

Controlling the melting kinetics of polymers : a route to a new melt state

Citation for published version (APA):

Lippits, D. R. (2007). *Controlling the melting kinetics of polymers : a route to a new melt state*. [Phd Thesis 1 (Research TU/e / Graduation TU/e), Chemical Engineering and Chemistry]. Technische Universiteit Eindhoven. <https://doi.org/10.6100/IR622737>

DOI:

[10.6100/IR622737](https://doi.org/10.6100/IR622737)

Document status and date:

Published: 01/01/2007

Document Version:

Publisher's PDF, also known as Version of Record (includes final page, issue and volume numbers)

Please check the document version of this publication:

- A submitted manuscript is the version of the article upon submission and before peer-review. There can be important differences between the submitted version and the official published version of record. People interested in the research are advised to contact the author for the final version of the publication, or visit the DOI to the publisher's website.
- The final author version and the galley proof are versions of the publication after peer review.
- The final published version features the final layout of the paper including the volume, issue and page numbers.

[Link to publication](#)

General rights

Copyright and moral rights for the publications made accessible in the public portal are retained by the authors and/or other copyright owners and it is a condition of accessing publications that users recognise and abide by the legal requirements associated with these rights.

- Users may download and print one copy of any publication from the public portal for the purpose of private study or research.
- You may not further distribute the material or use it for any profit-making activity or commercial gain
- You may freely distribute the URL identifying the publication in the public portal.

If the publication is distributed under the terms of Article 25fa of the Dutch Copyright Act, indicated by the "Taverne" license above, please follow below link for the End User Agreement:

www.tue.nl/taverne

Take down policy

If you believe that this document breaches copyright please contact us at:

openaccess@tue.nl

providing details and we will investigate your claim.

**Controlling the melting kinetics of polymers;
a route to a new melt state**

PROEFSCHRIFT

ter verkrijging van de graad van doctor aan de
Technische Universiteit Eindhoven, op gezag van de
Rector Magnificus, prof.dr.ir. C.J. van Duijn, voor een
commissie aangewezen door het College voor
Promoties in het openbaar te verdedigen
op dinsdag 6 maart 2007 om 16.00 uur

door

Dirk Reinier Lippits

geboren te Geldrop

Dit proefschrift is goedgekeurd door de promotoren:

prof.dr. S. Rastogi

en

prof.dr. P.J. Lemstra

A catalogue record is available from the Library Eindhoven University of Technology

ISBN: 978-90-386-0895-2

Copyright © 2007 by Dirk R. Lippits

The work described in the thesis is performed in the Faculty of Chemistry & Chemical Engineering group (SKT) Eindhoven University of Technology, The Netherlands. The work has been financially supported by DSM research, Geleen, The Netherlands.

Design Cover: D.R. Lippits and P. Verspaget (Grafische Vormgeving-Communicatie)
Printed at the Universiteitsdrukkerij, Eindhoven University of Technology.

Voor papa,

Table of Contents

Summary	7
Chapter 1 General Introduction	11
1.1 Brief overview of current the understanding of chain dynamics in polymer melts	11
1.2 Brief overview of current the understanding of polymer solids	12
1.3 Polymer crystallization	13
1.4 Control of the entanglements in the amorphous phase via direct synthesis	18
1.5 Outstanding issues	19
1.5.1 Loss of disentangled state upon melting	19
1.5.2 Melting behaviour of semi-crystalline polymers	19
1.6 The objectives of the thesis	21
1.7 References	22
Chapter 2 The formation of physical entanglements in an initially disentangled polymer melt	25
2.1 Introduction	25
2.2 Experimental	27
2.2.1 Materials	27
2.2.2 Experimental techniques	28
2.3 Results and discussion	29
2.3.1 Rheology of mono-disperse entangled high molecular weight polymers	29
2.3.2 Formation of entanglements in a disentangled polymer melt as probed by rheometry	31
2.3.3 Transverse spin-spin relaxation of entangled mono-disperse high molecular weight polymers	36
2.3.4 Formation of entanglements in the initially disentangled polymer melt as probed by solid state NMR	39
2.4 Conclusion	42
2.5 References	43
Chapter 3 Melting kinetics in polymers; The role of entanglements in the amorphous phase	45
3.1 Introduction	45
3.2 Experimental Section	47
3.2.1 Materials	47
3.2.2 Experimental techniques	48

3.3	Results and discussion	50
3.3.1	First Melting Point of UHMW-PE	50
3.3.2	Melting kinetics in UHMW-PE as probed by DSC	51
3.3.3	Reorganization in the solid state prior to melting as probed by Temperature Modulated DSC (TM-DSC)	57
3.3.4	Origin of the high melting point of nascent UHMW-PE on the 1 st heating	59
3.3.5	Melting in UHMW-PE as probed by solid state ¹ H NMR	62
3.3.6	Melt mechanism of melting nascent disentangled crystals	66
3.4	Conclusion	69
3.5	References	70
Chapter 4	Influence of melting kinetics on the chain dynamics; a route to the heterogenous melt	73
4.1	Introduction	73
4.2	Experimental	74
4.2.1	Materials	74
4.2.2	Experimental techniques	74
4.3	Results and Discussion	75
4.3.1	Melting and entanglement kinetics probed by Rheology	75
4.3.2	Influence of melting kinetics on the entanglements formation as probed by Solid state NMR	79
4.3.3	Additional experimental evidence for the existence of the heterogeneous melt	84
4.3.4	Molecular weight dependence of the appearance of heterogeneity in the melt	86
4.3.5	From a Heterogeneous to a Homogeneous melt	88
4.3.6	Heterogeneity in polymer melts	89
4.4	A theoretical Model	90
4.4.1	Salient findings of the McLeish model on the heterogeneous melt	90
4.4.2	Comparison with experiments	91
4.5	Conclusions	92
4.6	References	93
Chapter 5	Role of chain entanglements in crystallization; homogeneous vs. heterogeneous nucleation	95
5.1	Introduction	95
5.2	Experimental section	96
5.2.1	Materials	96
5.2.2	Experimental	97
5.3	Results and discussion	98
5.3.1	Influence of a heterogenous distribution of entanglements in the polymer melt on crystallization	98
5.3.2	Influence of entanglements in the polymer melt on crystallization	101
5.3.3	Solid state drawing of disentangled melt-crystallized UHMW-PE	104
5.4	Conclusion	106
5.5	References	107

Chapter 6	Implications of the melting kinetics on the melt state of the solution crystallized UHMW-PE	109
6.1	Introduction	109
6.2	Experimental	111
6.2.1	Materials	111
6.2.2	Experimental techniques	111
6.3	Results and discussion	112
6.3.1	Crystal morphology of solution-crystallized UHMW-PE	112
6.3.2	Melting behaviour of the solution-crystallized UHMW-PE	114
6.3.3	Heating rate dependence on the chain dynamics –from the disentangled to the entangled melt	118
6.3.4	Melting mechanism of solution-crystallized UHMW-PE as probed by ^1H NMR	120
6.3.5	Melt rheology of the disentangled UHMW-PE Fibers.	122
6.4	Conclusion	124
6.5	References	125
Chapter 7	Influence of the addition of single walled carbon nanotubes on the melt rheology of UHMW-PE	127
7.1	Introduction	127
7.2	Experimental	129
7.2.1	Materials	129
7.2.2	Experimental techniques	129
7.3	Results and discussion	130
7.3.1	Dispersion of SWNTs in UHMW-PE	130
7.3.2	Solution-crystallized films of SWNT/UHMW-PE nanocomposites	132
7.3.3	Crystallization of UHMW-PE in the presence of SWNTs	134
7.3.4	Rheology of SWNT/UHMW-PE nanocomposites	135
7.3.5	Electrical conductivity of SWNTs/UHMW-PE nanocomposites	143
7.4	Conclusion	144
7.5	References	145
Appendix	Experimental rheology of UHMW-PE	147
Samenvatting		151
Acknowledgement		155
Curriculum Vitae		157

Summary

Polymers play an important role, both in nature and in the modern society. In contrast to polymers in nature, the so-called biopolymers, man-made polymers are thermally more robust and are in majority processed via the melt (plastics). In the case of thermoplastic polymers (> 70% of all synthetic polymers), the viscosity of the polymer melt poses a limit on the processability, notably for polymers possessing a high(er) molar mass M . Based on experimental evidence, the (zero-shear) viscosity of polymer melts, η_0 , scales with $M_w^{3.4}$ (M_w is the weight-average molar mass). This implies that the melt-viscosity increases with more than a factor of 10 upon doubling the molar mass! Since the properties of polymers in the solid-state also increase with increasing molar mass, notably the strength and toughness, the processing of thermoplastic polymers, e.g. injection-moulding, extrusion, fiber spinning, is often a compromise between the ease of processing, viz. preference for lower molar mass (easy flow), and properties, with preference for high(er) molar masses.

The current knowledge of polymer melts is rather well developed and based on a simple but elegant model put forward by P.G. de Gennes (Nobel prize for Physics), the so-called reptation model. In this model, the motion of a polymer chain in the molten state is hindered by its neighbors (entanglement), which generate a virtual “tube” confining the chain on a one dimensional pathway. The constraint chain dynamics gives rise to a characteristic time for a chain to diffuse its own length in the tube. Scaling as M^3 . The same scaling is predicted for the zero-shear viscosity. The experimentally observed discrepancy, see above $\eta_0 \sim M^{3.4}$, from the 3.0 dependence is attributed to “contour-length fluctuations” i.e. fluctuation-driven stretching and contractions of the chain along the tube. In **Chapter 2**, it is shown that the zero-shear melt-viscosity of carefully prepared samples of high molar mass polyethylene (PE), possessing a narrow molecular weight distribution, indeed follow the predictions of the reptation model, viz. η_0 scales with M^3 . The advantage of high molar mass polyethylenes is that chain-end effects do not play an important role or can be ignored. **As a consequence of these results, high molecular weight polyethylenes have been used as a model substance throughout the thesis, notably ultra-high-molecular-weight PE (UHMW-PE).**

In the solid state, entanglements can be removed effectively by dissolution of the polymer. In dilute solutions, below the so-called overlap concentration ϕ^* , entanglements can be removed completely. In the case of crystallizable polymers, such as PE, the reduced entanglement density can be made permanent since the long chain molecules form folded-chain crystals, a well-studied phenomenon in polymer physics.

A more elegant and also technologically more advanced way to generate disentangled PE crystals is via direct polymerization in the reactor. At low polymerization temperatures and low catalyst activity/concentration, individual growing chains will form their own folded-

chain crystals. In the limiting case where the growing chains are separated far enough from each other, monomolecular crystals can be formed.

If completely disentangled PE structures can be obtained via solution-crystallization and/or via direct controlled synthesis, the intriguing question is whether this disentangled state will be preserved upon melting and what is the time scale to generate a fully entangled equilibrium polymer melt. **This question is the key issue of the thesis. What happens when we start from a non-equilibrium disentangled state and cross the melting temperature into the molten state? How does the equilibrium entangled melt state get restored?**

In **Chapter 2** it is shown that starting from the disentangled state, in this case nascent UHMW-PE powder, that it takes time to “build-up” the plateau modulus in the melt, indicative of an entanglement formation process. The entanglements formation scales as the reptation process (M_w^3). Parallel to rheology measurements, solid-state NMR is used to monitor the change in chain mobility. The time scale to reach the equilibrium melt as probed by the NMR and Rheology experiments is very different, suggesting that restrictions in local chain mobility monitored by NMR are realized at an earlier stage than restrictions in segmental mobility inferred from rheological experiments.

A peculiar phenomenon of nascent reactor powders is their high melting point, close to or equal to the so-called equilibrium melting point of PE. This phenomenon has puzzled researchers in the field for many years and various explanations have been given such as the growth of extended-chain crystals instead of folded-chain crystals or extensive reorganization during the melting process, but all these explanations were not supported by experimental data which show that nascent UHMW-PE reactor powders consist of “normal” folded-chain crystals without extensive reorganization (thickening) during the melting process. In **Chapter 3** it is shown that the unusual high melting temperature of nascent UHMW-PE is related to the tight-folding (adjacent re-entry mode) in the crystals. Melting is a cooperative process over several chain stems of the same crystal in contrast with e.g. melt-crystallized samples where a chain is incorporated in various folded-chain crystals and topologically, prior to the melt, is in contact to different chains.

The melting mechanism as discussed in chapter 3, can be utilized by controlling the melting process of UHMW-PE nascent reactor powders. When decreasing the heating rate, the melting process starts by detachment of single stems from the (lateral) surface of the crystals. In this process, the molten chain ends can entangle with chain ends from other partly molten crystals, whereas the core of the molecule is still in the crystal, viz. in the tight folded-chain conformation. As discussed in **Chapter 4**, after complete melting by this mechanism, a heterogeneous melt-state is obtained since the central part of the individual chains is prevented from taking part in the entangling process. By NMR experiments, it is observed that on decreasing the heating rate, the time required to restrict the chain conformations at the local scale increases. In rheometry it is observed that with the increasing time to restrict the

chain conformations, the time needed for the modulus to buildup increases. Ultimately, it is feasible to melt the sample so slowly that the restriction in the chain conformation in part of the sample can be inhibited, maintaining the partially high local mobility. Since restrictions in the chain conformations can not be achieved, the cooperative motion needed for the translational mobility is absent. As a consequence normal chain reptation is slowed down considerably and a long-living partially disentangled melt is obtained.

This new melt state shows a decreased plateau modulus and viscosity, whereas the terminal stress relaxation rates remain the same. The observations are that stress relaxation is achieved without “normal” reptation of chains in the tube. This is explained by the partial reptation of the chains since only a fraction of the whole chain is required for the stress relaxation.

The consequences of a heterogeneous melt-state are discussed in **Chapter 5**. The observations are that the disentangled chainsegments crystallize faster than the entangled chains. This suggests that intra-molecular homogeneous nucleation occurs faster than the heterogeneous nucleation. Moreover, after crystallization from the heterogeneous melt, the solid-state drawability is still remarkably high, indicative of a certain state of disentanglement. Thus can be drawn into a fiber in the solid state because large disentangled blocks are present in the crystal.

The melting behavior of solution-crystallized UHMW-PE is studied in **Chapter 6**. Similar to the nascent disentangled crystals, these folded-chain crystals can be melted by consecutive detachment of chain stems from the crystal substrate. The differences in melting behavior, revealed during different heating rates, have consequences on the chain dynamics. Unlike the nascent disentangled samples, where modulus builds up with time, the solution-crystallized sample entangles immediately upon fast heating. The remarkable difference in the rate of entanglements formation can be attributed to the differences in the stacking of crystals, prior to melt. The solution-crystallized samples double their crystal size via intermixing of the regularly stacked crystals which upon melting facilitate the entanglement formation process. contrary to the nascent disentangled samples where no regular stacking occurs.

An alternative route to achieve a reduction in the melt viscosity is explored in **Chapter 7**, by the addition of the single-walled carbon nanotubes (SWNTs). When varying the content of SWNTs, the dynamic viscosity/storage modulus shows a minimum. The decrease in viscosity is attributed to the selective adsorption of the high molar mass fraction onto the nanotube surface. The increase in viscosity upon further increasing the nanotube content is attributed to the formation of an elastic nanotube-polymer network.

The concepts presented in the thesis, based on experimental validation, could have an important impact on novel processing techniques for UHMWPE, e.g. sintering of UHMW-PE into products for demanding applications such as artificial hip-and knee joints and, solvent-free processing routes for UHMW-PE fibers and tapes.

Chapter 1

General Introduction

Preamble

Polymer Science & Engineering is the paradigm of a multi-disciplinary area in Materials Science. The path from monomer to polymer into functional materials and products (plastics) travels through various (sub)disciplines such as Chemistry, Catalysis, Thermodynamics, Polymer Reaction Engineering, Rheology, Physics, Mechanics, Processing & Product Design. The successful developments of new and/or improved polymeric materials and products from laboratory into industrial realization, requires ideally an integrated approach of the (sub)disciplines met en route.¹ At present, a full spectrum of knowledge in polymer science & engineering is available and many disciplines such as polymer catalysis and (molecular) rheology have been developed very well as evidenced e.g. by Nobel prizes given to researchers in these fields, e.g. Grubbs and de Gennes to name a recent few.

Not many attempts have been made up to now in academia to cross the borders between (sub) disciplines, viz. a “chain-of-knowledge” approach.

In the thesis an attempt is made to cross the border between the area of solid-state physics of polymers and (molecular) polymer rheology, aiming at improved processability and product performance.

Before discussing the goal of the thesis, the current know how about polymers in the molten state (melt) and in the solid-state will be reviewed in brief.

1.1 Brief overview of the current understanding of chain dynamics in polymer melts

Synthetic polymer molecules in the molten state are highly entangled, to be compared with cooked spaghetti. There is no apparent order in the molten state and the conformation of the individual chain is a so-called random-coil, as evidenced by various neutron scattering experiments on deuterated polymer chains.² Due to the presence of long chain polymer molecules, which are highly entangled, polymer melts exhibit a high viscosity which increases strongly with increasing molecular weight. Experimental results³ on many polymeric systems show that the (zero-shear) viscosity scales with $M^{3.4}$ which implies that on doubling the molar mass, the melt-viscosity increases with more than a factor of 10! Since the properties of synthetic polymers in the solid-state also depend on the molar mass, e.g. the toughness and strength increase with increasing molecular weight, the area of polymer processing (thermoplastic polymers) is a compromise between, on the one hand, the

maximum properties in the solid state (high molar mass) and, on the other hand, the ease of processability (lower molar mass).

Our current understanding of the behavior of long chain molecules in the molten state was boosted by the concept of “reptation” introduced by P.G. de Gennes^{4,5} in 1971. In his simple but elegant model, the polymer chain in the molten state (polymer melt) is envisaged to be entangled/surrounded by its neighbors, providing a virtual tube confining the pathway of a polymer chain to follow its own contour length. The chain dynamics in an equilibrium melt, Brownian motion, is, consequently, a snake-like motion (reptation) of the polymer chain to move out of their virtual tube into its new surrounding, another virtual tube. The constraint chain dynamics give rise to a characteristic time for a chain to diffuse one tube length, scaling (and thereby the zero-shear viscosity η_0) with M^3 , The experimentally observed discrepancy, see above, $\eta_0 \sim M^{3.4}$, from the 3.0 dependence is attributed to “contour-length fluctuations” i.e. fluctuation-driven stretching and contractions of the chain along the tube.⁶

The concept of “reptation” is nowadays generally accepted. Based on this model Doi and Edwards⁷ developed a theory to describe the experimental rheology of mono-disperse entangled polymer melts. Nowadays more quantitative predictions include chain contour length fluctuations (Millner and McLeish),⁸ and cooperative effects of constraint release, i.e., double reptation (des Cloizeaux)^{9,10} and dynamic tube dilation. (Marrucci, Pattamaprom and Larson)^{11,12}

1.2 Brief overview of the current understanding of polymer solids

Upon cooling from the melt into the solid state, the entanglement network in the molten state will be preserved to a large or some extent, depending on the type of polymer, viz. non-crystallizable (amorphous) vs. crystallizable polymers.

1.2.1 Amorphous polymers

In the case of amorphous, non-crystallizable polymers, it is tacitly assumed that the entangled polymer melt turns into a glassy solid polymer upon cooling below the glass transition temperature T_g without much change in the conformation and entanglement density, the number of entanglements c.q. constraints per chain molecule. The mechanical properties of amorphous polymers in the solid-state, such as the deformation behaviour, can be explained straightforwardly from the presence of an entanglement network, where entanglement loci act as physical crosslinks in the network and the deformation behaviour depends on the average molar mass, $\langle M_e \rangle$ between entanglements. The value of $\langle M_e \rangle$ is dependent on the polymer chemical structure and can be derived from the so-called plateau modulus. The deformation behaviour of amorphous polymers has been studied in depth by Govaert, Meijer^{13,14} c.s. and

they determined the intrinsic deformation behaviour of polymers such as polycarbonate (PC), polystyrene (PS) and PMMA and related the strain-hardening modulus G_R to the entanglement density. The paradox that a polymer such as polystyrene (PS) with a relatively high $\langle M_e \rangle$, is ductile on a local scale, but brittle macroscopically, can be understood straightforwardly from the value of the yield stress vs. the (lack of) strain hardening. The intrinsic deformation behaviour of amorphous polymers can thus be understood from the simple model of trapped entanglements in the glassy solid state.

1.2.2 Crystallizable polymers

In the case of crystallizable polymers, a completely different situation can be encountered, which is highly dependent on the way the polymer is crystallized. It can not be assumed that the entanglement density, or the $\langle M_e \rangle$, the average molar mass between entanglement loci, will not change significantly as is the case for amorphous polymers. Upon crystallization from the melt, the long chain molecules are withdrawn from the entanglement network in order to form a crystalline structure, consequently crystallization is an inherent chain-disentangling process. The extent of disentangling as a result of crystallization is a matter of crystallization conditions. In general, low supercoolings promote disentangling during crystallization. But apart from crystallization from the melt, there are other possibilities for crystallization such as crystallization from dilute solutions or crystallization during polymerization, as will be discussed below. In these special cases, complete disentangled structures in the solid state can be obtained! In order to explain the change in entanglement density as a result of crystallization, the current understanding of polymer crystallization will be summarized below in 1.3.

1.3 Polymer crystallization

1.3.1. Crystallization from dilute solutions

The observations that long chain polymer molecules can crystallize is an intriguing phenomenon which puzzled scientist for many years and still is a topic of interest. The prerequisite for crystallization is that the chains are linear and stereo regular. The original idea was that long chain molecules, which are highly entangled in the melt, are not able to form well defined crystallites upon cooling below the melting temperature. It was anticipated in the early years when polymers became known, the beginning of last Century, that at most segments of polymer chains come together to form the so-called fringed-micellar crystals, see figure 1.1a, a logical conclusion in view of the fact that the long chain molecules are highly entangled in the polymer melt and, moreover, do not possess the same molar mass!

In 1938, however, Storks pointed out the possibility of chain folding during crystallization but his finding remained unnoticed for many years.¹⁵ In the 1950s, more or less independently, folded-chain crystals have been discovered by Keller, Fischer and Till¹⁶⁻¹⁸ by crystallizing linear polyethylene (discovered in 1953 by Ziegler) from dilute solution. Based on electron-diffraction experiments, Keller showed that the long polymer chains are folded in the platelet (lamellar) crystals, see figure 1.1b.

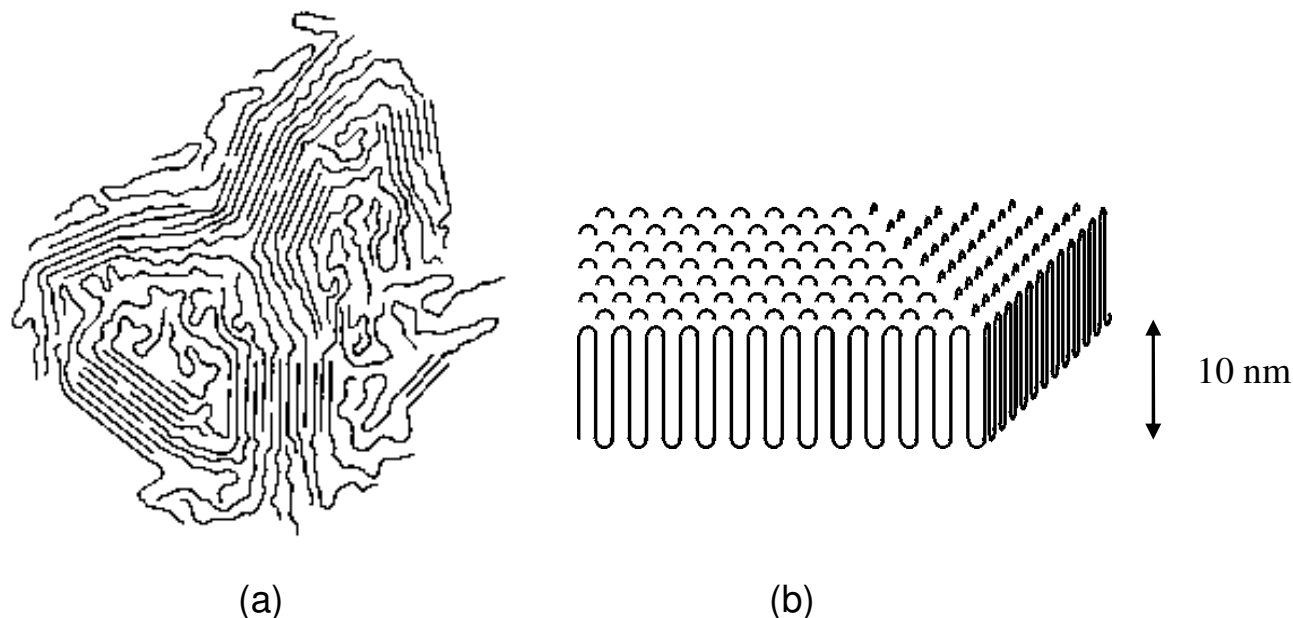


Figure 1.1: (a) Schematic representation of the fringed micelle concept and (b) folded chain crystals (after A. Keller)^{19,20}

The observation of well-defined PE single crystals was related to two facts, the availability of linear polyethylene, discovered by Ziegler in 1953, and crystallization from very dilute solutions with concentrations $< \phi^*$, the so-called overlap concentration. Hence, the chains in solution are completely disentangled to start with. Many studies have been devoted in the mean time to crystallization from dilute solutions using linear PE as a model substance. In general, low molecular weight PE chains form platelet single crystals upon crystallization from a dilute solution.^{16,17,21,22}

These single crystals are thin, in the order ten nanometers, and at least 1 order of magnitude larger in the lateral direction. The chains in these crystals are folded along the lateral faces of the growing lamellae, thereby subdividing the crystal in different sectors.

Observations of Toda et al. are, that within a polyethylene single crystal, polymers chains tilt at an angle of 15° - 30° to the folding surface of lamellar crystals.²¹ The tilting direction can be different for each growth sector leading to characteristic tri-dimensional forms (Figure 1.2a). In figure 1.2a a well known the tent shape morphology is shown. The existence of a non-planar shape (the base of the tent with the $\{110\}$ lateral faces is not planar) is indicative for

regular chain folding, where each chain along the periphery of the crystal is shifted a certain distance along the chain axis with respect to the nearby chain.²²

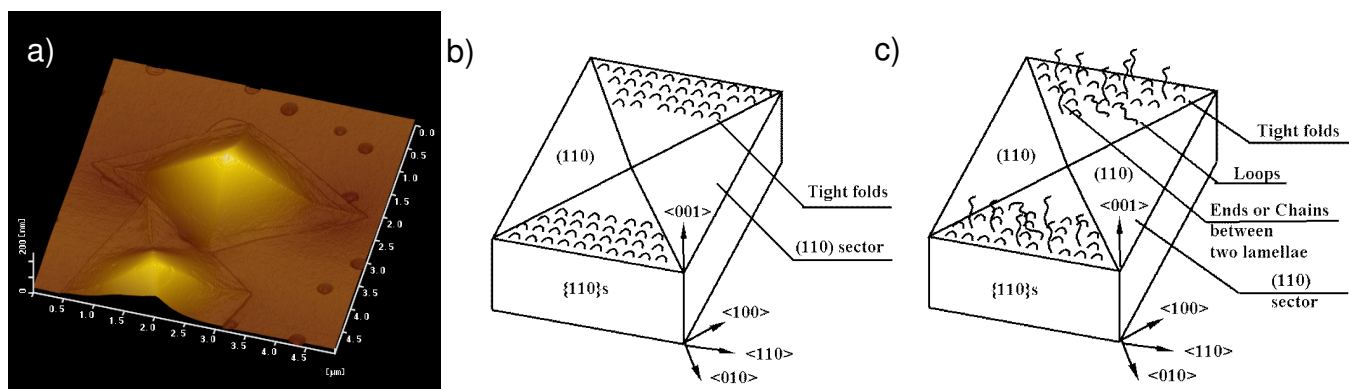


Figure 1.2: **a)** AFM Topographic image of polyethylene single crystals of 30 kg/mol grown from dilute solution (Copied from Toda et al.) In the picture crystals having convex hollow pyramidal type morphology is shown as an example.²¹ **(b)** Sketches of the fold surface organization with tight adjacent re-entrant folds (After Keller)²⁴ and **(c)** loose folds of the switchboard concept. (After Flory)^{25,26}

1.3.2. Crystallization from the melt

In the case of crystallization from the melt, the polymer chains must disentangle from the highly entangled melt, achieve a regular conformation and then chain segments align parallel to each other and fold to form folded-chain crystals. In contrast to crystallization from dilute solutions, in the case of crystallization from the melt, regular chain-folding resulting into well defined crystals does not occur. Upon isothermal crystallization at relatively low supercoolings, spherulites can be observed, viz. spherical aggregates of folded-chain crystallites. In practice, due to fast cooling/quenching e.g. during injection moulding, the morphology becomes rather complex and oriented structures with row nucleation can be observed. A full description of these phenomena is outside the context of the thesis.

What is relevant for the concepts put forward in the thesis, that long polymer chains upon crystallization have the tendency to form folded-chain crystal structures but due to topological constraints, viz. entanglements, the process of folding, notably adjacent re-entry of crystals stems, is usually hampered. There are two techniques to infer the organization of polymer molecules within the crystals, respectively solid-state NMR and solid-state drawing.

NMR-studies

Using solid state NMR,²⁸ it is shown that the non-crystalline region of the solution-crystallized sample reveals anisotropy, indicative for restricted (tight) folds in the amorphous phase as shown in figure 1.2b. Tight folds are the result of adjacent re-entry of folded chain stems. In the case of melt-crystallized samples, an isotropic motion is detected, indicative for the mobile (loose) folds in the amorphous phase. Using 1D ¹³C exchange spectra,²⁹ below the alpha relaxation temperature (< 90 °C), it is shown that chain segments exchange from the amorphous phase to the crystal domain in the solution-crystallized sample. At these low temperatures, in the melt-crystallized sample such an exchange is hardly observed. It is concluded that though local chain dynamics in the amorphous phase of the solution-crystallized sample is restricted; the anisotropy present in the amorphous phase (tight folds) favors the cooperative motion between the crystal and amorphous domains. NMR is a powerful technique to study chain dynamics.

Solid-state drawing

Upon crystallization from the melt the polymer chains are reeled-in on the crystal surface and hence disentangle. The properties in the solid-state are governed by the presence of an entanglement network, not only for amorphous polymers but for semi-crystalline polymers as well. In the literature many researchers try to correlate the mechanical properties of semi-crystalline polymers to the crystal size/perfection, lamellar thickness etc. and the presence of a trapped entanglement network is overlooked. For example, upon slow cooling or prolonged isothermal crystallization, the chains have more time to reel-in, viz. to withdraw from the entanglement network. A standard PE sample can be made tough, fast cooling/quenching from the melt, or brittle, by slow cooling from the melt. The link between drawability in the solid state and the presence of an entanglement network will become clearer from section 1.3.3 below.

1.3.3. Crystallization from semi-dilute solutions, polymer gels.

The number of entanglements is dependent on the polymer concentration in solution. In general, the M_e will increase about proportional with the inverse of the polymer concentration ϕ . In the limit of dilute solutions, viz. the polymer concentration ϕ is $< \phi^*$, there is no chain overlap and individual single crystals grow. Upon crystallization from semi-dilute solutions, also folded-chain crystals will form, but they can be still entangled. Since the individual crystals are connected, via trapped entanglements, and the solvent molecules are in between the crystals, a gel-like material is formed. Figure 1.3 shows a simple 2-D scheme of the topology of polymer molecules.

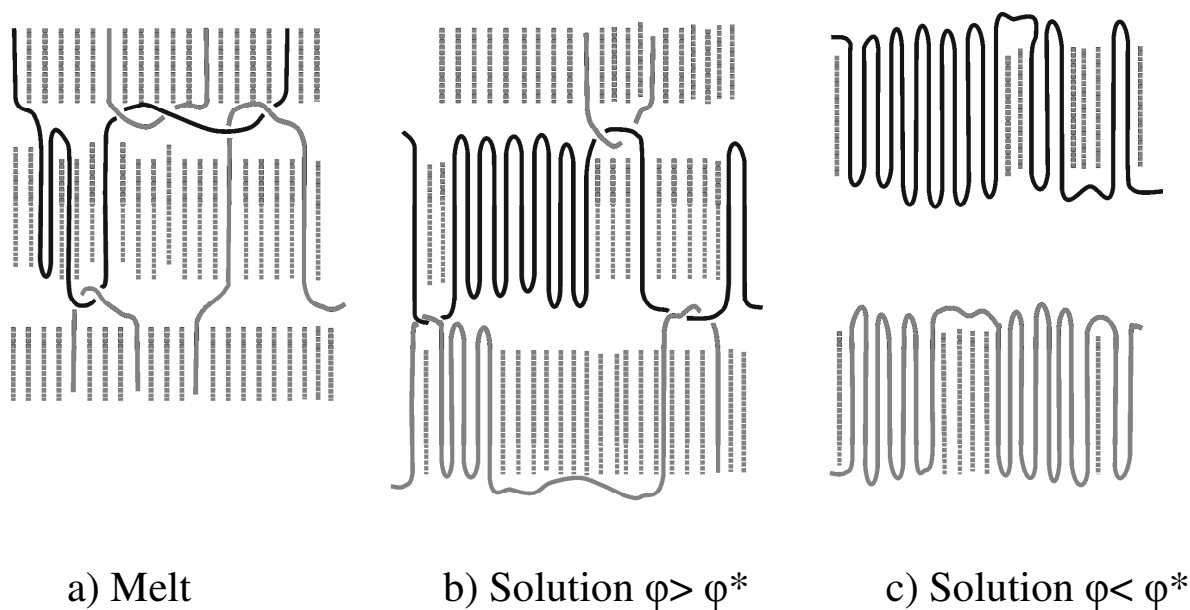


Figure 1.3: 2-D schematic representation of the chain trajectory upon crystallization from the melt (a) semi-dilute solutions (b) and dilute solutions (c)²³ ϕ^* is the critical overlap concentration for polymer chains.

In the case of crystallization from semi-dilute solutions, the solvent can be removed from the polymer gels, and the thus obtained dry film shows a remarkable high drawability in the solid state, demonstrating that the number of trapped entanglements control the ultimate drawability. This phenomenon is the basis for the so-called solution (gel)-spinning of ultra-high-molecular-weight PE at DSM, discovered in 1979. The fibers spun from semi-dilute UHMW-PE solutions, after removal of the solvent, can be drawn to high draw ratios (above 100) into fibers and tapes.^{23,30} The thus obtained fibers possess a tensile strength of > 3 GPa and a Young's modulus of > 100 GPa, which approaches the theoretical value for the fully extended chain crystals.

1.4 Control of the entanglements in the amorphous phase via direct synthesis

To generate disentangled polymers via crystallization from dilute solutions is rather cumbersome and requires more than 90% of solvent, thus recycling of solvent. A more elegant route to obtain disentangled UHMW-PE, and thus to control the entanglements in the amorphous phase, is by direct polymerization in the reactor. For UHMW-PE, a relatively low polymerization temperature is required in order to obtain high molar mass. Such synthesis conditions allow for successive polymerization and crystallization of a polymeric chain at the surface of the catalyst. In commercial processes, UHMW-PE is synthesized by a slurry process using a Ziegler-Natta catalyst with a hydrocarbon as diluent. As the active sites in such catalyst systems are relatively close together, the chains grow in close proximity to each other. Due to the relatively high polymerization temperature of 60-100°C, crystallization of the polymer chains is slow compared to the polymerization. These conditions facilitate the entanglements formation during synthesis.

By decreasing the temperature a situation is encountered where the rate of polymerization is relatively slower than the rate of crystallization. In this situation, the growing chains on the catalyst surface tend to crystallize independently of each other during the polymerization process and consequently less entangled UHMW-PE is obtained. These UHMW-PE reactor powders often referred to as ‘nascent’ or ‘virgin’ UHMW-PE, can be remarkably ductile in the solid state.³¹ It was shown by Smith et al.³² that films of reactor powders, in the same manner as solution cast UHMW-PE, could be drawn easily into high-modulus structures.

An even more elegant approach is to polymerize disentangled polymers directly in solution. In the case of PE, there is ample experience with so-called homogeneous catalysts, metallocene- or post-metallocene-based catalyst, in which case the molecularly dissolved catalyst initiates a polymer chain in solution.³³ In order to make high molecular weight PE, the temperature is kept low, e.g. at room temperature, and the growing chain is far below the dissolution temperature, hence will crystallize. In the case of low catalyst concentration, the chains will grow individually and will crystallize directly in the reactor. In the limit of low catalyst concentration and low catalyst activity, one could anticipate that the PE chains will form their own crystal, viz. monomolecular crystals. In this case, UHMW-PE crystals are generated which are completely disentangled.³⁴⁻³⁶

In recent NMR studies Yao et al.²⁸ showed that the nascent disentangled samples reveal anisotropy in the non-crystalline regions, similar to the solution grown crystals, indicative for tight adjacently re-entrant folds.

1.5 Outstanding issues

1.5.1 Loss of disentangled state upon melting

In the past, attempts have been made to use disentangled solution-crystallized polymer for the melt-processing of the intractable UHMW-PE. The basic idea was that the disentangled molecules will require considerably long time to (re)establish the equilibrium entanglement network. Ideally, melt-processing should become feasible for intractable polymers such as UHMW-PE, due to a lower initial viscosity in the melt. However, against the predictions, within the given experimental time, no memory effect of the disentangled state could be obtained.

It was shown also, that after melting and crystallization of the solution-crystallized polymer, the high drawability in the solid state is lost, even when the polymer was left in the melt for a few seconds. The thus crystallized samples behaved similar to the entangled melt crystallized samples.^{37,38} Rheological properties of the melt obtained from the initially disentangled crystals, such as G' , G'' and $\tan \delta$ are identical to the fully entangled melt state. In view of the long relaxation times for these high molar masses the absence of any memory effect is rather puzzling.

1.5.2 Melting behaviour of semi-crystalline polymers

The melting behaviour of semi-crystalline polymers can be complicated. Depending on the reorganization process of the amorphous and crystalline regions, which are connected by chains, the heating rate dependence on the melting temperature can be either positive or negative. For polymers where crystal thickening and/or crystal perfectioning is feasible, the measured melting temperature increases with decreasing heating rate.⁸ On the other hand, in polymers where no such reorganization occurs (e.g. extended chain crystals), the measured melting temperature decreases with decreasing heating rate. The increase of the melting temperature with increasing heating rate is attributed to superheating, as well as thermal lag.⁹ Other complications in the melting of semi-crystalline polymers arise from the experimental observations that melting temperatures of the solution, nascent and melt-crystallized samples of the same polymer having approximately the same crystal thicknesses are distinctly different. For example, on heating at 10 K/min, nascent UHMW-PE melts around 141 °C (independently of synthesis route!), close to the reported equilibrium melting temperature for polyethylene of 141.5 °C. Such a high melting point normally found for “chain-extended” polyethylene crystals which are extremely thick ($>1 \mu\text{m}$), has been a subject of debate. Using electron microscopy and DSC, Engelen et al.⁴¹ conclusively showed that the nascent crystals are folded-chain crystals. Thus the high melting temperature was attributed to fast reorganization leading to thickening prior to melting. However, no experimental evidence of thickening was provided. On the

contrary, Kurelec et al. showed that even on annealing close to the melting point for several hours these nascent crystals do not exceed a value of 26 nm.^{42,43} The melting temperature predicted from Gibbs-Thomson equation for polyethylene [$T_m = 414.2 - 259.7/l$]⁴⁴ for a lamellae thickness of 26 nm is 131 °C.⁴⁵ Furthermore, the high melting temperature of 141 °C, is lost on second heating, where a melting temperature of 135 °C is measured.⁴¹ A similar discrepancy is observed between the first and second heating run of solution crystallized UHMW-PE, where the lamellae double their initial thickness upon annealing below the melting temperature to a maximum of 25 nm.⁴⁵ The melting temperature predicted from the Gibbs-Thomson equation for a lamellae thickness of 25 nm, 131 °C is 5 °C lower than the experimentally observed melting point of 136 °C. Furthermore, the high melting temperature of 136 °C, is lost on second heating where a melting temperature of 131 °C is measured, which now coincide with the prediction of the Gibbs-Thomson equation.

The melting aspects involved in nascent, melt- and solution-crystallized polymers cannot be explained by existing thermodynamic concepts alone. A different approach is needed to resolve the high melting point of the nascent and solution-crystallized polyethylenes.

1.6 The objectives of the thesis

From controlled synthesis it is feasible to obtain completely disentangled nascent crystals. In the equilibrium melt, the chains are highly entangled. Consequently, nascent disentangled reactor powders provide a unique opportunity to follow the entanglements formation upon melting, viz. from a completely disentangled solid state into a fully entangled molten state. Making use of powerful techniques such as solid-state NMR, combined with rheological experiments, the chain dynamics of a non-equilibrium disentangled melt state is followed to elucidate the outstanding issues as highlighted in paragraph 1.5.

As a model substance, ultra-high-molecular-weight polyethylenes, UHMW-PEs are chosen in order to increase the time required for the entanglements formation and to minimize the effect of chain ends.

Thanks to synthesis possibilities in the group SPC (Koning, Duchateau) and cooperation with others (Hessen et al. (University of Groningen, The Netherlands)³⁴ and B. Wang (DSM Research, Geleen, The Netherlands),³⁵ the following systems could be studied:

- The melt-rheology of well-defined narrow molar mass UHMW-PE to verify current theories regarding reptation;
- With the help of advanced NMR and Rheology, the entanglements formation of the disentangled UHMW-PE samples in the melt could be followed.
- With the help of DSC and Dynamic DSC, the melting kinetics/behaviour of polyethylene could be studied.
- With combined DSC, advanced NMR and Rheology the influence of the melt mechanism on the melt state could be studied.
- By controlled melting, the number/concentration of entanglements in the melt can be adjusted and varied, providing a unique opportunity to study the influence of entanglements on chain dynamics and on polymer crystallization.
- In the last chapter an alternative route to influence the melt rheology of UHMW-PE by addition of single walled nano tubes is explored

It has to be noted that the studies performed are extended to low molecular weight polyethylenes and in principle can be extended to flexible semi-crystalline polymers where the adjacent re-entry is feasible. This thesis is based on a collection of papers which have been published or submitted to various journals.⁴⁹⁻⁶⁰

1.7 References

1. Lemstra, P.J., *Macromolecular Reaction Engineering*, **2007**, 1, 15.
2. Flory, P.J. *Principles of Polymer Chemistry*. Cornell University Press, Ithaca, New York, **1953**.
3. Ferry, J.D. *Viscoelastic Properties of Polymers* **1980**, John Wiley & Sons: Toronto.
4. de Gennes, P.J., *J. Chem. Phys.*, **1971**, 55, 572.
5. de Gennes P.G., *Scaling Concepts in Polymer Physics* **1979** (Cornell University Press, Ithaca, NY).
6. Doi M. *J. Polm. Sci. Ed.* **1983**, 21, 667.
7. Doi, M.; Edwards, S.F. *The Theory of Polymer Dynamics* **1986**; Oxford Press: Oxford.
8. Milner S.T.; McLeish T.C.B.; *Phys. Rev. Lett.* **1998**, 81, 725.
9. des Cloizeaux, J., *Europhys. Lett.* **1988**, 5, 437.
10. des Cloizeaux, J., *Macromolecules* **1990**, 23, 3992.
11. Marrucci, G., *J. Polym.Sci.: Polym. Phys. Ed.* **1985**, 23, 159.
12. Pattamaprom, C.; Larson, R. G.; Van Dyke, T.J. *Rheol. Acta* **2000**, 39, 517.
13. Ho, J.; Govaert, L.; Utz, M. *Macromolecules* **2003**, 36, 7398.
14. van Melick, H. G. H.; Govaert, L. E.; Meijer, H. E. H. *Polymer* **2003**, 44, 457.
15. Storks, K.H.; *J. Am. Chem. Soc.*, **1938**, 60, 1753.
16. Keller, A. *Philos. Mag* **1957**, 2, 1171.
17. Fischer, E.W., *Nature* **1957**, 12, 753.
18. Till, P.H. *J. Polym. Sci.* **1957**, 24, 301.
19. http://materials.dept.shef.ac.uk/liquid_crystal/minim/alkgen.html.
20. <http://www.chem.rochester.edu/~chem421/cryst.htm>.
21. Toda, A.; Okamura, M.; Hikosaka, M.; Nakagawa, Y. *Polymer* **2000**, 44, 6135.
22. Gedde, U.W.; Mattozzi, A. *Adv Polym Sci* **2004**, 169, 29.
23. Lemstra, P.J.; Bastiaansen, C.W.M; Rastogi, S. In: Salem DR (ed) *Structure formation in polymeric fibers*. Hanser **2000**, 185.
24. Keller, A.; Pedemonte, E. *J. Crystal Growth.* **1973**, 18, 111.
25. Flory, P. J. *J. Am. Chem. Soc.* **1962**, 84, 2857.
26. Tian, M. Ph.D. thesis, Eindhoven University of Technology, *Understanding the Organization and Reorganization of Polymer Crystals* ISBN 90-386-2705-x <http://alexandria.tue.nl/extra2/200412853.pdf>
27. Rastogi, S.; Terry, A.E. *Adv. Polym. Sci.*, **2005**, 180, 161.
28. Yao, Y. PhD Thesis Max Planck Institute für Polymerforschung, Mainz, **2007**.
29. Schmidt-Rohr, K.; Spiess, H. W. *Multidimensional Solid-State NMR and Polymers* **1994** (Academic, New York).
30. Smith, P.; Lemstra, P.J.; Booij H.C. *J. Polym. Sci. Part B: Polym. Phys.*, **1982**, 20, 2229.
31. Smith, P.; Chanzy, H.D.; Rotzinger, B.P. *Polym, Comm.*, **1985**, 26, 258.
32. Smith, P.; Chanzy, H.D.; Rotzinger, B.P. *J. Mater. Sci.*, **1987**, 22, 523.
33. Scheirs, J.; Kaminsky, W. *Metallocene-based polyolefins: preparation, properties and technology*, Wiley: Chichester, **2000**.
34. Evans, W.J.; De Coster, D.M.; Greaves, J. *Macromolecules*, **1995**, 28, 7929.
35. Gruter, G.J.M.; Wang, B.; van Beek, J.A.M. *European Patent Application* EP 1057837 A1 **2000**.

36. Sharma-Garkail K Ph.D. thesis, Eindhoven University of Technology *Easily processable ultra high molecular weight polyethylene with narrow molecular weight distribution* **2005** ISBN 90-386-2836-6,
<http://alexandria.tue.nl/extra2/200510552.pdf>
37. Bastiaansen, C.W.M; Meijer, H.E.H; Lemstra, P.J. *Polymer*, **1990**, *31*, 1435.
38. Bastiaansen, C.W.M. Ph.D. thesis, Eindhoven University of Technology, *Oriented structures based on flexible polymers*, **1991**,
<http://alexandria.tue.nl/extra1/PRF7B/9104295.pdf>
39. Wunderlich B.; Czornyj G, *Macromolecules* **1977**, *10*, 906.
40. Toda A.; Hikosaka M.; Yamada K.; *Polymer* **2002**, *43*, 1667.
41. Tervoort-Engelen, Y.M.T.; Lemstra P.J. *Polym. Comm.* **1991**, *32*, 343.
42. Rastogi S.; Kurelec L.; Lippits D.; Cuijpers J.; Wimmer M.; Lemstra P.J.; *Biomacromolecules* **2005**, *6*, 942.
43. Corbeij-Kurelec L. Ph.D. thesis, Eindhoven University of Technology, *Chain mobility in polymer systems* **2001** Chapter 3 ISBN 90-386-3032-8
<http://alexandria.tue.nl/extra2/200113706.pdf>
44. ATHAS data bank (<http://web.utk.edu/~athas/databank/> Ed. M. Pyda)
45. Depending on the experimental methods used, different numerical Gibbs-Thomson equations exist, see Cho T.Y.; Heck B.; Strobl G.; *Colloid Polym Sci.* **2004**, *282*, 825
46. Rastogi S.; Spoelstra A.B.; Goossens J.G.P.; Lemstra P.J.; *Macromolecules* **1997**, *30*, 7880.
47. Bambirra, S.; Leusen, van D.; Meetsma, A.; Hessen, B.; Teuben, J. H. *Chem. Commun.* **2003**, 522.
48. Gruter G. J. M.; Wang B. (DSM N.V. The Netherlands), *EP 1057837*, **2000**.
49. Rastogi, S.; Lippits, D.R.; Peters, G.W.M.; Graf, R.; Yao, Y.; Spiess, H.W. *Nature Mat.*, **2005**, *4*, 635.
50. Lippits, D.R.; Rastogi, S.; Höhne, G.W.M.; *Phys Rev Lett*, **2006**, *96*, 218303.
51. Lippits, D.R.; Rastogi, S.; Höhne, G.W.M.; Mezari, B.; Magusin, P.C.M.M. *Macromolecules*, **2007**, in press.
52. Lippits, D.R.; Rastogi, S.; Talebi, S.; Bailly, C. *Macromolecules*, **2006**, *Macromolecules*, **2006**, *39*, 8882
53. Lippits, D.R.; Rastogi, S.; Bailly, C. *To be submitted to Phys Rev. Lett* **2007**.
54. Lippits, D.R.; Yao, Y.; Rastogi, S.; Magusin, P.C.M.M.; *Manuscript in preparation*.
55. Rastogi, S.; Lippits, D.R.; Terry, A.E.; Lemstra, P.J. In Reiter G.(ed), Strobl G.(ed) *Progress in understanding of polymer crystallization*, Lecture Notes in Physics, Springer **2006**, 285.
56. Zhang, Q.; Lippits, D.R.; Rastogi, S.; Lemstra, P.J. *Macromolecules* **2006**, *39*, 658.
57. Zhang, Q.; Rastogi, S.; Chen, D.; Lippits, D.R.; Lemstra, P.J. *Carbon* **2006**, *44*, 778.
58. Rastogi, S.; Kurelec, L.; Lippits, D.R.; Cuijpers, J.; Wimmer, M.; Lemstra, P.J., *Biomacromolecules*, **2005**, *6*, 942.
59. Rastogi, S., Kurelec, L., Cuijpers, J., Lippits, D.R., Wimmer, M.A., Lemstra, P.J., *Macromol. Mater. Eng.*, **2003**, *288*, 964.
60. Duchateau, R; Garkhail, K.; Rastogi S.; Gruter G.J.M.; Lippits D.R., *Process for the preparation of a shaped part of an ultra high molecular weight polyethylene*, Patent: WO 2004113057 (2004)

Chapter 2

The formation of physical entanglements in an initially disentangled polymer melt

With the help of controlled synthesis, it is possible to obtain disentangled polyethylene crystals, which upon melting form an out of equilibrium disentangled melt. With time, this system will return to the equilibrium entangled state. Though initially, chain dynamics in the disentangled melt is faster than in the entangled melt, the time required to reach thermodynamic equilibrium scales as the reptation process of the corresponding fully entangled system (third power of molar mass). When probed by advanced NMR or rheometry, the observed times to reach equilibrium are distinctly different in value and scaling behavior. This difference is indicative of differences between the notions of local and segmental mobility probed by the two techniques in out of equilibrium situations, i.e. the formation of entanglements.

2.1 Introduction

Chain dynamics in polymer melts is a complex process. Using the concept of chain reptation introduced by de Gennes¹, Doi and Edwards² developed a theory to describe the experimental rheology of mono-disperse entangled polymer melts. The model reduces the intricate problem of topological constraints to the notion of a virtual tube. The tube provides a pathway for the chain dynamics and its diameter is defined from the constraints on the test chain by its neighbors. The constrained chain dynamics give rise to a characteristic time (τ_d), for a chain to diffuse one tube length. A salient feature of the theory is that it requires a very few parameters: the tube diameter, a (or equivalently the molecular weight between topological

Reproduced in part from:

Lippits, D.R.; Rastogi, S.; Talebi, S.; Bailly, C. *Macromolecules*, **2006**, *39*, 8882.

Lippits, D.R.; Rastogi, S.; Bailly, C. *Phys. Rev Lett.* in preparation.

constraints, M_e , or the plateau modulus G_N^0 and the monomeric friction coefficient $\zeta_0(T)$ (or equivalently $\tau_e(T)$ the characteristic relaxation time for a segment between two entanglements).

The average molecular weight between entanglements, $\langle M_e \rangle$, is inversely proportional to the entanglement density. It is related to the elastic modulus in the rubbery plateau region, G_N^0 according to:

$$G_N^0 = g_N \rho R T / \langle M_e \rangle, \quad (2.1)$$

where g_N is a numerical factor (1 or 4/5 depending upon convention), ρ is the density, R the gas constant and T the absolute temperature. From these basic concepts it appears that the plateau modulus is an intrinsic property as it arises from the elastic response of the entangled polymer melt. It is therefore independent of the total number of entanglements per chain, which increases with the molar mass.

In the solid state of a semi-crystalline polymer, as discussed in chapter 1, the distribution of entanglements can be highly heterogeneous, since entanglements are normally confined to the amorphous phase, whereas the crystal domains are void of them. Usually this heterogeneous distribution is lost upon melting, which causes an immediate entropy gain, and the entanglements are again uniformly distributed along the chain. So far studies have only been performed on such entangled melts. As was discussed in chapter 1, by control of polymer synthesis, it is possible to obtain disentangled crystals i.e. a single chain forming a single crystal.³ When such disentangled crystals are melted, the chains will tend to entangle to reach the thermodynamic equilibrium state, where the entanglements are homogeneously distributed and their density is constant.

The objective of this chapter is to compare the molecular dynamics of fully entangled and initially disentangled melts of UHMW-PE. This is made possible by the availability of UHMW samples with low polydispersity as well as disentangled nascent crystal samples. Two methods are used to probe molecular dynamics: rheology and solid state NMR and the results are compared. The chapter is organized in four corresponding sections and a conclusion.

2.2 Experimental

2.2.1 Materials

Entangled Polyethylene samples

Narrow distributed molecular weight polymers possessing a low polydispersity of approximately 1.1 (± 0.1) were kindly provided by Professor Bart Hossen of RU Groningen, NL.⁴ These polymers were synthesized using a homogenous, living Yttrium based catalyst. The samples and their basic characterization are reported in Table 2.1. Considering the high synthesis temperature and high catalyst activity, the samples are considered to be fully entangled.

Table 2.1 *Molecular properties and rheological characterization of the entangled Polyethylene samples.*⁴

	M_w [kg \cdot mol $^{-1}$] [*]	M_w/M_n	η_0 [Pa \cdot s] ^{**}
PE-1	430	1.2	5.5×10^5
PE-2	640	1.2	1.9×10^6
PE-3	850	1.2	4.5×10^6
PE-4	1200	1.1	1.6×10^7

^{*} The molecular weight is determined by size exclusion chromatography.

^{**} Rheological characterization is performed at 180 °C.

Nascent disentangled Polyethylene samples

As discussed in chapter 1, to obtain the desired disentangled crystals a simple concept is applied. The active sites of the catalyst are diluted to an extent that growing chains do not overlap in solution.³ Immediate crystallization upon polymerization is achieved by performing the synthesis at high supercooling. A single site catalyst in dilute solution is used to meet the requirements for “single chain forming single crystals”. A series of linear polyethylene samples described in Table 2.2 have been synthesized using this concept. The materials A-E have been synthesized by DSM research, Geleen,⁵ The Netherlands. For all samples 0.5 wt% Irganox is used to prevent oxidation. All GPC measurements have been performed in DSM Geleen, The Netherlands. The nascent disentangled samples are compared

with the fully entangled samples (obtained after leaving the samples for 4 hours in the melt) of the same grade.

Table 2.2 *Molecular properties and rheological characteristics of the nascent disentangled Polyethylene samples.*

	M_w [kg* mol ⁻¹]*	M_w/M_n	η_0 [Pa*s]**	Build-up time (s)**
A	90	1.4	1.3×10^4	120
B	380	2.6	6.0×10^5	200
C	800	1.8	2.9×10^6	600
D	1400	3.6	1.6×10^7	4000
E	3600	2.8	3.4×10^8	54000

*The molecular weight is determined by size exclusion chromatography.

**Rheological characterization is performed at 180°C. The buildup time will be explained the text.

2.2.2 Experimental techniques

Rheometry

Oscillatory shear and transient stress relaxation measurements in the linear viscoelastic regime have been performed on a Rheometrics ARES strain controlled spectrometer for a broad range of temperatures (140 °C-220 °C) angular frequencies ω (from 0.001 to 100 rad/s), and a constant strain of 0.5 %. It has been checked with the help of a strain sweep that at this strain level, the response of all samples is within the linear viscoelasticity regime (LVE). Due to high sample stiffness, a 8 mm parallel plate geometry is used with a sample thickness of 1 mm. The time-temperature superposition⁷ is applied at a reference temperature of 180 °C. For the high molar mass materials stress relaxation experiments have been performed to expand the time window of the measurements.

To follow the entanglements formation in the melt, the build-up (increase) of the plateau modulus with time is investigated via oscillatory shear measurements. Prior to measurements, the disentangled nascent powders listed in Table 2.2 are first sintered at 50 °C and 200 bars and the resulting disks of 8 mm diameter are heated fast (~ 30 K/min) to 180 °C in the

rheometer. A constant strain of 0.5 % is applied at a fixed angular frequency of 10 rad/sec or 100 rad/sec. The frequency is chosen to be in the plateau region of the fully entangled material. The change of the modulus is followed in time. As explained in the Appendix, special care has been taken to avoid experimental artifacts such as non-linear effects or slippage between the sample and sample holder.

Solid state ^1H NMR.

NMR experiments have been performed without sample rotation on a Bruker DMX spectrometer operating at a ^1H NMR frequency of 500 MHz and equipped with a special (2-mm MAS) probe head that resists temperatures above 150 °C. The transverse spin-spin relaxation time T_2 is measured using a Hahn echo pulse sequence; 90° - τ - 180° - τ -acquisition, with a variable τ time starting from $\tau = 2 \mu\text{s}$. The repetition time is 3 s. The transverse relaxation function is characterized by 60 data points at properly selected echo times. Temperature calibration is carried out by monitoring peak separation in the ^1H NMR spectrum of glycol and the melting-induced ^1H NMR line-narrowing of a series of compounds often employed for DSC calibration. ^1H NMR transverse relaxation functions are obtained from the total integral of the spectra after Fourier transformation, phase- and baseline correction.

To follow the formation of entanglements of the initially disentangled melt, the samples are pre-heated in a nitrogen-oven at 120 °C for 30 minutes. The hot samples are next transferred to the NMR spectrometer pre-heated to 160 °C and the measurement is started instantaneously. A pulse sequence with 8 different echo times is used to follow the time dependence of the transverse spin-spin relaxation at 5 minutes interval.

2.3 Results and discussion

2.3.1 Rheology of mono-disperse entangled high molecular weight polymers

In the LVE regime the basic reptation theory predicts the reptation time τ_d (and thereby the zero-shear viscosity η_0) to scale with chain length N as $\tau_d \sim N^{3.0}$. On the other hand, numerous experiments in the usual molecular weight range⁷ give $\tau_d \sim N^{3.4}$. The discrepancy from the power 3.0 dependence is usually attributed to “contour-length fluctuations” i.e. thermal fluctuations-driven stretching and contraction of the chain along the tube.⁸ Recently Vega et al., reported that relaxation times of different UHMW-PE possessing a narrow molecular weight distribution follow a viscosity power law close to 3.0 vs. molar mass.⁹ This is in agreement with the model of Milner and Mcleish,¹⁰ which predicts a crossover from exponent 3.4 to a 3.0 for very long chains. The crossover point is predicted¹⁰ to be at $(M_w/M_e =) 200$, i.e. 240.000 g/mol for polyethylene.¹¹ Experimentally Vega et al. have shown a

crossover at $440 \times M_e$ ($= 530.000$ g/mol in the case of linear polyethylene) but these experiments have been performed on samples possessing a polydispersity in the range of 2-3. Figure 2.1 presents the dynamic moduli of the entangled nascent samples described in table 2.1 which can be used as model grades.

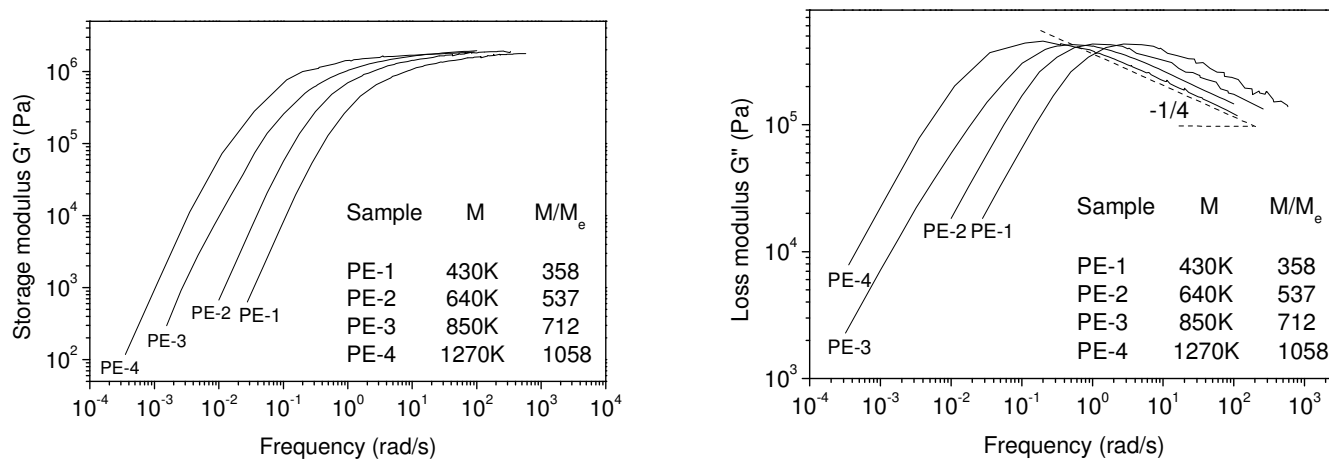


Figure 2.1: Storage modulus $G'(\omega)$ and loss modulus $G''(\omega)$ data of the narrow molecular weight polyethylenes listed in Table 2.1. A well developed plateau modulus is observed approaching 1.92 MPa. The loss modulus G'' in the high-frequency zone shows a characteristic power law with an exponent of $-1/4$.

A typical rheological response for narrow disperse samples, i.e. a sharp transition from the plateau region at high frequencies to the terminal region ($G' \propto \omega^2$, $G'' \propto \omega$) at low frequencies, is observed. A distinct rubber-plateau value of $G_N^0 = 1.92$ MPa is obtained for all samples. Using eq. 2.1, this result in a molecular weight between entanglements of 1200 g/mol, this is in agreement with earlier work.^{9,11} From Figure 2.1 it is evident that the loss modulus G'' in the high-frequency zone shows a characteristic power law with an exponent of $-1/4$. These observations are in agreement with the Milner and McLeish's contour length fluctuations theory.¹⁰ From the rheological data presented in Figure 2.1 the zero shear viscosity can be estimated using the equation $\eta_0 = \lim_{\omega \rightarrow 0} G^* / \omega$. Figure 2.2 shows the zero shear viscosity dependence on molar mass. The viscosity follows a pure reptation scaling (molar mass to the power 3.0) and disagrees with the more usual 3.4 exponent but is consistent with the Milner-McLeish model. For linear polyethylenes the crossover to pure reptation is expected around 240000 g/mol. The samples investigated have a molar mass greater than the anticipated crossover molar mass, and hence a slope of 3.0 is expected.

The reptation dominated $\omega^{-1/2}$ dependence anticipated between the maximum value of G'' and the fluctuations dominated $\omega^{-1/4}$ region is not observed, even for $M/M_e > 1000$. This interesting observation contradicts the predictions of the most recent tube models.

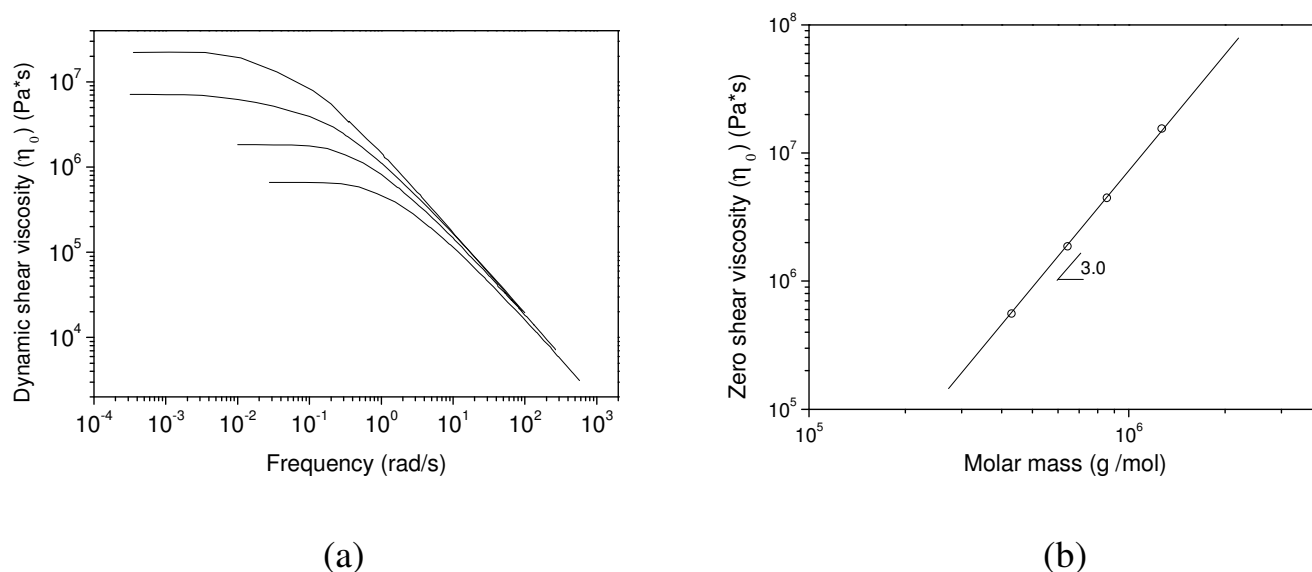


Figure 2.2: (a) *Dynamic viscosity as function of frequency for the fully entangled narrow molecular weight polymer melts listed in table 2.1 at 190 °C.* (b): *Zero-shear viscosity vs. molar mass. The data points for different molar masses are obtained by the extrapolation of the dynamic viscosity in Figure 2.2a to zero frequency. A slope of 3.0 is observed.*

2.3.2 Formation of entanglements in a disentangled polymer melt as probed by rheometry

To investigate the formation of entanglements in the melt from an initially disentangled sample, we use disentangled nascent crystals directly obtained by synthesis (see Table 2.2). Once the disentangled crystals are rapidly heated (~ 30 K/min) above the melting point, the chains are likely to adopt a random coil conformation following the reported “chain explosion” process.^{13,14} Immediately thereafter, the chains are essentially disentangled because the formation of entanglements unavoidably takes time. Indeed, immediately after melting a lower plateau modulus than expected (1.92 MPa) is observed. The low plateau modulus presumably reflects the low entanglements density according to eq 2.1 (which, is assumed to at least qualitatively hold in this non-equilibrium situation). With time, as chains tend to mix, entanglements formation should take place and should be reflected by an increase in modulus. Figure 2.3 summarizes a series of experiments showing a build-up of the modulus as function of time for different molar masses.

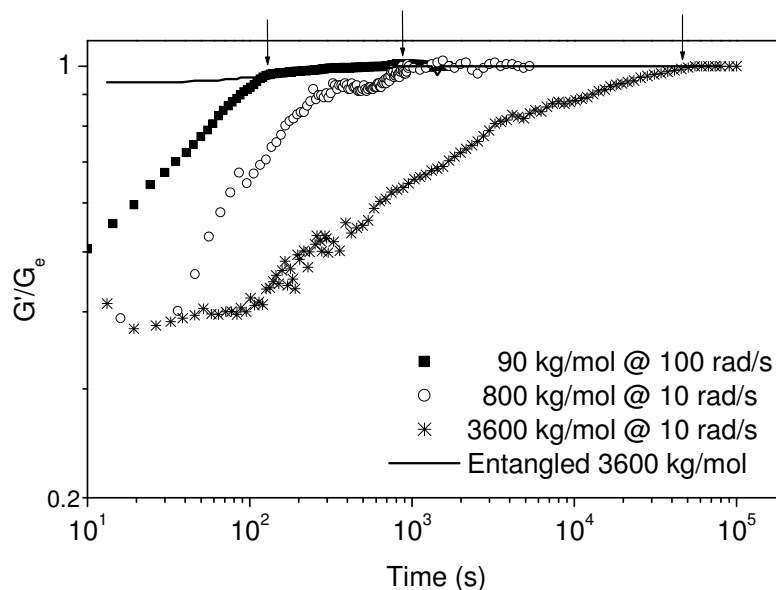


Figure 2.3: *Modulus build-up in initially disentangled polymer melts as a function of time. The measured plateau modulus (G') is normalized by the equilibrium plateau modulus (G_N) at the measurement frequency. Arrows in the figure correspond to the build-up time where $G'/G_N = 0.98$. For comparison, the corresponding entangled melt is also shown. The entangled melt is obtained after leaving the sample in the melt for 4 hours.*

During the modulus build-up, the melt is in a thermodynamically unstable state where the existing rheological concepts applicable to equilibrium melts are not valid. Ultimately, as the modulus reaches its asymptotic value, the chains return to the equilibrium state where de Gennes' tube is present and classical reptation takes place. It has to be noted that when a fully entangled sample of the same molar mass and molar mass distribution is melted under the same conditions, no such build-up of modulus is observed (see Figure 2.3).

The time required for the modulus build-up increases with the molar mass. From Figure 2.3, the build-up time (at 180 °C) can be approximately determined.¹⁵ Arrows in Figure 2.3 illustrate the time required for the modulus to reach 98 % of the asymptotic equilibrium value of the fully entangled melt. The build-up time vs. average molar mass is plotted in Figure 2.4. For molar masses with build-up time larger than the thermal stabilization time, the buildup time appears to scale as molar mass to the third power. The sample with the molar mass 90.000 g/mol falls off the curve but has to be discounted as the stabilization time for the temperature is longer than the time required for build up of the modulus.

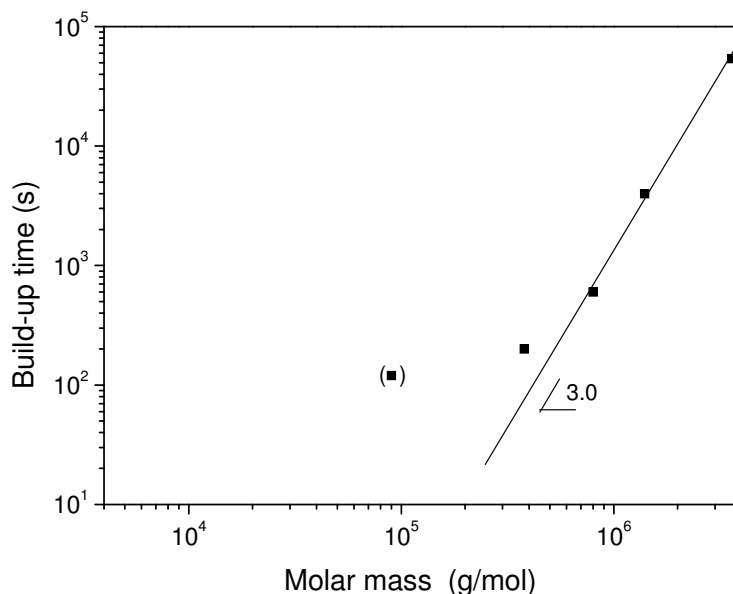


Figure 2.4: Data point represent build-up time obtained from the Figure 2.3 for a range of molar masses. When the build-up time is comparable with the time required reaching thermal equilibrium (< 200 s.), the data are not reliable.

Ultimately, the initially disentangled chains become a fully entangled thermodynamically stable melt. Frequency sweep measurements have been performed on these fully entangled samples. Figure 2.5, shows the corresponding dynamic viscosity vs. angular frequency for different molar masses. The unfilled symbols at low frequencies are determined by stress-relaxation experiments, which cover the very low frequencies inaccessible to the dynamic experiments. Extrapolation of the plateau to zero frequency yields the zero shear viscosity (η_0). The excellent overlap between the two types of measurements guarantees the accuracy of the extrapolated zero shear viscosity values.

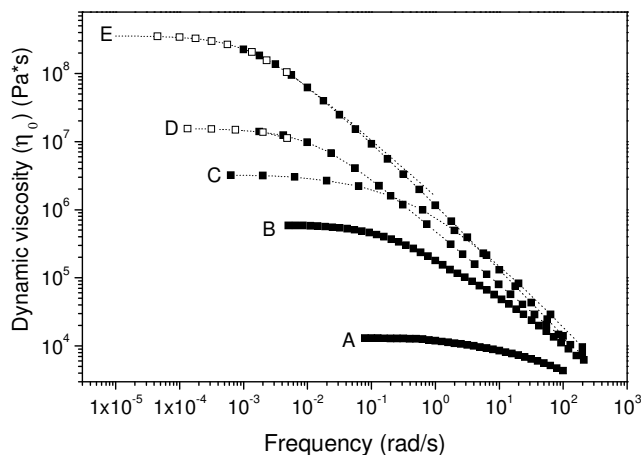


Figure 2.5

Figure 2.5: *Dynamic viscosity as function of frequency for the fully entangled polymer melts of different molar masses at 190 °C. Unfilled symbols in the figure represent the data points obtained from stress-relaxation experiments.*

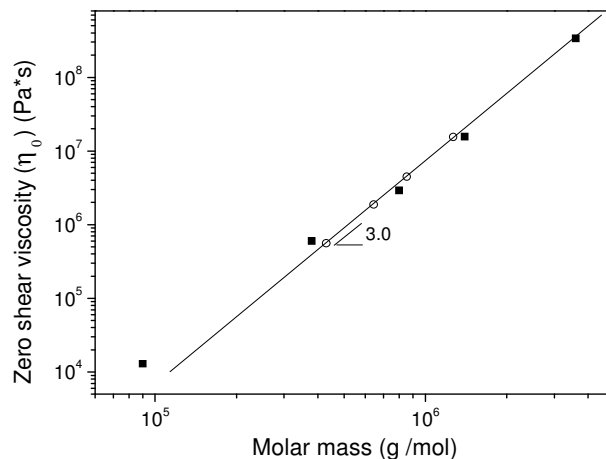


Figure 2.6

Figure 2.6: *Zero-shear viscosity vs. molar mass. The data points for different molar masses are obtained by the extrapolation of the dynamic viscosity in Figure 2.5 to zero frequency. A slope of 3.0 is observed. Unfilled symbols represent the narrow molar mass polyethylenes of Figure 2.2*

Similar to situation for the mono-disperse polyethylenes plotted in the Figure 2.2, the zero shear viscosity vs. molar mass curve plotted in Figure 2.6 shows a pure reptation scaling (molar mass to the power 3.0)

Figure 2.4 shows that the time required for the formation of entanglements scales as the third power of molar mass. To gain more insight in the mechanism of entanglements formation, we now compare the modulus buildup of a disentangled sample with the stress relaxation of the same sample when it is fully entangled. The unfilled symbols in Figure 2.7 represent the relaxed fraction as a function of time ($=1-G(t)/G_N^0$) obtained for a molar mass of 3.6 million g/mol (sample E in Table 2.2). The filled symbols in Figure 2.7 represent the modulus buildup of the initially disentangled melt for the same molar mass. Both curves are representative of chain dynamics in the initially disentangled and fully entangled environments, respectively.

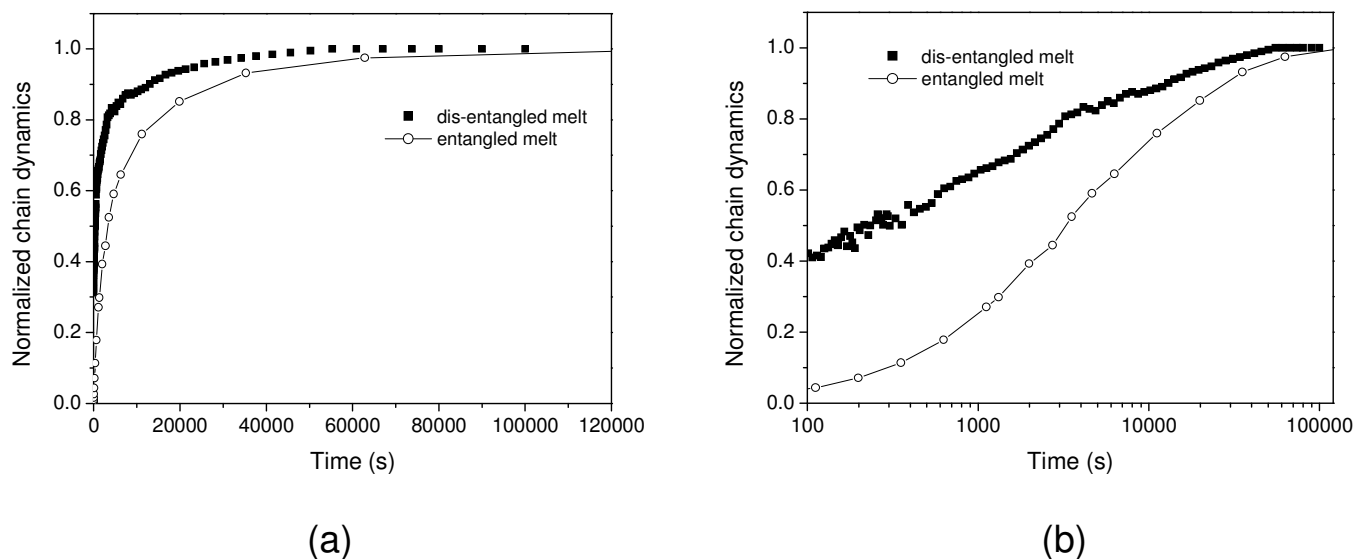


Figure 2.7: Chain dynamics of the disentangled and entangled melt state for a polymer of molar mass 3.6×10^6 g/mol at 180 °C. Chain dynamics of the disentangled melt state is represented as the normalized plateau modulus during the buildup phase ($G'(10 \text{ rad/s})/G_N^0$) (filled symbols). Chain dynamics of the entangled melt is obtained from a stress-relaxation experiment as the relaxed fraction ($1 - (G(t)/G_N^0)$) (open symbols). In the figure (a) the data are plotted on a linear scale and in figure (b) on a semi-log scale.

From Figure 2.7, it is evident that at all times, the modulus buildup is faster than the stress relaxation curve, highlighting faster chain dynamics of the disentangled sample. The two curves only merge at very long times of the order of 100.000 s. Since 200 seconds are required for stabilization of the rheometer, it is not possible to comment on the very early stages of modulus build-up.

The much faster initial chain dynamics of the disentangled sample than the dynamics of the corresponding entangled melt can be attributed to the lower amount of physical restrictions present in the disentangled melt state compared to the entangled melt. On the other hand, the convergence of the two curves at long times suggests that chain dynamics of the initially disentangled melt later on become dominated by chain reptation. To confirm this suggestion, the zero shear viscosity of different fully entangled samples (Figure 2.4) has been compared with the modulus buildup time (Figure 2.3). This is shown in Figure 2.8. A linear correlation is observed. From here can be concluded that the modulus build-up time of the disentangled samples scales as the reptation time of the corresponding fully entangled system. Whereas the initial stages of entanglement formation are fast and probably follow a different scaling, the later stages have to occur at the approximate rate of fully entangled melt reptation.

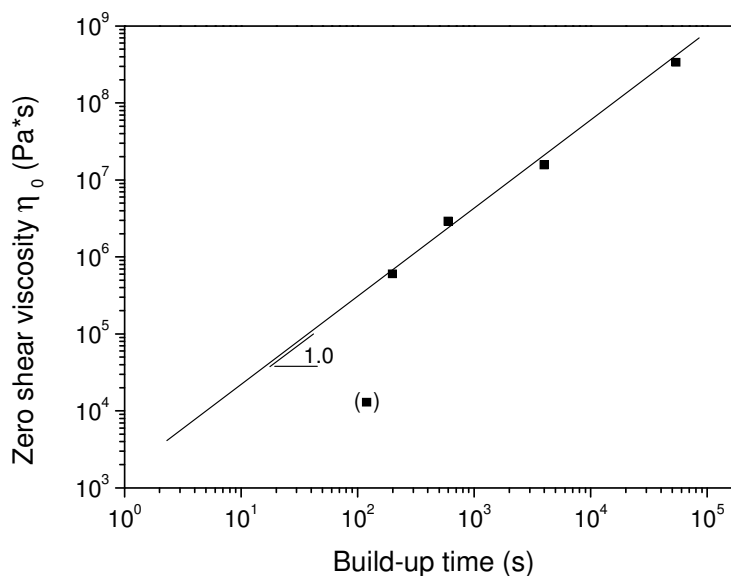


Figure 2.8: Correlation between chain dynamics of entangled and disentangled samples, represented by the zero shear viscosity and the modulus buildup time respectively, for the samples listed in Table 2.2.

To probe, detailed mechanisms involved in the entanglements formation of the disentangled melt at the initial stages, advanced NMR sensitive for local polymer chain dynamics is used. Prior to the NMR studies performed on the disentangled nascent samples described in table 2.2 the observation of the transverse spin-spin relaxation in the model entangled polymers summarized in table 2.1 is presented.

2.3.3 Transverse spin-spin relaxation of entangled mono-disperse high molecular weight polymers

Besides rheology, advanced NMR can be used as a sensitive probe for local chain dynamics to investigate detailed mechanisms of entanglements formation in the disentangled melts. Prior to the NMR studies performed on the disentangled nascent samples, first our observations about the transverse spin-spin relaxation in the model entangled polymers are described (table 2.1).

¹H NMR can be used to determine cross linking density in rubbers¹⁶⁻¹⁹ and entanglement density in polymers melts, respectively.²⁰⁻²² At $T \gg T_g$, the transverse spin-spin relaxation time T_2 of a polymer melt is very sensitive to the conformational mean position of the chains, which depend on the number of statistical segments between entanglements with lifetimes greater than 10^{-3} s. However, the shape of the transverse spin relaxation function can be complex. Brereton et al.²² have observed that for high molecular weights ($>3 \times 10^4$ g/mol) the

transverse spin relaxation function is decisively non-exponential and clearly reflects complex dynamics. In line with other groups^{23,24} they show that two parameters can be used to characterize the shape of these curves: T_2^* , the time for the relaxation to decay $1/e$ of its original value, and T_2' , the characteristic time constant to fit the tail of the function. T_2^* is mainly dominated by the amount of un-averaged dipolar coupling, whereas T_2' is affected by many variables such as free chains, chain ends and partially averaged dipolar coupling. Brereton et al. conclusively demonstrate that the actual shape of the transverse spin relaxation function can be described by theoretical calculations²⁵ based on two additional parameters: T_R and M_R , where T_R is a single relaxation time of an entangled chain segment of molecular weight M_R . For high molar masses ($>3 \times 10^4$ g/mol), the initial decrease of the relaxation function is largely independent of T_R and can be determined by the single parameter M_R . Therefore in the NMR transverse spin relaxometry experiments at $t \ll T_R$ the entanglements (with relaxation time T_R) are considered to be fixed in space.

Since the main goal of the present study is to use the transverse spin relaxation function as a tool for the physical interpretation of rheological data, we first discuss the transverse spin relaxation of the bulk. To correlate the influence of the number of entanglements per unit chain on the transverse spin relaxation, simple Hahn echo experiments are performed on the entangled mono-disperse polyethylene samples listed in table 2.1.

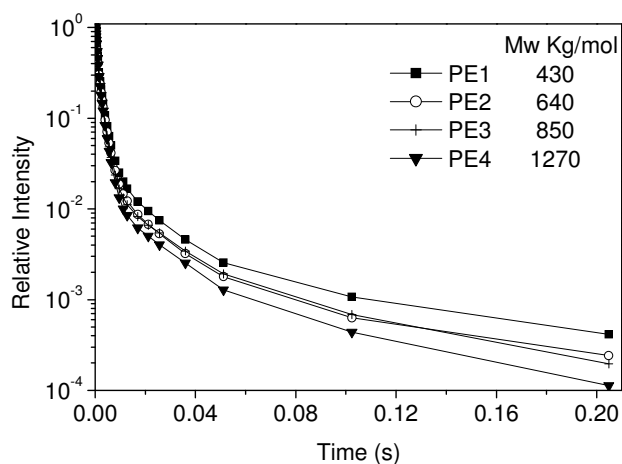


Figure 2.9

Figure 2.9: *Transverse spin relaxation curve of high molecular weight entangled mono-disperse polyethylenes at 160 °C, see table 2.1.*

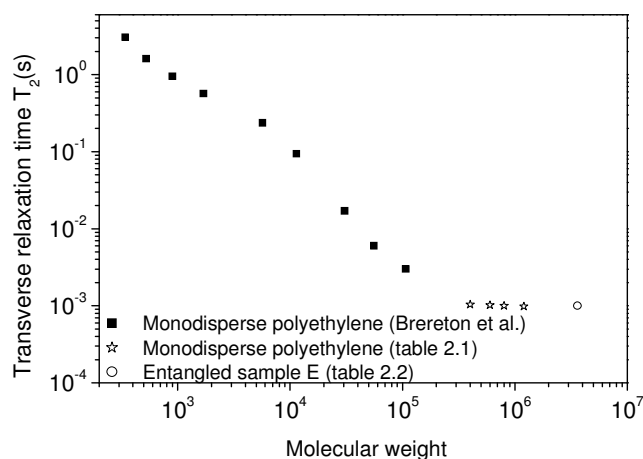


Figure 2.10

Figure 2.10: *Relationship between T_2^* and molar mass for fully entangled PE. T_2^* is obtained after fitting the initial decrease of the transverse spin relaxation function (Figure 2.9) with a single exponential decay. Filled symbols are obtained from ref 22. The behavior of sample E (table 2.2) after full entanglement is represented by the circle.*

Figure 2.9 shows that the initial decrease of the transverse spin relaxation curve of the samples listed in Table 2.1 is similar for all samples. Considering the high molar masses used in this study (ranging from 4×10^5 to 1.3×10^6 g/mol) and low polydispersity (1.1-1.2), it can be assumed that free disentangled chains possessing a molecular weight smaller than 2500 g/mol are negligible and the influence of chain ends on the bulk of the sample is small. Therefore the initial decrease (from 1 to 0.05) of the transverse relaxation curve is correlated to the entanglement network by a single exponential decay time (T_2^*) of approximately 1 ms. The determined relaxation time is independent of temperature in the measured temperature range of 145 °C to 170 °C for all samples.

In Figure 2.10 the determined relaxation time T_2^* is compared with the values obtained in previous studies.²²⁻²⁴ From the figure, it is evident that the initial transverse spin relaxation is sensitive to the molar mass up to approximately 2×10^5 g/mol. It can be assumed that beyond this molar mass the translational motion of chain segments is too slow to affect the transverse spin relaxation measurement and the number of chain ends is too small to have any effect on the transverse spin relaxation measurements of the bulk material. At these high molar masses T_2^* is dominantly sensitive to the entanglement density, which is an intrinsic property of polyethylene and independent of molecular weight. The minor differences in the tail of the transverse relaxation function can be related to the few chain ends present in the samples. A detailed discussion of these differences is out of the scope of the present study. It is to be noted that the molar mass of 2×10^5 g/mol observed as initiation point for the plateau region in Figure 2.10 is roughly similar to the molar mass for the crossover from the 3.4 to the 3.0 power law exponent for viscosity vs. molar mass, as described earlier in this chapter.

The T_2^* relaxation time of the high-temperature plateau (T_2^{pl}) can be correlated to the number of elementary chain units N_u between the network junctions^{16,17} by:

$$T_2^{pl} = a T_2^{rl} N_u / n_{ss} \quad (2.2)$$

Where a is molecular-structure specific constant ~ 6.2 for aliphatic polymers, and n_{ss} represents the number of elementary chain units per statistical segment in the Kuhn model, which for polyethylene is 9.25 CC bonds.²⁷ T_2^{rl} represents the decay time of the spin-spin relaxation in the rigid limit and is typically in the order of 13 μ s. The underlying assumption is that polymer motions are divided into fast and slow polymer motions at the 10^{-3} -s timescale without significant intermediate fraction. Using eq. 2.2 the molecular weight between entanglements for polyethylene is calculated to be 1.500 ± 300 g/mol. This value is in accordance with the value obtained from the rheological studies presented above (1.200 g/mol).

2.3.4 Formation of entanglements in the initially disentangled polymer melt as probed by solid state NMR

Experimental observations on the transverse spin-spin relaxation on the entangled polymer melts described in the section above will be applicable in our understanding of the entanglements formation in the disentangled nascent polymers (Table 2.2). To recall, rheology experiments presented above show; that upon melting of the disentangled nascent crystals (30 K/min), entanglements formation occurs with time. The initial stages of entanglements formation occurs fast, and at later stages the entanglements formation is correlated to the reptation time. To gain insight in the mechanism of the entanglements formation at the local scale, similar experiments on the disentangled samples are performed using advanced NMR spectroscopy. To probe the formation of entanglements in the initially disentangled melts, we use a Hahn echo pulse sequence. The Fourier transformed peak of the 8 echo times is integrated and the area of the peak is followed with time.

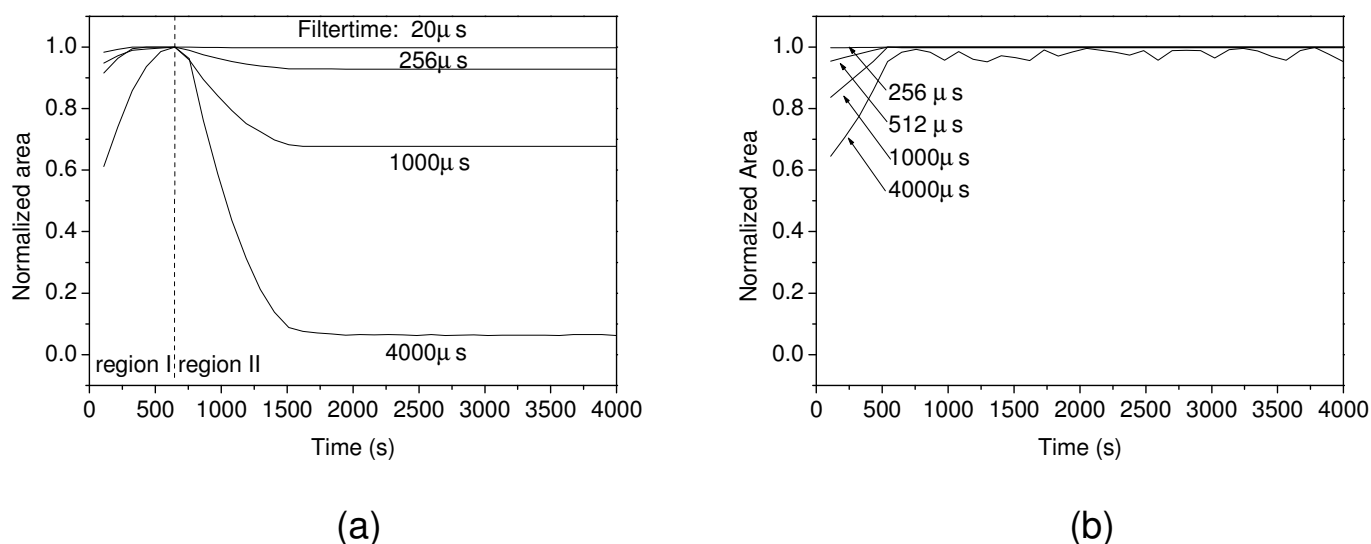


Figure 2.11: Normalized area of the NMR spectra peaks at 160 °C using different spin-echo filter times at 160 °C as a function of time of **a)** the initially disentangled sample E (3.6×10^6 g/mol) and **b)** the same sample after entanglement formation.

In the Figure 2.11a the normalized total integral of the spectra after Fourier transformation, phase- and baseline correction is plotted as a function of time for four different echo filter times for sample E (3.6×10^6 g/mol). In the region I ($0 < t < 700$ s) the areas of the four integrated peaks increase. This region corresponds to the time needed to reach thermal equilibrium. During this period, the sample melts and its temperature increases. Therefore the local mobility of the chains in the melt increases and hence the area of the integrated peak increases. This effect is best seen when using a T_2 -filter of 4000 μs, probing the more mobile

fraction of the sample. Similar results can be found when using the same procedure to melt an entangled sample of the same grade, as seen in Figure 2.11b.

In region II ($t > 700$ s), the peaks of the four different filter times are constant as a function of time in the case of the entangled sample (Figure 2.11b). In contrast, for the initially disentangled sample the peak area changes with time, irrespective of filter time. The most striking change is seen in the peak area of the highest T_2 -filter time of $4000 \mu\text{s}$. Applying this filter, the less-mobile fractions of the melt are suppressed, while the local mobility is highlighted. Thus a decrease in the peak area can be related to a decrease in the local mobility of the melt. By comparison with the rheological studies presented above, this decrease in the local mobility must be related to the formation of entanglements. After 1750 s changes in the peak areas are no longer seen. After the experiment, the transverse spin relaxation of the initially disentangled sample is characterized by a Hahn spin-echo experiment using 60 echo times at 160°C . No differences are observed between the fully entangled and the initially disentangled sample.

The spin-echo experiments on disentangled samples are repeated for all molar masses described in Table 2.2. Figure 2.12 shows the results and compares them with the corresponding rheology build-up times.

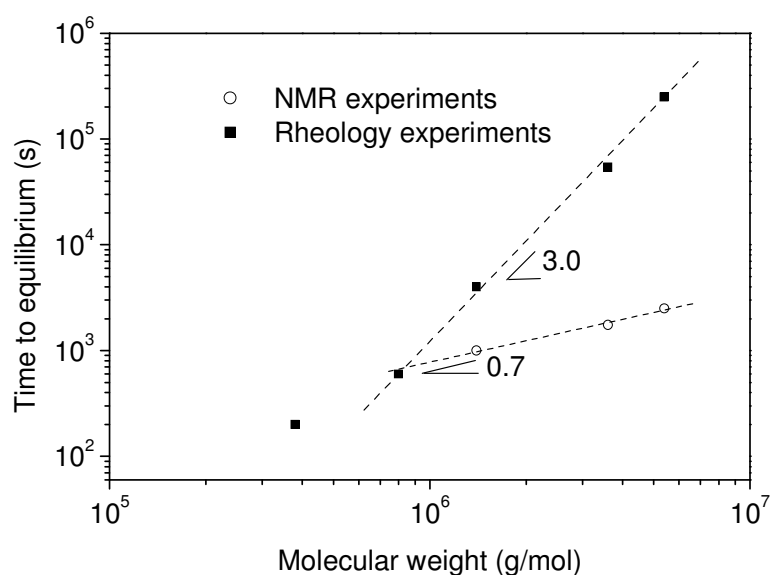


Figure 2.12: Time to reach equilibrium of the T_2 relaxation using ^1H NMR (Figure 2.11) compared to the time required to reach the equilibrium plateau modulus in the rheology experiments (Figure 2.4) for the nascent disentangled samples.

Unlike the $M^{3.0}$ scaling for the plateau modulus build-up, the time to reach equilibrium of the spin-spin relaxation scales with molar mass as $M^{0.7}$ (Figure 2.12). Furthermore in the NMR experiments, the time required to reach the equilibrium of the T_2 relaxation is considerably

shorter than the time required for the modulus build-up in the rheology experiments. This suggests that the restriction in the local mobility probed by the T_2 relaxation is realized much earlier than the restriction in the stress relaxation arising from the formation of entanglements as probed by the rheology experiments.

For instance, for the 3.6×10^6 g/mol sample (Figure 2.11) the time required for T_2 to reach its equilibrium value is 1750 s, whereas the time required for the modulus to reach the equilibrium value is 50000 s. This suggests that after 1750 s, while the melt probed by T_2 relaxation experiments is fully entangled, the same melt probed by rheology is still partially disentangled. These findings clearly suggest that the two different techniques used for probing the entanglements formation explore the dynamics on a different length scale.

The T_2 relaxation time is sensitive to the conformational mean position of the chains, which depends on the number of statistical segments between entanglements. When contact points are formed with lifetimes greater than 10^{-3} s, chain interactions are effective in restricting the local mobility as seen by NMR. On the other hand, the rheological measurements probe the stress relaxations of topological constraints on longer time scale. In equilibrium melts contact points and topological constraints are considered to be the same (i.e. entanglements), however in the case of an out of equilibrium situation differences can be observed.

Similar differences between contact points and topological constraints as is obtained by solid state NMR and rheometry have been reported for cross-linked rubbers^{28,29} In these studies, using a series of samples with varying cross linking density, no distinction could be made by NMR between permanent chemical crosslinks and temporary or trapped chain entanglements, without swelling the samples. On the other hand, rheology experiments were able to make a distinction between permanent and temporary entanglements.

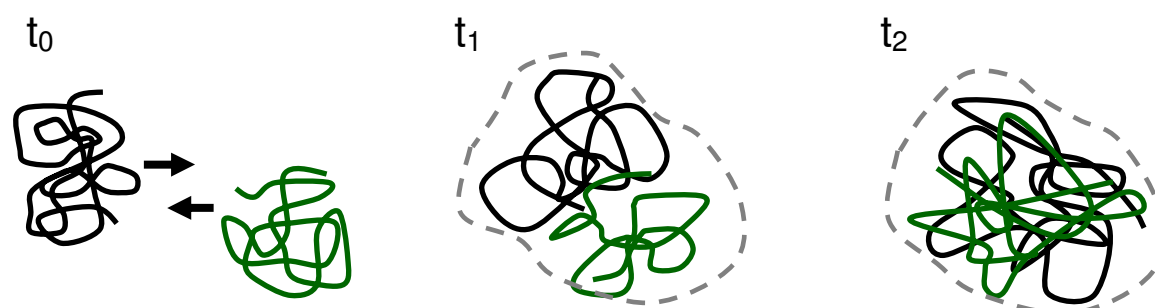


Figure 2.13: Schematic picture of entanglement formation adapted from reference 30, 31. Two disentangled chains (t_0) first diffuse into one another and the number of contact points increase (t_1). From here the chains now become increasingly entangled (t_2). For the sake of clarity only two chains are pictured.

For the formation of entanglements in the initially disentangled melt, it is therefore hypothesized that; in order to effectively entangle the two separated disentangled chains, the chains first need to come into contact. This process is relatively fast since ideally the

disentangled chains can follow Rouse motions. This hypothesis is pictured after Graessly,³¹ in Figure 2.13. After a given time (t_1) considerable overlap of the chains occurs and the local mobility of the test chain is restricted by the interaction with the other chains. (i.e. the T_2 relaxation time reaches the equilibrium value) The weak molecular time dependence of the time t_1 of $M^{0.7}$ is not in accordance with a disentangled Rouse chain (M^2) therefore the time t_1 is related to form contact points not to the diffusion of the whole chain but to the diffusion of a part of the chain.

Beyond $t=t_1$, the test chain that interacts with the neighboring chains, entangles to an extent that the segmental mobility is restricted. In rheology this is seen as an increase in modulus.

At $t=t_2$ the modulus reaches the equilibrium value 1.92 MPa associated to a fully entangled state.

2.4 Conclusion

From the rheology experiments presented above it can be inferred that, when nascent disentangled UHMW-PE is molten, the modulus build-up time of the disentangled samples scales as the reptation time of the corresponding fully entangled system. Though the initial stages of entanglements formation are fast and probably follow different scaling, at the later stages once the entanglements are formed chains tend to reptate following the classical concepts. Using advanced NMR, details in the entanglements formation mechanism of the disentangled melt at the initial stages is elucidated. The time required for the entanglements formation when probed by NMR using T_2 relaxation is shorter than the time required for the modulus build-up in the rheology experiments. This suggests that the restriction in the local mobility probed by the T_2 relaxation is realized much earlier than the restriction in the segmental mobility arising from the formation of entanglements as probed by the rheology experiments. These experiments suggest that with the interaction of the disentangled test chain with its neighboring chains, restrictions in the conformation arise, which is probed by NMR. Restrictions thus developed at the local length scale, promote the chain reptation, which is required to form an equilibrium entangled melt as envisaged by the classical theories.

2.5 References

1. de Gennes P.G., *Scaling Concepts in Polymer Physics* **1979** (Cornell University Press, Ithaca, NY).
2. Doi M.; Edwards S.F., *The Theory of Polymer Dynamics* **1986** (Clarendon Press, Oxford,).
3. Rastogi S.; Lippits D.R.; Peters G.W.M.; Graf R.; Yao Y.; Spiess H.W.; *Nature Mat.* **2005**, *4*, 635.
4. Bambirra, S.; Leusen, van D.; Meetsma, A.; Hessen, B.; Teuben, J. H. *Chem. Commun.* **2003**, 522.
5. Gruter G. J. M.; Wang B. (DSM N.V. The Netherlands), *EP 1057837*, **2000**.
6. Talebi S. *Paper in preparation*
7. Ferry, J.D. *Viscoelastic Properties of Polymers* **1980**, John Wiley & Sons: Toronto.
8. Doi M. *J. Polm. Sci. Ed.* **1983**, *21*, 667.
9. Vega, J.F.; Rastogi S.; Peters G.W.M.; Meijer, H.E.H. *J. Rheol.* **2004**, *48*, 663.
10. Milner S.T.; McLeish T.C.B.; *Phys. Rev. Lett.* **1998**, *81*, 725.
11. Fetters, L.J.; Lohse, D.J.; Richter D.; Witten, T.A.; Zirkel *Macromolecules* **1994**, *27*, 4639.
12. Likhtman, A. E.; McLeish T.C.B.; *Macromolecules* **2002**, *35*, 6332.
13. Barham, P.; Sadler, D.M. *Polymer* **1991**, *32*, 393.
14. Lippits D.R.; Rastogi S.; Höhne G.W.M.; *Phys Rev Lett* **2006**, *96*, 218303.
15. It is to be noted that since the glass transition temperature of linear polyethylene is below -100°C, any changes in the chain dynamics due to a shift in the experimental temperature +/- 20°C hardly causes substantial changes.
16. Fry C.G.; Lind A.C. *Macromolecules* **1988**, *21*, 1292.
17. Gotlib Y.Y.; Lifshits M.I.; Shevelev V.A.; Lishanskii I.A.; Balanina I.V. *Poly Sci USSR* **1976**, *18*, 2630.
18. Litvinov V.M.; Barendswaard W.; van Duin M. *Rubber Chemistry and Technology* **1998**, *71*, 105.
19. Orza R.A.; Magusin P.C.M.M.; Litvinov V.M.; van Duin M.; Michels M.A. *Macromol. Symp* **2005**, *230*, 144.
20. Cosgrove, T.; Turner, M. J.; Griffiths, P. C.; Hollingshurst, J.; Shenton, M. J.; Semlyen, J. A. *Polymer* **1996**, *37*, 1535.
21. Guillermo, A.; Addad, J-P. C; Bytchenkoff, D. *J. Chem. Phys.* **2000**, *113*, 5098.
22. Brereton M.G.; Ward I.M.; Boden N.; Wright P. *Macromolecules* **1991**, *24*, 2068.
23. Fleisher, G. *Colloid Polym. Sci.* **1987**, *265*, 89.
24. Kimmich, R.; Koch, H. *Colloid Polym. Sci.* **1980**, *258*, 261.
25. Brereton M.G. *Macromolecules* **1990**, *23*, 1119.
26. Saalwachter K. *J. Chem. Phys.* **2004**, *120*, 454.
27. Fetters, L.J.; Lohse D.J. Greassley W.W. *J. Polym. Sci. Part B* **1999**, *37*, 1023.
28. Litvinov V.M.; Barendswaard W.; van Duin M. *Rubber Chem. and Tech.* **1998**, *71*, 105.
29. Orza R.A.; Magusin P.C.M.M.; Litvinov V.M.; van Duin M.; Michels M.A.J. *in preparation* **2007**.
30. Makosco C.W. *Rheology principles, measurements, and applications.* **1994** (Wiley, Toronto).
31. Graessley W.W *Adv. Polym. Sci.* **1974**, *16*, 1.
32. de Gennes P.G. *C.R. Acad.Sci. Paris*, **1995**, *321*, 363.

Chapter 3

Melting kinetics in polymers; The role of entanglements in the amorphous phase

In the previous chapter it is shown that entanglements present in the amorphous phase of the semi-crystalline polymer can be controlled by synthesis.¹⁻³ Ultimately, it is possible to obtain nascent disentangled polyethylenes, which on melting form a initially disentangled melt. Chains in the disentangled melt tend to entangle with time. A homogeneous distribution of the entanglements occurs instantaneously on melting of the entangled nascent semi-crystalline polyethylene. From the thermal analysis and solid state NMR studies reported in this chapter, it is apparent that the melting temperature and melting process of crystal depends on the topological constraints present in the amorphous phase of the semi-crystalline polymer. Contrary to the melt-crystallized sample, the nascent entangled or disentangled UHMW-PE powders melt close to the equilibrium melting temperature. A distinction in the melting process of the entangled and the disentangled nascent polyethylenes becomes apparent on annealing just below the equilibrium melting temperature. On annealing of the disentangled nascent UHMW-PE, melting occurs by simple consecutive detachment of chain segments from the crystalline substrate. However, complication in the melting process of the entangled UHMW-PE arises, when the chain in the process of detachment from the surface is shared between different crystals. Experimentally, a clear distinction in the different melting processes is observed, by the differences in the activation energies required for the consecutive detachment of chain stems or of the chain segments having topological constraints. The consecutive detachment of chain stems starts at the melting temperature predicted from the Gibbs-Thomson equation, whereas higher temperature or time is required if the chain has to overcome the constraints. The consecutive detachment of chain stems from the crystal lattice results into the evolution of a 'heterogeneous melt' state having two different segmental mobilities.

3.1 Introduction

Melting of solids can be described using a thermodynamic approach, where the melting temperature is defined as a first-order transition at the intersection of the Gibbs free energy of

Reproduced in part from:

Lippits D.R.; Rastogi S.; Höhne G.W.M.; *Phys Rev Lett* **2006**, 96, 218303 .

Lippits D.R.; Rastogi S.; Höhne G.W.M.; Mezari B.; Magusin P.C.M.M. *Macromolecules* **2007**, in press.

the solid and liquid state. The transition temperature is then fixed as long as both phases coexist. However, the thermodynamic approach starts from equilibrium conditions and infinite sizes of both phases. For polymers these conditions are not fulfilled; there is no equilibrium, crystallization is not complete and the crystal size is finite. Many semi-crystalline polymers form lamellae crystals, which are 10-30 nm thick and at least one order of magnitude larger in the lateral direction.^{4,5} The melting transition is not sharp but covers a certain temperature range that is correlated to the thickness distribution of the lamellae, which has been quantitatively described by the Gibbs-Thomson equation.⁶

$$T_m = T_m^\infty \left[1 - \frac{2\sigma_e}{l \cdot \rho \cdot \Delta H_m} - \frac{2\sigma}{A \cdot \rho \cdot \Delta H_m} - \frac{2\sigma}{B \cdot \rho \cdot \Delta H_m} \right] \quad (3.1)$$

where T_m is the experimentally determined melting point, T_m^∞ is the equilibrium melting point for infinite perfect crystals (141.5°C for polyethylene⁷), σ_e is the surface free energy of the fold planes, σ is the surface free energy of the lateral planes, l is crystal thickness in the chain direction (fold length), ΔH_m is the heat of fusion, A and B are the lateral crystal dimensions and ρ is the crystal density. Normally, the last two terms are ignored due to relatively large lateral dimensions of the melt and/or solution-crystallized samples (in the order of a few microns) and consequently the melting temperature is only related to the lamellar thickness, l . If l approaches infinity, T_m approaches T_m^∞ , which is the equilibrium melting temperature. This classical thermodynamic approach is sufficient to correlate the crystal dimensions of melt-crystallized ultra high molecular weight polyethylene (UHMW-PE) having molar mass greater than a million to the melting point of 135 °C.

However melting in semi-crystalline polymers can be highly complicated. Depending on the reorganization process of the amorphous and crystalline regions, which are connected by chains, the heating rate dependence on the melting temperature can be either positive or negative. For polymers where crystal thickening and/or crystal perfectioning is feasible, the measured melting temperature increases with decreasing heating rate.⁸ On the other hand, in polymers where no such reorganization occurs (e.g. extended chain crystals), the measured melting temperature decreases with decreasing heating rate. The increase of the melting temperature with increasing heating rate is attributed to superheating, as well as thermal lag.⁹

Other complications in the melting of semi-crystalline polymers arise from the experimental observations that melting temperatures of the solution, nascent and melt-crystallized samples of the same polymer having approximately the same crystal thicknesses, are distinctly different. For example, on heating at 10 K/min, nascent UHMW-PE melts around 141 °C, close to the reported equilibrium melting temperature for polyethylene of 141.5 °C; such a high melting

point normally found for “chain-extended” polyethylene crystals which are extremely thick (>1 μm) has been a subject of debate. Using electron microscopy and DSC, Engelen¹⁰ et al. conclusively showed that the nascent crystals are folded chain crystals. Thus the high melting temperature was attributed to fast reorganization leading to successive thickening prior to melting. However, no experimental evidence of successive thickening was provided. On the contrary, Kurelec et al. showed that even on annealing close to the melting point for several hours the thickness of these nascent crystals do not exceed a value of 26 nm.^{11,12} The melting temperature predicted from Gibbs-Thomson equation for polyethylene⁷ [$T_m = 414.2 - 259.7/l$] for a lamella thickness of 26 nm is 131 °C.¹³ Furthermore, the high melting temperature of 141 °C, is lost on second heating, where a melting temperature of 135 °C is measured.¹⁰ A similar discrepancy is observed between the first and second heating run of solution-crystallized UHMW-PE, where the lamellae double their initial thickness upon annealing below the melting temperature to a maximum of 25 nm.¹⁴ The melting temperature predicted from the Gibbs-Thomson equation for a lamella thickness of 25 nm, 131 °C, is 5 °C lower than the experimentally observed melting point of 136 °C. Furthermore, the high melting temperature of 136 °C, is lost on second heating where a melting temperature of 131 °C is measured, which now coincide with the prediction of the Gibbs-Thomson equation.

The melting aspects involved in nascent, melt- and solution-crystallized polymers cannot be explained by existing thermodynamic concepts. In this chapter, time as well as the temperature required for melting of ultra high molecular weight polyethylene (UHMW-PE) is correlated to the chain topology in the amorphous interphase. The introduced kinetic aspect of melting is probed by different experimental techniques; Differential Scanning Calorimetry (DSC), Temperature Modulated Differential Scanning Calorimetry (TM-DSC), Rheometry and solid-state ¹H NMR relaxometry. The key observation is that at sufficiently low heating rates disentangled nascent polyethylene melts at lower temperatures than observed in normal heating runs.¹⁵ The lowest temperature where melting is observed, corresponds to the value predicted by the Gibbs-Thomson equation. This point out the influence of the topological constraints in the amorphous phase on the melting of the crystalline regions in the semi-crystalline polymer.

3.2 Experimental Section

3.2.1 Materials

To correlate the melting behavior of UHMW-PE to the chain topology, four different samples are used as described in Table 3.1. The nascent grades differ in synthesis conditions and catalyst type. The nascent entangled sample is a commercial grade of Montell (1900CM)

synthesized with a heterogeneous Ziegler-Natta catalyst. The nascent disentangled grade is provided by DSM (The Netherlands) synthesized at temperatures below the dissolution temperature using a homogeneous metallocene catalyst.

Tensile testing is used to investigate drawability of the materials. In our definition drawable materials (>150 times) are “disentangled” and not-drawable (<7) materials are “entangled”.

Table 3.1 *Molecular properties of the UHMW-PE samples*

	M_w ($g^* mol^{-1}$)	M_w/M_n	Melting point on first heating	Draw ratio at 120°C
Nascent, Entangled (<i>commercial grade</i>)	4.5×10^6	8	141°C	7
Nascent, Disentangled	3.6×10^6	2.8	141°C	>150
Solution Crystallized	4.5×10^6	8	136°C	>150
Melt Crystallized	4.5×10^6	8	135°C	7

3.2.2 Experimental techniques

Differential scanning calorimetry (DSC)

DSC has been performed using a standard Perkin-Elmer DSC-7. Samples of 0.7-2.0 mg mass are weighed with a precision balance and encapsulated in standard (crimped) aluminium pans of known mass. An identical empty pan is used as a reference. Nitrogen is purged at a rate of 25 ml/min. DSC is calibrated using indium and tin.

Tensile Testing.

For draw ratio determination dumb-bell-shaped samples having a gauge length of 10 mm and a width of 0.5 mm is used. The samples are drawn in the solid-state at a crosshead speed of 50 mm/min at 125 °C. The draw ratio is determined by measuring the separation of the ink marks prior and after the deformation.

Rheometry

Oscillatory shear measurements in the linear viscoelastic region are performed using an Advanced Rheometrics Expansion System (ARES). Measurements are carried out using parallel plate geometry (8 mm diameter) at constant temperature of 134 °C below the peak melting point in the nitrogen atmosphere. Elastic modulus is followed as a function of time at

a constant frequency of 10 rad/s, at a constant strain of 0.5 %. Before measurements the samples are heated with 1 K/min from 120 °C to 134 °C. The pre-melting of the polymer is used to achieve good adhesion between the sample and the plates. To monitor any slippage between the plates and the polymer an oscilloscope is attached to follow any changes in the applied strain. More detailed information of the experimental rheology of UHMW-PE can be found in the Appendix.

Temperature Modulated Differential scanning calorimetry (TM-DSC)

TM-DSC has been performed using a standard Perkin Elmer DSC-7 apparatus modified for temperature modulation.¹⁶ For the TM-DSC measurements an underlying heating rate of 0.5 K/min is used, which is low enough to ensure good linearity and stability during measurements. The time dependent temperature-modulated measurements are performed in quasi-isothermal mode at different temperatures (110 °C, 120 °C, 130 °C, 135 °C, 136 °C, 137 °C and 138° C) at a frequency of 12.5 mHz. The temperature amplitude T_A of 53 mK is kept low enough to ensure a linear response. Before evaluation, the empty pan run (taking the same measuring parameters and phase position) is subtracted from the curve of the sample to reduce surroundings and apparatus influences. The measured (modulated) heat flow rate signal $\Phi(T,t)$ consists of two parts: The underlying part $\Phi_u(t)$ and the periodic part $\Phi_{per.}(T,t)$. Gliding integration over one period provides the underlying part $\Phi_u(t)$ which, when subtracted from the total measured signal, yields the periodic part $\Phi_{per.}(T,t)$. The apparent heat capacity is calculated using a mathematical procedure described in reference 24.

Solid state ¹H NMR

NMR experiments are carried out without sample rotation on a Bruker DMX spectrometer operating at a ¹H NMR frequency of 500 MHz and equipped with a special (2-mm MAS) probe head that resists temperatures above 150 °C. The transverse relaxation time T_2 is measured using a two pulse sequence $90^\circ-\tau-180^\circ-\tau-aq$ with a variable τ time starting from $\tau=2 \mu s$. The 90° pulse length was $5 \mu s$ and the repetition time was 3 s, which proved long enough for quantitative measurements. The relaxation decay is characterized by 60 data points at properly selected echo times. This pulse sequence is chosen because it offers the possibility to both qualitatively as well as quantitatively analyse relaxation of the amorphous and crystalline components. Temperature calibration is carried out by monitoring peak separation in the ¹H NMR spectrum of glycol and the melting-induced ¹H NMR line-narrowing of a series of compounds often employed for DSC calibration. ¹H NMR spin-spin relaxation decays are obtained from the total integral of the spectra after Fourier transformation, phase- and baseline correction. The relaxation decay is analyzed by a non-linear least-square fitting. The relaxation times are determined by fitting the relaxation data with a sum of two or three exponentials. From the determined relaxation times below the melting point appropriate τ -delay times are chosen for real-time monitoring of the T_2

relaxation by 8 data points. In this way it is possible to follow the changes in the sample with 5 minutes intervals.

3.3 Results and discussion

3.3.1 First Melting Point of UHMW-PE

Figure 3.1 shows a standard DSC run performed at 10 K/min on the entangled and disentangled nascent UHMW-PE. The observations are that, independent of the synthesis route, no differences in the melting peak, onset and end temperatures exist, though the polydispersity and the topological constraints present in the amorphous phase (estimated by differences in the drawability of the two samples in the solid state^{1,2} and the different entanglement density upon melting, Chapter 2) provided during synthesis of the two samples are different.

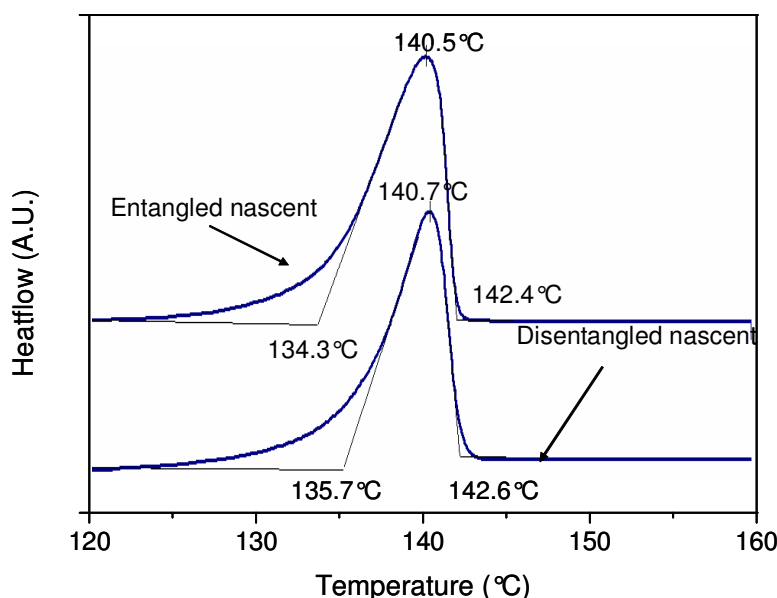


Figure 3.1: DSC curves obtained on heating the nascent entangled and the nascent disentangled samples at 10 K/min. Independent of the synthesis route the peak melting temperature of the polymer melts around 140.5 °C, close to the equilibrium melting point of the linear polyethylene.

The observed high melting point of 141 °C of the nascent powders is 5-6 °C higher than for melt-crystallized UHMW-PE.¹⁸ In the heating rate region of 20 to 0.1 K/min, a non-linear relationship between the peak temperature and the heating rate of entangled and disentangled nascent UHMW-PE polymer is observed. However, similar to the observations reported by Toda et al,⁹ the melting temperature, plotted vs. the heating rate to the power 0.2, shows a linear relationship (Figure 3.2). The ‘true’ melting temperature is determined by extrapolation to zero heating rate. The shift in the observed melting temperature at nonzero heating rates is

attributed to “superheating”. This superheating is caused (i) by thermal inertia (the transport of heat from the heater to the sample) and (ii) by a time dependence of the melting process. Adopting this existing knowledge, the extrapolated, “true” melting temperature for these nascent polymers is 138.4 °C and 138.2 °C for the disentangled and entangled samples, respectively (Figure 3.2).

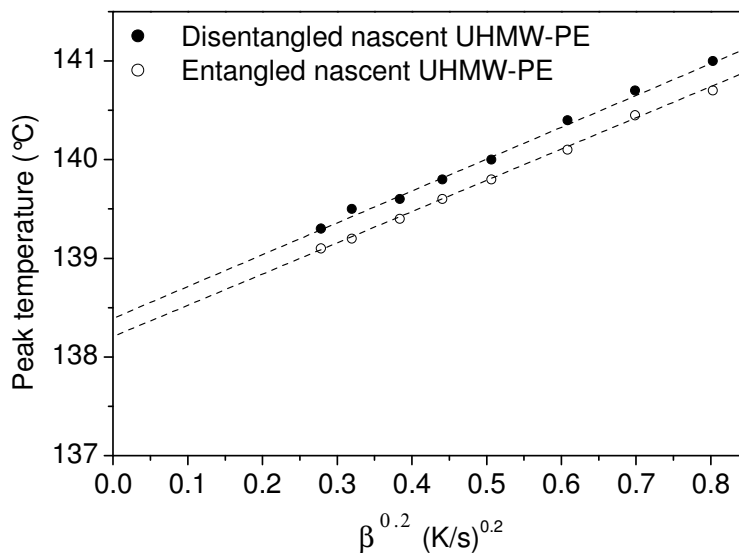


Figure 3.2: The measured melting peak temperatures for entangled and disentangled nascent UHMW-PE at different heating rates β . The non-linear abscissa allows extrapolation to zero heating rate. The extrapolation is needed to determine the “true” melting temperature. From the slope superheating can be determined.⁹

Corresponding to the mentioned Gibbs-Thomson equation this melting temperature belongs to a crystal thickness of approximately 100 nm.¹⁹ However, the experimental observations are that the crystals do not thicken more than to a maximum 26 nm even when the sample is left to anneal for several hours at 120 °C,^{11,12} distinction between the nascent entangled and nascent disentangled polymers starts to feature with decreasing heating rates below 1 K/min.

3.3.2 Melting kinetics in UHMW-PE as probed by DSC

Figure 3.3 shows that on decreasing the heating rate to 0.1 K/min during the first heating of the nascent disentangled UHMW-PE, a second peak at lower temperature appears, whereas in the nascent entangled UHMW-PE a single peak is observed. These findings suggest the influence of topological constraints present in the amorphous phase on the melting behaviour of polymer crystals. To get more insight in this melting mechanism, annealing experiments below the “true” melting point of 138.4 °C (determined from Figure 3.2) are performed.

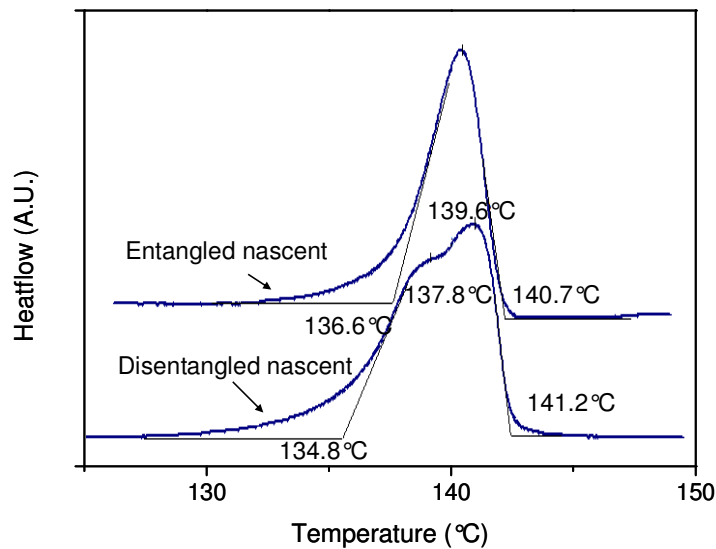


Figure 3.3: Heating of the nascent entangled UHMW-PE and the nascent disentangled UHMW-PE at 0.1 K/min. On slow heating; a second melting peak appears in the disentangled nascent sample.

Using differential scanning calorimetry (DSC), the sample is kept for a certain time at annealing temperatures ranging from 132 °C to 139 °C. Next to the annealing at the requisite temperature, the sample is cooled to room temperature and reheated (at 10 K/min) to 150 °C. On re-heating, two melting peaks are observed at 135 °C and 141 °C, respectively (Figure 3.4). The peaks are associated with the melting of material re-crystallized during cooling from the annealing temperature (peak at 135 °C), and crystal domains in the initial nascent state (peak at 141 °C), respectively. The ratio between the areas of the two peaks changes with the annealing time at the given annealing temperature.

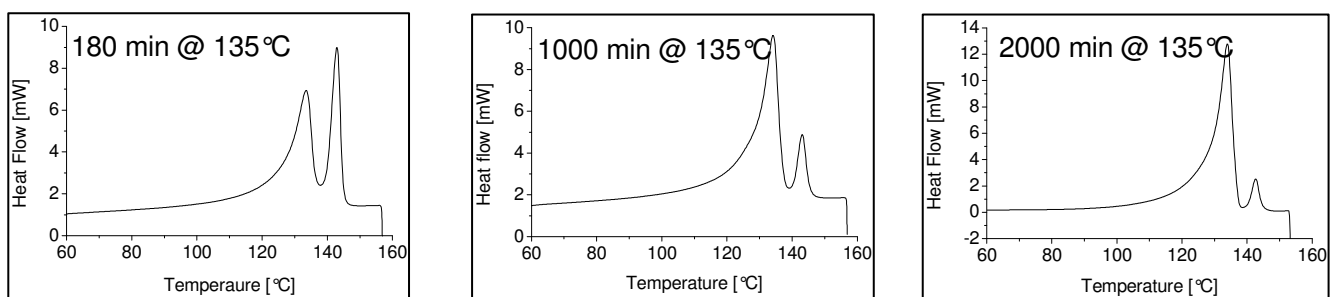
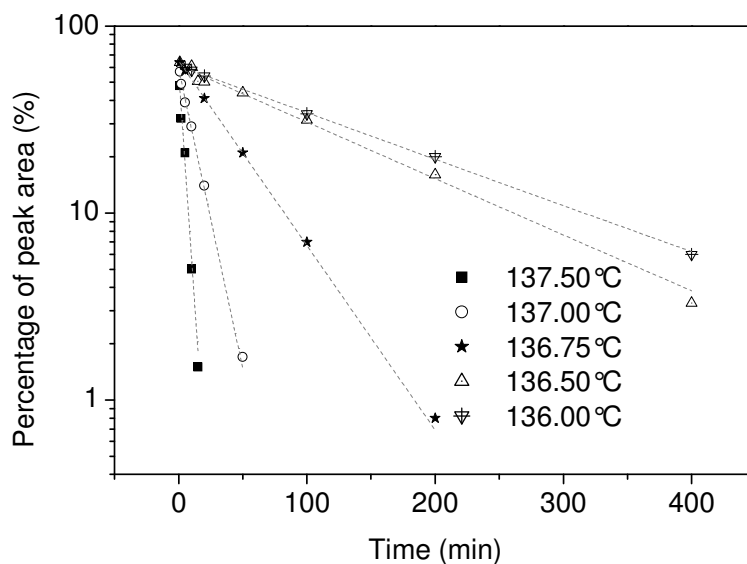
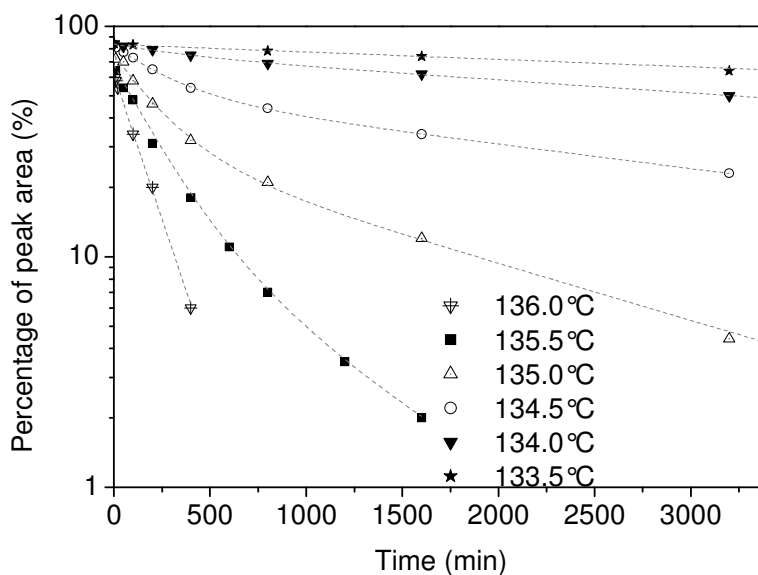


Figure 3.4: Heating run of the nascent disentangled UHMW-PE, after annealing at 135 °C for different annealing times. The annealing times are mentioned in the corresponding figures. The first peak at 133 °C corresponds to melting of the crystals which are crystallized from the melt obtained on annealing. The second peak at 141 °C corresponds to the nascent crystals. The high temperature melting peak disappears on prolonged annealing the sample at 135 °C.

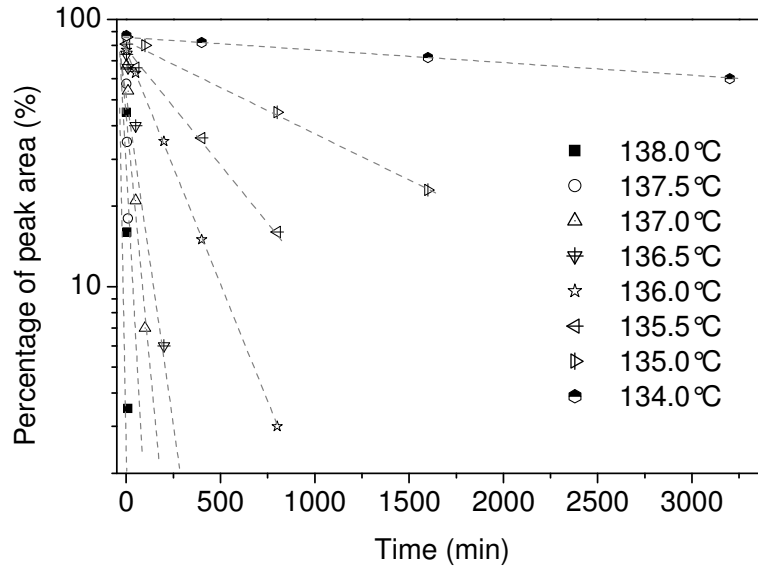
In the annealing temperature region above 135.5 °C, the experiments with the nascent disentangled UHMW-PE show an exponential decrease of the high temperature peak area, with one characteristic time constant; Figure 3.5a. Whereas, Figure 3.5b shows the existence of more than one time constant at annealing temperatures below 135.5 °C, suggesting at least two different processes. Similar experiments have been performed on the nascent entangled UHMW-PE. (Figure 3.5c)



(a)



(b)



(c)

Figure 3.5: The relative decrease in the area of the 141 °C melting peak of the nascent disentangled UHMW-PE with annealing time at different temperatures. (a) In the higher annealing temperature region (137.5 – 135.5 °C) a first order behavior with only one time constant for each annealing temperature is observed. (b) In the lower annealing temperature region (135.5 – 133.5 °C) for each annealing temperature two time constants are observed. (c) In nascent entangled UHMW-PE a first order behavior with only one time constant for each annealing temperature is observed

From Figure 3.5, it is possible to determine the enthalpic relaxation times for melt processes of the different nascent samples. Starting from a time law of Debye (Arrhenius) type for the fusion process in question, the enthalpy change reads

$$H(T, t) = H_0(T)e^{-t/\tau(T)} \quad (3.2)$$

where the time constant (τ) can be related to an activation energy (E_A) by

$$\tau = \tau_0 e^{E_A/RT} \quad (3.3)$$

Figure 3.6 summarizes the relaxation times determined from the slopes in Figure 3.5. Closed symbols represent the relaxation times for the disentangled nascent UHMW-PE sample. Open symbols in the figure represent the relaxation times for the nascent entangled sample. For the disentangled sample only one single relaxation time exists above 135.5 °C (Region I in the figure), whereas below this temperature two relaxation times are observed (Region II in the

figure). Unlike the disentangled sample, the entangled sample can be characterized by a single relaxation time over the whole temperature range of 133-138 °C.

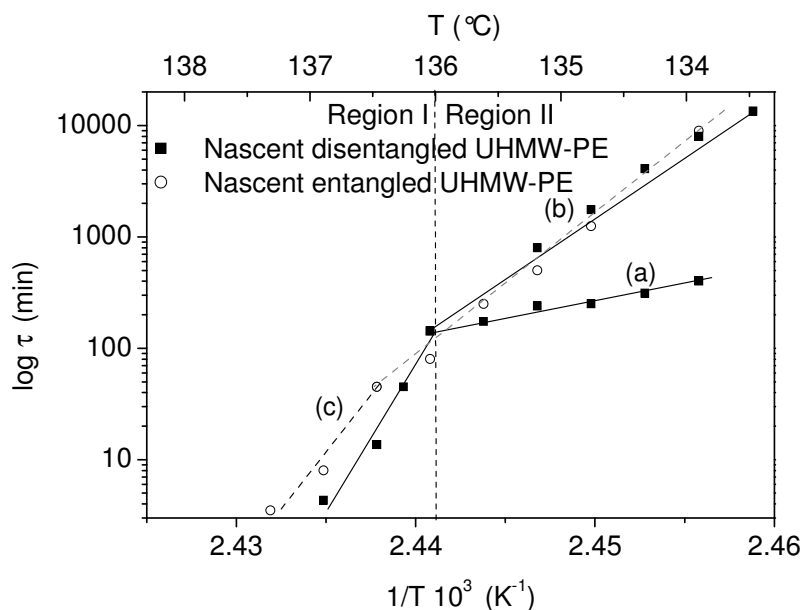


Figure 3.6: Arrhenius plot of the time constants determined from the slopes of the curves in Figure 3.5 for the nascent entangled and nascent disentangled UHMW-PE. The activation energies of the involved processes follow from the different slopes of the plotted fit curves in the figure.

Three different slopes of the relaxation times are observed in the $\log \tau$ versus $1/T$ plot (Figure 3.6), indicating the involvement of three different activation energies in the two different temperature regions as shown in Table 3.2. The activation energies vary from $5.0 \pm 1.0 \times 10^3$ kJ/mol (from slope (c)) for temperatures above 136 °C to $2.1 \pm 0.2 \times 10^3$ kJ/mol (from slope (b)) and $0.6 \pm 0.05 \times 10^3$ kJ/mol (from slope (a)) for temperatures below 136 °C, respectively. In the nascent disentangled UHMW-PE, the three activation energies suggest the involvement of three different melting processes. The measured activation energies can be assigned to detachment/removal of chain stem(s) from the crystal, followed by the diffusion of the detached chain into the melt.²⁰ The measured lowest activation energy of 600 ± 50 kJ/mol (slope (a)) can be assigned to the detachment of a chain segment of ~ 28 nm. (this has been calculated considering the activation energy for detachment of one CH_2 group and its diffusion into the melt, 2.7 kJ/mol and the C-C distance in the orthorhombic lattice along the c-axis 0.127 nm.)²¹ This equals roughly one chain (stem) at the lateral surface of the lamellar crystal. The activation energy of 2100 ± 200 kJ/mol (slope (b)) then refers to the simultaneous detachment of 3-4 stems from the crystalline substrate and their cooperative diffusion and the activation energy of 5000 ± 1000 kJ/mol (slope (c)) refers to the cooperative breakdown of the crystal by simultaneous randomization of at least 7-8 stems.

The low activation energies determined from the slopes (a) and (b) suggest the involvement of a new melting behavior, whereas the slope (c) refers to the conventional melting at higher temperatures.

Table 3.2 Activation energy determined from the Arrhenius plot shown in Figure 3.6

	Activation energy ($\times 10^3$ kJ mol ⁻¹)*	Number of CH ₂ units involved	Chain length involved (nm)	Lamellae thickness (nm) Prior to melt	Stems involved
Nascent entangled	4.3±1.0 (c)	1600±370	202±50	26 ^{11,12}	6-10
	2.4±0.2 (b)	900±90	110±10	26 ^{11,12}	4-5
Nascent disentangled	5.0±1.0 (c)	1850±370	235±50	26 ^{11,12}	7-11
	2.1±0.2 (b)	780±50	99±7	26 ^{11,12}	4
	0.6±0.05 (a)	220±20	28±2	26 ^{11,12}	1

* (a),(b),(c) refer to the three slopes determined from the Figure 3.6 The activation energies in the Table are determined from the three slopes.

Contrary to the disentangled polymer, the nascent entangled polymer exhibits the absence of the process leading to the slope of (a), suggesting the absence of melting by consecutive detachment of single chain stems from the crystalline substrate. Apparently this process is not possible due to constraints in the amorphous layers. The slopes of (b) and (c) of the entangled and the disentangled samples are similar, which indicate that melting of the entangled sample occurs in clusters of several chain stems. Differences in the melting behavior of the nascent entangled and disentangled UHMW-PE arises due to differences in the topological constraints present in the amorphous phase of the polymer.

The melting phenomenon similar to the nascent disentangled UHMW-PE can be obtained with entangled nascent UHMW-PE on crystallization from dilute solution (for example 1 wt. % of UHMW-PE in decalin). As will be discussed in chapter 6 slope (a) in Figure 3.6 associated to the removal and diffusion of a single chain stem is also found for the solution-crystallized disentangled samples (Figure 6.4).

The melting processes shown above for the nascent samples are distinctly different from the melting behavior observed for the melt-crystallized samples, where only one melting process occurs at 135 °C (at a heating rate of 10 K/min) without any time dependence of melting at low heating rates or at annealing temperatures below 135 °C.

3.3.3 Reorganization in the solid state prior to melting as probed by Temperature Modulated DSC (TM-DSC)

From the above described experiments it is evident that different processes are involved in the melting of crystals. Temperature-modulated differential scanning calorimetric (TM-DSC) investigations provide the opportunity to separately measure the individual contributions of different processes to the TM-DSC apparent heat capacity signal. In the quasi-isothermal operation mode it is possible to study the contributions of time dependent processes occurring inside the sample upon small temperature fluctuations. Detailed information about such processes and the TM-DSC method can be found in a review article of Wunderlich^{22,23} Recently, Höhne et al. reported a study on the pre-melting behaviour of entangled nascent UHMW-PE.²⁴ It was shown that with TM-DSC it is possible to determine the time constants of thermal activated processes, such as α -relaxation and reorganization processes, taking place within the crystal lattice.

By the use of TM-DSC Höhne et al. showed that the magnitude of the complex apparent heat capacity of the nascent entangled UHMW-PE in the pre-melting region is higher than the heat capacity obtained by conventional DSC in that region. This indicates that chain reorganization occurs in the solid state which contributes to the apparent heat capacity. The magnitude of this “excess heat capacity” decreases on second heating suggesting that the process is irreversible in nature and is observed only on the first heating of the nascent sample. Quasi-isothermal TM-DSC experiments revealed that this apparent heat capacity is time dependent. To evaluate the relaxation times of the processes contributing to the apparent heat capacities requires the assumption that the relaxation processes are of Arrhenius type (i.e. follow an exponential decay). With such an assumption an evaluation of the measured apparent heat capacity signal is possible, but it should be mentioned that due to the large uncertainty of the determined relaxation times the results are not clear and an interpretation may be difficult.

The same method used for the nascent entangled sample, described in ref. 24, is used for the determination of different relaxation times in nascent disentangled UHMW-PE. Quasi-isothermal TM-DSC measurements with the disentangled nascent UHMW-PE samples are performed at different temperatures below the melting peak and the change of the apparent heat capacity in time is followed (Figure 3.7).

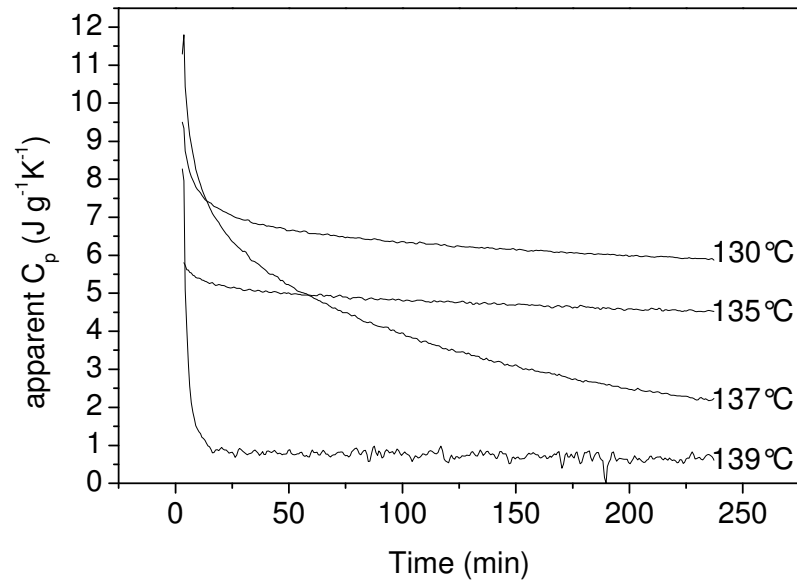


Figure 3.7: Apparent heat capacity from four quasi-isothermal TM-DSC measurements in the melting region of the disentangled nascent UHMW-PE (frequency 12.5 mHz, period 80 s, $T_A = 53$ mK)

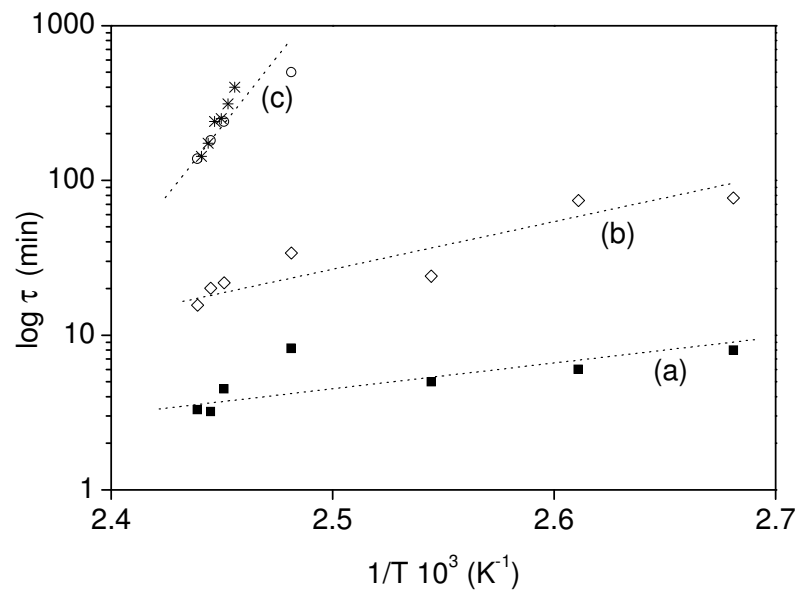


Figure 3.8: Activation diagram of the three processes determined from Figure 3.7. The slope gives the activation energy (solid symbol: exothermic, open symbols: endothermic). The stars represent the time constants determined from the slope (a) of the Figure 3.6. This is attributed to the melting and diffusion of the stems from the crystal sides. The Activation energy is determined from the slopes

The respective excess heat capacity function is fitted with a sum of 2 or 3 exponentials $a_1e^{-t/\tau_1} + a_2e^{-t/\tau_2} (+ a_3e^{-t/\tau_3})$ and the result of the best fit, within the experimental accuracy, are plotted in Figure 3.8. The approximately linear behavior in this so-called Arrhenius-plot, support the assumption that the respective processes are of Arrhenius type (Eq. (3.3)). Therefore the activation energies can be determined from the slopes in the $\log \tau$ via $1/T$ plot (Figure 3.8). Thus determined activation energies for reorganization in the solid state are 30 ± 10 , 60 ± 10 and 500 ± 150 kJ/mol, respectively, for the three processes found in this sample. The first process (shown by solid symbols along line (a), in Figure 3.8) is exothermic and can be attributed to ordering and perfectioning of the crystals. The activation energy of process (a) is in the same order of magnitude as the activation energy of the α -process (i.e. the chain diffusion within the crystallites) determined from mechanical measurements.²⁵ The second process (shown by the unfilled symbols along line (b), in Figure 3.8) is endothermic and can be attributed to irreversible crystal thickening (and/or melting of small crystallites), processes well known in literature.^{23,24,26} These two processes start already at approximately 100 °C, well below the onset of the melting temperature, therefore these processes are attributed to reorganization in the solid state. Considering the small activation energy (30 ± 10 , 60 ± 10 kJ/mol), such a process is likely to involve a few methylene units.

The third process, observed above 130 °C in the TM-DSC experiments (unfilled symbols along line (c), in Figure 3.8) is linked to irreversible melting. It seems to be one of the melting processes seen by the conventional DSC studies mentioned in the section 3.3.2.above. To show the similarity, the data points obtained from the slope (a) of Figure 3.6 are inserted as star symbols (*) in Figure 3.8. Both data sets coincide, indicating the two relaxation processes to be of similar origin. Considering, the similar relaxation times and activation energy for line (c) in Figure 3.8 and line (a) in Figure 3.6, we attribute the third process from the TM-DSC experiments, to the detachment of one chain stem from the crystal substrate and its diffusion to the melt. Considering the results from TM-DSC and annealing experiments with conventional DSC are in good agreement, the assumptions made for the evaluation of the TM-DSC should be valid. Thus the processes seem to be of Arrhenius type and their characterization with the given parameters to be realistic.

3.3.4 Origin of the high melting point of nascent UHMW-PE on the 1st heating

When comparing the low activation energy of 30 and 60 kJ/mol for the first and second process of the TM-DSC evaluation with the activation energy required for the detachment of a chain stem (~ 600 kJ/mol), it is concluded that both the crystal perfection (first process) and the thickening (second process) takes place with the involvement of a few methylene units within the crystal. The reorganization occurs without any detachment of a whole chain stem. The third process takes place when the disentangled polymer sample is annealed close to the

onset melting temperature, in this case melting proceeds by successive detachment of chain stems from the crystal substrate and diffusion into the neighboring melt. The minimum temperature of 133 °C required for this process is in good agreement with the melting temperature determined from Gibbs-Thomson equation. At higher annealing temperatures (>135.5 °C) another melting process occurs where bigger clusters, exceeding the size of one stem, are co-operatively involved.

The relaxation times required for the successive detachment of chain stems from the crystal substrate (>150 minutes) are considerably longer than the relaxation times for melting in clusters. Apparently, at standard heating rates, melting mainly proceeds via cluster melting involving 7-8 chain stems. The experiments show clearly that such a cluster melting of the nascent UHMW-PE leads always to a high melting temperature of 141 °C, normally representative of extended chain crystals only. In the second heating of the nascent samples (i.e. melt-crystallized), no time dependent melting on annealing is observed and the normal melting temperature is 5 °C lower than the nascent polymer during the first run. From here it is concluded that distinction in the melting behaviour and temperature depends on the topological differences of the chains in the amorphous phase of the semi-crystalline polymers rather than on the crystal size.

Topological differences in the amorphous phase will arise from the nature of chain folding on the crystal surface, i.e. tight or loose folds.²⁷ In general, crystal melting is described by the increasing the number of defects in the crystal lattice, ultimately leading to complete breakdown of the lattice. In semi-crystalline polymers, where a chain within the lattice is connected by the chain segments in the amorphous phase, melting requires a cooperative motion of chain segments within the lattice and in the amorphous phase. Tight or loose chain folds connecting chains in the amorphous and crystalline regions will have implications in the breakdown of the crystal lattice. This concept is shown schematically in Figure 3.9. In the case of nascent UHMW-PE with adjacent or tight folds a greater number of -CH₂- groups have to move cooperatively (Figure 3.9 b,c), thus the melting process, where the whole chain has to acquire a random coil state, requires the number of -CH₂- groups to be higher than those present in a single chain stem residing within the crystal lattice. This cooperative melting will involve several chain stems connected by tight folds, thus higher melting temperature than that predicted from the Gibbs-Thomson equation.

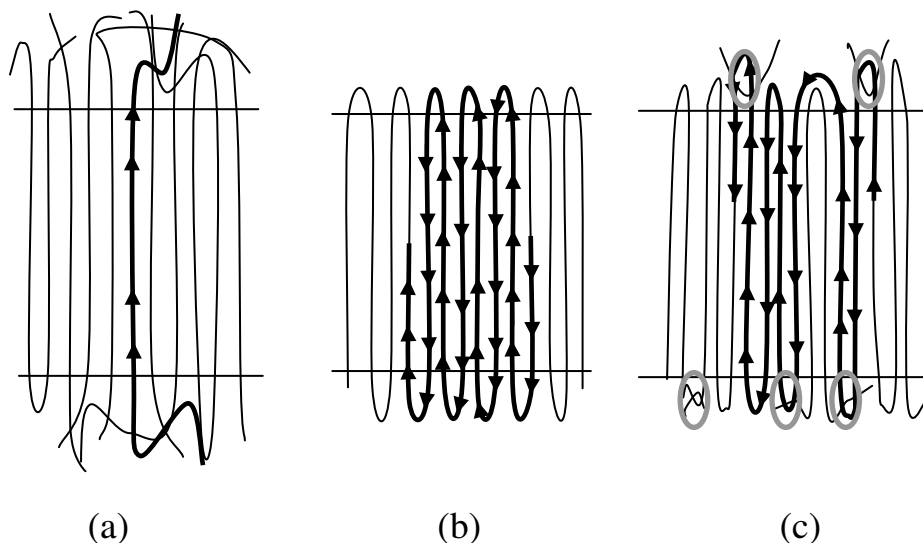


Figure 3.9: *Illustration of the crystal structure of a) melt-crystallized sample having inter crystal molecules and loose loops. It is to be noted that the highlighted test chain represents melting of single chain connected by loose folds or chain segments. b) Nascent disentangled sample having tight folds c) Nascent entangled sample having tight folds. The depicted entanglements in the figure are circled. The highlighted test chains in the figures b and c are connected by tight folds with the neighbouring chain. Thus melting in the nascent samples is a cooperative process involving several chain stems.*

In the melt-crystallized UHMW-PE sample, chain segments in the amorphous phase are free to adopt a larger number of chain conformations, thus the crystal stems are connected by loose folds. Therefore melting requires an entropy gain of the chain stem corresponding to crystal thickness (shown schematically in Figure 3.9a). And the number of repeating units involved in the melting process corresponds to the lamella thickness of the crystal, resulting in a melting point of 135 °C, as predicted from the Gibbs-Thomson equation.

By modifying the Gibbs-Thomson equation, Höhne^{18,22} correlated the number of CH₂ units with the melting temperature. In this approach the number of –CH₂– groups of the respective molecule, incorporated into the crystallite via tight folds (methylene units present in the amorphous phase having restricted chain conformation²⁷) is the essential variable, rather than the crystal thickness. In this approach the basic idea is that the total (molar) enthalpy $\Delta_m H_{\text{mol}}$ and entropy $\Delta_m S_{\text{mol}}$ of fusion (melting) of chain molecules each consisting of n repeating units in the crystals is composed of the respective values of the subunits.

The modified Gibbs-Thomson equation replaces crystal thickness by the number of repeating units;

$$\frac{1}{T_m^n} \approx \frac{1}{T_m^\infty} \left(1 - \frac{\Delta_m G_e}{\Delta_m H_{r.u.}^\infty} \frac{1}{n} \right) \quad (3.4)$$

which contains the number n of repeating units of the chain molecule ($-\text{CH}_2-$ in UHMW-PE) rather than the crystal thickness and a quantity which is the total excess (Gibbs) free energy rather than only the surface free energy. Usually the number n of repeating units of the chain is unambiguously connected with the thickness of the respective lamella crystal via the well-defined distance between two repeating units in the chain and possible tilt angle of the chain inside the crystal. In the case of cluster melting of 7-8 stems, from the number of CH_2 units (± 1800) involved in the melting process a melting temperature of 138.5°C is predicted by using equation 3.4. This value is in agreement with the experimentally determined melting temperature (138.2°C) obtained on the extrapolation to the zero heating rate. (Figure 3.2)

From the thermal analysis studies, it is apparent that melting temperature and melting process strongly depends on the topological constraints present in the amorphous phase of the semi-crystalline polymer. Figure 3.6 clearly shows two distinct melting regions, i.e. slow melting ranging from 133.5°C to 135.5°C and fast melting ranging from 136°C to 141°C . To probe the structural changes during the melting processes in the fast and slow melting regions, solid state NMR studies are performed.

3.3.5 Melting in UHMW-PE as probed by solid state ^1H NMR

In polymers ^1H NMR lineshapes and spin-spin (T_2) relaxation are strongly affected by rotational chain motions at timescales $< 10^{-3}$ s. The more restricted the motion, the broader is the resonance and the faster the relaxation decay of the so-called Hahn-echo produced by a $90^\circ\text{-}\tau\text{-}180^\circ\text{-}\tau$ pulse sequence versus the echo time 2τ . Spin-spin relaxation is a better measure for polymer chain motion than the line shape, because the latter is also broadened by other mechanisms, which are eliminated in the Hahn-echo experiment. ^1H NMR T_2 relaxometry is a versatile tool to determine entanglement in rubbers²⁸⁻³¹ and polymer melts.³²⁻³⁴ At $T \gg T_g$, the transverse spin-spin relaxation time, T_2 , for a polymer melt is very sensitive to the conformational mean position of the chains, which depend on the number of statistical segments between entanglements with lifetimes greater than 10^{-3} s. To distinguish the crystalline and amorphous phases of nascent entangled and nascent disentangled UHMW-PE, the relatively robust and quantitative Hahn-echo method as a tool is applied.

The ^1H NMR transverse spin relaxation curve of the samples is monitored at different constant temperature and are characterized by 60 data points at properly selected echo times (Figure 3.10). The transverse spin relaxation curves are analyzed by a non-linear least-square fitting. The relaxation times are determined by fitting the relaxation data with a sum of two or

three exponents. The Figure 3.11 shows the T_2 -relaxation time as a function of temperature of the nascent entangled (3.11a) and the nascent disentangled (3.11b) UHMW-PE samples.

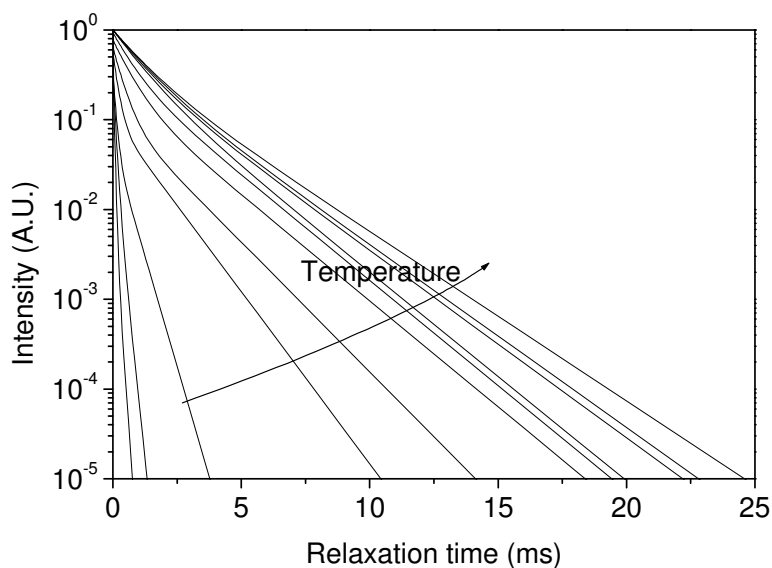
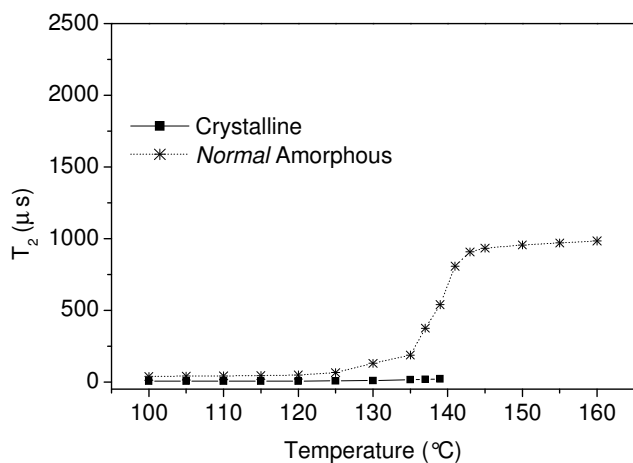
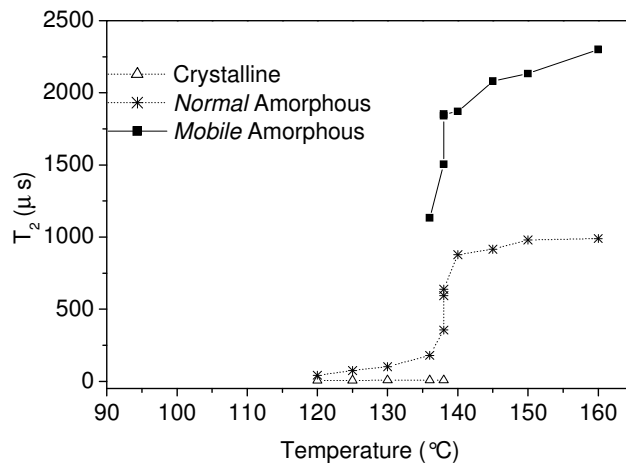


Figure 3.10: Transverse spin (T_2) relaxation curve of nascent disentangled sample at different temperatures.



(a)



(b)

Figure 3.11: T_2 relaxation time versus temperature of (a) the nascent entangled and (b) the nascent disentangled UHMW-PE. The T_2 relaxation time is determined using curve fitting the ^1H NMR transverse spin relaxation curves.

Between the experiments at different temperatures, the sample is heated at a rate of 0.1 K/min. Below the onset of melting temperature, the observed transverse spin relaxation curves of the nascent entangled UHMW-PE sample are well described in terms of two exponential components (Figure 3.11a). The fastest component has a fairly temperature-independent short T_2 value $\sim 10 \mu\text{s}$ and disappears above 140 °C. This fast relaxation time is assigned to the rigid, crystalline phase. Above 120 °C, the long T_2 relaxation time of the amorphous fraction increases strongly with temperature. The steepest increase occurs around the melting point $T_m \sim 140 \text{ °C}$. Apparently, below T_m chain motion in the entangled amorphous phase is confined by the crystalline domains. The resulting melt state is described by a single T_2 relaxation time (T_2^{pl}) of $\sim 1 \text{ ms}$.

Using similar heating protocol a third T_2 component seems to show up in the transverse spin relaxation curves of the nascent disentangled sample (Figure 3.11b). This component appears in addition to the crystalline and amorphous T_2 components also found for the nascent entangled UHMW-PE. The short T_2 attributed to the crystalline phase and the long T_2 attributed to the amorphous phase of the disentangled nascent sample are similar to the T_2 relaxation times determined for the crystalline and the amorphous phases of the nascent entangled sample. The value of this third T_2 component is about 2 – 3 times longer than that of the amorphous phase. Because of its long T_2 value, we attribute the third T_2 component to a more *mobile* type of amorphous phase to be distinguished from the *normal* amorphous phase observed for the entangled and disentangled nascent UHMW-PE.

Quantitative determination of the nascent disentangled sample is shown in Figure 3.12. The crystalline fraction (shortest T_2 component) of approximately 72 % determined from the transverse spin relaxation curves at 120 °C is consistent with the crystallinity of the sample estimated from DSC. As the crystallinity decreases with increasing temperature from 130 °C to 137 °C, the *normal* amorphous fraction increases (Figure 3.12). On increasing the temperature further above 137 °C, with the disappearance of the remainder of the crystalline phase, simultaneous increase in the more *mobile* amorphous phase occurs.

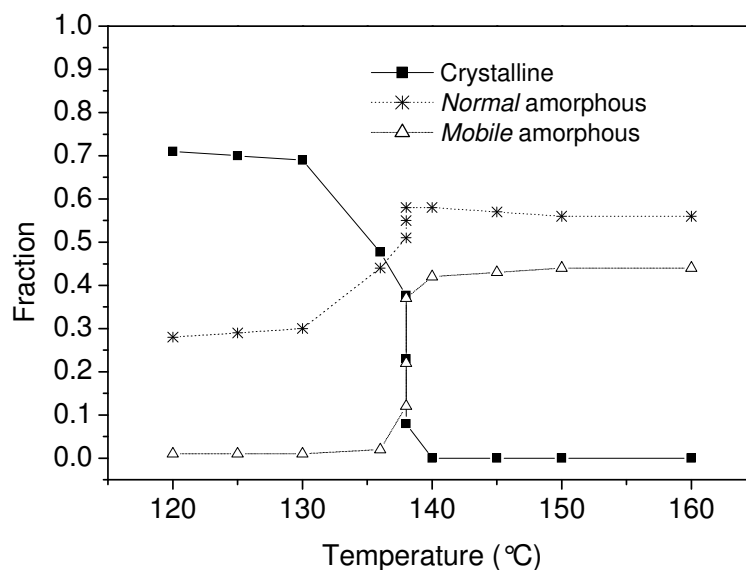


Figure 3.12: Quantitative changes in the relative fractions of the crystalline, mobile amorphous and normal amorphous components of the nascent disentangled UHMW-PE sample with temperature as probed from the Hahn echo pulse program.

To recall, melting at the low temperatures (*‘slowly’* with 0.1 K/min from 130 °C to 137 °C, Region II in Figure 3.6) is associated with the successive detachment and diffusion of a few crystal stems from the crystal surface. The increase of the normal amorphous fraction suggests that the polymer chain stems that are molten by the successive detachment are able to entangle with the surrounding amorphous phase. Upon increasing the temperature further, with the melting of the remainder of the disentangled crystalline fraction (approximately 40 %) a highly *mobile* amorphous component, of the same fraction, evolves. The amount of the highly *mobile* amorphous fraction as well as the *normal* amorphous fraction remains almost constant on increasing temperature. This suggests a barrier for the mixing of the two amorphous-phases. From the NMR studies, it can be concluded that since the polyethylene chains are chemically uniform, on the slow melting of the disentangled nascent crystals the presence of the two amorphous fractions with two different mobility’s above 140 °C, will arise from the ‘heterogeneous’ distribution of entanglements. I.e. with more entangled regions, where the chains are mixed, and less entangled ones, composed of individually separated chains.

Contrary to the *‘slow’* melting upon *fast* heating the nascent disentangled sample (10 K/min, cluster melting depicted in Region I of Figure 3.6), a single T_2 -relaxation time is found on melting at 150 °C (Figure 2.11). These dynamic NMR results suggest that upon fast melting,

associated to melting in clusters of 7-8 polymer chain stems, a homogenous distribution of entanglements occurs – this result into the evolution of ‘normal’ amorphous phase and the absence of the ‘mobile’ amorphous phase in T_2 relaxation experiments. Rheological aspects and physical implications of the ‘heterogeneous’ melt will follow in chapter 4.

3.3.6 Melt mechanism of melting nascent disentangled crystals

Combining the results from DSC and Solid state NMR experiments a hypothesis for the melt mechanism involved in the melting of the nascent disentangled UHMW-PE can be proposed. Figure 3.13 depicts the slow melting of the disentangled nascent crystals. The adjacently re-entrant chains first melt by consecutive detachment of a chain segments equal to the crystal thickness (from the crystal sides) from the crystal lattice (AA' and BB' in Figure 3.13). The initially disentangled chains will form entanglements by reptation (circles) and will result in an increase of the fraction of the “normal” amorphous. Upon melting the whole crystal at higher temperatures, the section AB in Figure 3.13, will transform from a disentangled crystal to a “mobile” amorphous phase (as was shown in the NMR experiments).

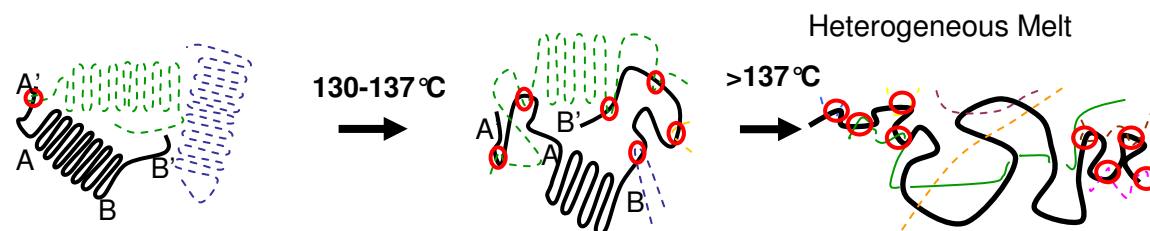


Figure 3.13: *Depicting melting process of the disentangled nascent crystals during slow heating. On annealing below 137 °C, with the consecutive detachment of chain stems from the crystal substrate and their diffusion in the melt normal entangled amorphous phase is formed. On heating above 137 °C, the center of the crystal melts invoking the mobile amorphous phase. The two amorphous phases, mobile and normal, do not mix even above the melting temperature. This leads to the origin of a melt having differences in the local mobility of the two amorphous components. Entanglements are encircled.*

As a result of the absence of physical entanglements, the disentangled component of the amorphous fraction can be described by a high T_2 value referring to the overall higher local mobility. Thus depending on the heating rate, chain dynamics in the resultant melt state of the disentangled nascent crystals can be altered.

Contrary to the slow melting, a complete collapse of the crystal lattice occurs upon fast melting of the nascent disentangled UHMW-PE. This causes an instant free movement of the chain ends in the melt, resulting in a homogenous distribution of entanglements (Figure 3.14).

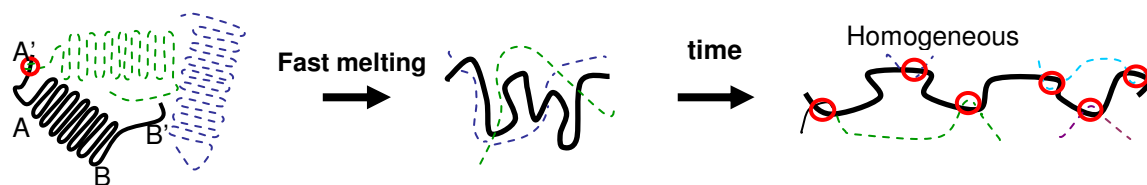


Figure 3.14: *Depicting the melting process of the disentangled nascent crystals during fast heating. Upon fast heating the chains are likely to get mixed, leading to a gradual increase in the storage modulus with the formation of entanglements (see chapter 2), ultimately resulting into a homogenous distribution of the entanglements in the melt.*

In the nascent entangled samples, physical entanglements present in the amorphous phase of the semi-crystalline polymer restrict the consecutive detachment of chains. Therefore the low activation energy component (slope a) in Figure 3.6 is absent. Thus on melting, independent of the heating rate, entanglements present in the amorphous phase get homogeneously distributed along the main chain, Figure 3.15

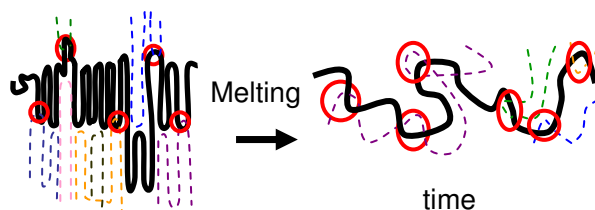


Figure 3.15: *Depicting the melting process of the entangled nascent crystals. On melting, entanglements initially present in the amorphous phase get homogeneously distributed.*

Differences in the melting process of the entangled and disentangled nascent polymers can be also be probed by rheometry. The melting process can be followed by keeping the entangled and disentangled samples at a constant annealing temperature of 134 °C. The elastic modulus is followed as a function of time at a constant strain of 0.5 % (inside the visco-elastic linear regime) and frequency of 10 rad/s (inside the rubbery plateau modulus time frame). On annealing the disentangled and entangled nascent samples the phase angle decreases with time, Figure 3.16. This decrease in phase angle and the modulus is attributed to melting of the crystals. Distinction between the modulus of the entangled and disentangled polymers is evident. On melting of the nascent entangled sample, the elastic modulus decreases to 2 MPa corresponding to the plateau modulus of the fully entangled melt state, whereas the

disentangled sample shows an initial drop in the modulus to 0.6 MPa followed by an increase with time. These rheological differences originating from the melting behavior of the nascent entangled and nascent disentangled UHMW-PE are in agreement with the differences observed on crystal melting by solid state NMR. To recall on melting of the entangled nascent sample a *normal* melt state arises which is entangled. Whereas on slow melting of the disentangled nascent sample a *mobile* melt state together with a normal melt state is realized. The presence of this mobile melt state causes a lower plateau modulus than that anticipated from the normal melt state (see Chapter 4). Hence we can designate the origin of the *mobile* component in the melt to be disentangled. In Figure 3.16 the increase in plateau modulus of the disentangled nascent polymer after 15000 seconds is due to the increasing number of entanglements.

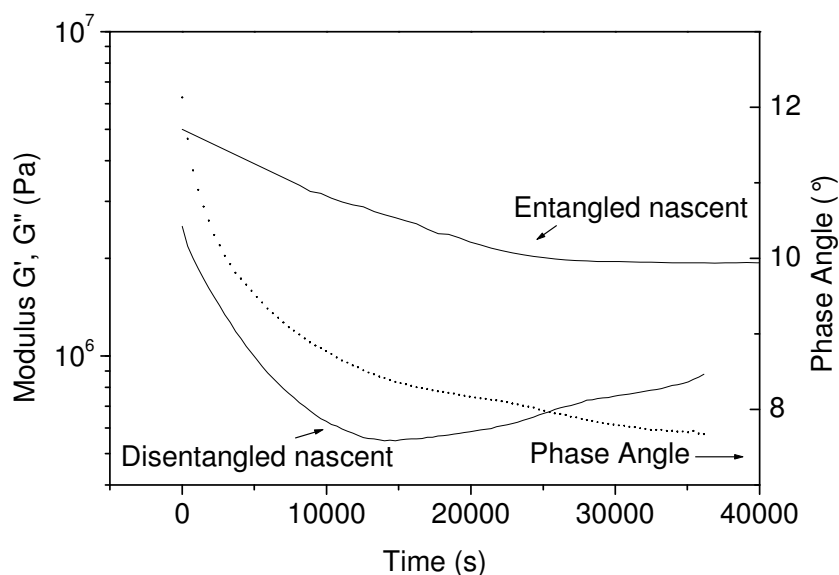


Figure 3.16: Elastic Modulus of the entangled and disentangled nascent UHMW-PE as a function of time at a fixed frequency of 10 rad/s, strain (0.5 %) and temperature 134 °C. The phase angle plotted in the figure is from the annealing experiment of the disentangled sample.

3.4 Conclusion

From the series of experiments reported above it is evident that the differences in the topological constraints present in the amorphous phase of the nascent entangled, nascent disentangled and melt-crystallized UHMW-PE, influences the melting behavior of the crystal. From the experiments reported in this chapter the number of CH₂-groups involved in the melting process depends on the annealing temperature and time. Melting in the low temperature region (130 °C-135 °C) occurs by cooperative detachment of chain stems from the surface involving a time-dependent melting process, whereas melting in the high temperature region (136 °C-141 °C) leads to a breakdown of larger parts of the lattice. Therefore the normal extrapolation to zero heating rate of Figure 3.2 needs modification at slow heating rates, as shown in Figure 3.17. The figure shows that in nascent polymers, if melting kinetics is taken into account, the normal extrapolation to zero heating rate does not hold good.

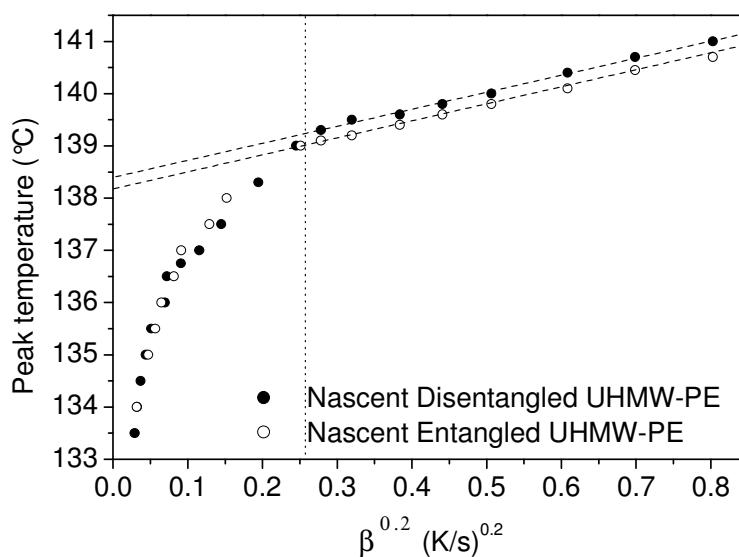


Figure 3.17: The measured melting peak temperatures for the entangled and the disentangled nascent UHMW-PE at different heating rates. The non-linear abscissa allows extrapolation to zero heating rate.⁹ However, the extrapolation fails at the lower heating rates.

The high melting temperature of nascent UHMW-PE compared to that of melt-crystallized UHMW-PE is explained by the differences in the crystal topology i.e. depending on the nature of chain folds in the amorphous phase, loose or tight, the number of CH₂ units that

require cooperative motion for melting differs. Melt-crystallized sample having loose folds melt at the temperature predicted by the Gibbs-Thomson equation i.e. the number of CH₂ units that require cooperative motion to adopt the random coil state is equal to the crystal thickness. In nascent samples, having tight folds, the number of CH₂ units required for cooperative melting is much larger than that of the crystal thickness. Therefore melting point of the samples shifts to higher temperatures than the melt-crystallized sample.

From the structural information probed by solid state ¹H NMR, the influence of the different melting processes (consecutive detachment of chains from the crystal substrate and their reeling in the melt or cluster melting) of the disentangled nascent crystals on the local mobility of the resultant melt state is shown. On melting via consecutive chain detachment from the crystal substrate, the chain ends of the disentangled nascent sample form *normal* entangled amorphous domains. Ultimately, melting of the remainder of the crystal at a higher temperature forms a melt with *mobile* disentangled and *normal* entangled amorphous domains. This melt will be discussed in more detail in chapter 4.

3.5 References

1. Smith, P.; Chanzy, H.D.; Rotzinger, B.P. *Polym. Com.* **1985**, *26*, 258.
2. Rotzinger, B.P.; Chanzy, H.D. Smith, P. *Polymer* **1989**, *30*, 1814.
3. Rastogi S.; Lippits D.R.; Peters G.W.M.; Graf R.; Yao Y.; Spiess H.W.; *Nature Mat.* **2005**, *4*, 635.
4. Keller A. *Phil. Mag.* **1957**, *2*, 1171.
5. Fischer E.W., *Nature* **1957**, *12a*, 753.
6. Strobl G., *The Physics of Polymers.* **1997**, p166, Springer-Verlag, New York.
7. ATHAS data bank (<http://web.utk.edu/~athas/databank/> Ed. M. Pyda)
8. Wunderlich B.; Czornyj G, *Macromolecules* **1977**, *10*, 906.
9. Toda A.; Hikosaka M.; Yamada K.; *Polymer* **2002**, *43*, 1667.
10. Tervoort-Engelen, Y.M.T.; Lemstra P.J. *Polym. Comm.* **1991**, *32*, 343.
11. Rastogi S.; Kurelec L.; Lippits D.; Cuijpers J.; Wimmer M.; Lemstra P.J.; *Biomacromolecules* **2005**, *6*, 942.
12. Corbeij-Kurelec L. Ph.D. thesis, Eindhoven University of Technology, Chain mobility in polymer systems **2001** Chapter 3 ISBN 90-386-3032-8
<http://alexandria.tue.nl/extra2/200113706.pdf>
13. Depending on the experimental methods used, different numerical Gibbs-Thomson equations exist, see Cho T.Y.; Heck B.; Strobl G.; *Colloid Polym Sci.* **2004**, *282*, 825. A difference arises because of different surface free energy values resulting in a somewhat different melting temperature of 136°C for a crystal thickness of 25nm. But such discrepancies in the calculated melting temperatures have no implications on our experimental findings.
14. Rastogi S.; Spoelstra A.B.; Goossens J.G.P.; Lemstra P.J.; *Macromolecules* **1997**, *30*, 7880.
15. Lippits D.R.; Rastogi S.; Höhne G.W.M.; *Phys Rev Lett* **2006**, *96*, 218303.

16. Höhne G.W.H; Kurelec L.; Rastogi S.; Lemstra P.J.; *Thermochima Acta*, **2003**, 396, 97.
17. Höhne G.W.H.; *Thermochima Acta*, **1997**, 304/305 209.
18. Höhne, G.W.H. *Polymer* **2002**, 43, 4689.
19. From Cho T.Y.; Heck B.; Strobl G.; *Colloid Polym Sci.* **2004**, 282, 825, the calculated crystal thickness for the melting temperature of 138.4°C is 47nm, this is also larger than the measured thickness
20. Atkins P.W. *Physical chemistry* chapter 24.6, 27,4, 28,12
21. Considering 1/3rd lesser neighbor interactions on the surface than in bulk, the detachment energy and its diffusion into the melt is likely to be 2.7kJ/mol since the melting enthalpy of the bulk is 4.1kJ/mol CH₂ a value obtained from the ATHAS data bank (<http://web.utk.edu/~athas/databank/> Ed. M. Pyda)
22. Höhne, G.W.H. *Thermochimica Acta* **2003**, 403, 25.
23. Wunderlich B., *Prog. Polym Sci* **2002**, 391, 51.
24. Höhne, G.W.H.; Kurelec L.; Rastogi S.; Lemstra P.J. *Thermochimica Acta* **2003**, 396, 97.
25. Mayr P.U., Dissertation, Universität Ulm, **1998**.
26. Wunderlich B. *Macromolecular Physics*, Vol 3: Crystal melting. Academic Press, New York, **1980**.
27. Yao Y.; Graf R; Rastogi S.; Spiess H.W. IUPAC Macro 2004, Paris
28. Fry C.G.; Lind A.C, *Macromolecules* **1988**, 21, 1292.
29. Wouters M. E. L.; Litvinov V.M.; Binsbergen F.L.; Goossens J.G.P.; van Duin M.; Dikland H.G.; *Macromolecules* **2003**, 36, 1147
30. Tillier D.L.; Meuldijk J.; Magusin P.C.M.M.; van Herk A.M.; Koning C.E. *J. Pol. A*, **2005**, 43, 3600
31. Orza R.A.; Magusin P.C.M.M; Litvinov V.M.; van Duin M.; Michels M.A. *Macromol. Symp.* **2005** 230,144
32. Cosgrove, T.; Turner, M. J.; Griffiths, P. C.; Hollingshurst, J.; Shenton, M. J.; Semlyen, J. A. *Polymer* **1996**, 37, 1535
33. Guillermo A.; Cohen Addad J.P.; Bytchenkoff, D. *J. Chem. Phys.* **2000**, 113, 5098.
34. Brereton M.G.; Ward I.M.; Boden N.; Wright P. *Macromolecules* **1991**, 24, 2068.
35. Mandelkern L. *Macromol Chem* **1991**, 3, 347.
36. Baker A.M.E.; Windle A.H. *Polymer* **2002**, 42, 667.
37. Rastogi S.; Lippits D.R.; Terry A.E.; Lemstra P.J. In: Reiter G.; Strobl G.R.(ed) *Progress in understanding of polymer crystallization*. Lecture Notes in Physics, Springer **2006**, 285-328.
38. Lemstra P.J.; Bastiaansen C.W.M.; Rastogi S.; Chapter 5 in *Structure Formation in Polymeric Fibers*, **2000**, Hanser (Munich) edited by D.R. Salem ISBN 1-56990-306-9.
39. Y.Yao Ph.D Thesis, Max Planck institute, Mainz

Chapter 4

Influence of melting kinetics on the chain dynamics; a route to the heterogenous melt

Semi-crystalline polymers containing amorphous and crystalline regions usually have intimately mixed chains. The resulting topological constraints (entanglements) in the amorphous phase limit the drawability in the solid state. By controlled synthesis the number of entanglements can be reduced. Ultimately, crystals composed of single chains are feasible, where the chains are fully separated from each other. If such separation can be maintained in the melt, a new melt state can be formed. In this chapter we show that through slow and carefully controlled melting such polymer crystals form a heterogeneous melt with more entangled regions, where the chains have restricted mobility, and less entangled ones, composed of mobile segments. Chain reptation, required for the homogenization of the entanglement distribution, is found to be considerably hindered. The long-lived heterogeneous melt shows a decreased melt viscosity. This novel route to create a long-lived heterogeneous melt should be applicable to polymers in general.

4.1 Introduction

In the previous chapter it is shown that the melting process of nascent disentangled UHMW-PE depends on the annealing temperature and time. To recall, melting in the region 130-135 °C occurs by consecutive detachment of chain stems from the lateral surface of the crystal, whereas melting in the temperature region 136-141 °C occurs by cluster melting where immediate randomization of several chain stems take place. On melting of the nascent disentangled polymer, initially a disentangled melt is formed, where the distribution of entanglements depends on the heating rate. With the help of solid state NMR, it is shown that on “*slow*” (<0.1 K/min) heating or annealing in the low temperature region (130-135 °C), a heterogeneous melt is obtained having entangled and disentangled domains. Whereas, when the same polymer is heated “*fast*” (>10 K/min) or annealed in the high temperature region, (136-141 °C), a homogenous distribution of entanglements occurs. The different distribution

Reproduced in part from:

Rastogi, S.; Lippits, D.R.; Peters, G.W.M.; Graf, R.; Yao, Y.; Spiess, H.W.; *Nature Mat.* **2005**, *4*, 635.

of entanglements in the melt should lead to different chain dynamics. In chapter 2 of this thesis the entanglements formation upon “fast” heating (10 K/min) has been discussed. In this chapter, we address the influence of the heating rate on the chain dynamics of the melt state. Rheometry and ^1H NMR are the experimental tools used to probe the entanglements formation on two different length scales. Thereafter the characteristics of a heterogeneous melt are discussed. To strengthen the concept of the two different melt states, the influence of molecular weight on the appearance of heterogeneity in the melt state and the mutual transformation from the heterogeneous to the homogeneous melt state is discussed. In the last part of the chapter the predictions of a theoretical model of T.C.M. McLeish is compared with the experiments.

4.2 Experimental

4.2.1 Materials

In this chapter, nascent disentangled polyethylene samples of molar masses 0.8×10^6 g/mol and 3.6×10^6 g/mol are used, both having a polydispersity around 2-3. These are the samples C and E described in the Table 2.2. The nascent disentangled samples are compared with the fully entangled samples of the same grade. The fully entangled samples are obtained by leaving the disentangled samples in the melt for 4 hours prior to crystallization. For comparison, a commercial available UHMW-PE nascent entangled grade (Montell 1900 CM) possessing a molar mass of 4.2×10^6 g/mol and a polydispersity ~ 8 is used.

4.2.2 Experimental techniques

Rheometry

Oscillatory shear and transient stress relaxation measurements in the linear viscoelastic regime are carried out on a Rheometrics ARES strain controlled spectrometer for a broad range of temperatures (140 °C-220 °C) angular frequencies ω (from 0.001 to 100 rad/s), and constant strain of 0.5 %. It has been checked with the help of a strain sweep that at this strain level, the response of all samples is within the linear viscoelasticity regime (LVE). To follow the entanglements formation in the melt, the build-up of the plateau modulus with time is investigated via oscillatory shear measurements. Prior to measurement, the disentangled nascent powders listed in Table 2.2 are first compressed at 50 °C and 200 bars and the resulting disks of 8 mm diameter are heated with the desired heating rate to 145 °C in the rheometer. Thereafter the samples are heated fast (~ 30 K/min) to 180 °C, and a constant strain of 0.5 % is applied at a fixed angular frequency of 10 rad/sec or 100 rad/sec. The frequency is chosen to be in the plateau region of the fully entangled material. The change of

the modulus is followed in time. As detailed in the Appendix, special care has been taken to avoid experimental artifacts such as non linear effects or slippage between the sample and sample holder.

Solid state ^1H NMR

NMR experiments are carried out without sample rotation on a Bruker DMX spectrometer operating at a ^1H NMR frequency of 500 MHz and equipped with a special (2-mm MAS) probe head that resists temperatures above 150 °C. The transverse spin-spin relaxation time T_2 is measured using a Hahn echo pulse sequence; 90° - τ - 180° - τ -acquisition, with a variable τ time starting from $\tau = 2 \mu\text{s}$. The repetition time is 3 s. The transverse relaxation function is characterized by 60 data points at properly selected echo times. Temperature calibration is carried out by monitoring peak separation in the ^1H NMR spectrum of glycol and the melting-induced ^1H NMR line-narrowing of a series of compounds often employed for DSC calibration. ^1H NMR transverse relaxation functions are obtained from the total integral of the spectra after Fourier transformation, phase- and baseline correction.

To follow the formation of entanglements of the initially disentangled melt as a function of heating rate, the samples are heated inside the NMR spectrometer from 120 °C to 145 °C. Next the samples are heated fast (10 K/min) to 160 °C and the experiment is started. A short Hahn echo experiment with 8 different echo times is used to follow the time dependence of the transverse spin-spin relaxation with 5 minutes interval.

4.3 Results and Discussion

4.3.1 Melting and entanglement kinetics probed by Rheology

Oscillatory shear rheometry, sensitive to chain dynamics on mesoscopic length scales, is performed on the out of equilibrium melts obtained by melting the nascent disentangled sample at different heating rates. Oscillatory rheometry can be viewed as a ‘mechanical microscope’ that allows the chain dynamics affected by heterogeneities in the melt to be probed over broad frequency and temperature ranges. Tube models can be used (at least qualitatively for out equilibrium samples) to provide a link between rheological functions and melt structure.¹ The most recent models for linear polymers in the melt are presented in references 2-5.

The average molecular weight between entanglements $\langle M_e \rangle$, which is inversely proportional to the entanglement density in a thermodynamically stable melt having a homogeneous

distribution of entanglements is related to the elastic modulus in the rubbery plateau region, G_N^0 according to⁶:

$$G_N^0 = g_N \rho RT / \langle M_e \rangle, \quad (4.1)$$

where g_N is a numerical factor (1 or 4/5 depending upon convention), ρ is the density, R the gas constant and T the absolute temperature.

In the previous chapter it is shown that the melting process of nascent disentangled UHMW-PE can be probed by rheometry. Figure 3.16 shows that on keeping the samples at a constant temperature of 134 °C, the elastic modulus initially decreases with time because of progressive melting of the crystals. A major difference is observed between the entangled and disentangled sample: for the former, the modulus decreases monotonously to the equilibrium value, while the latter initially shows a much sharper decrease followed by very slow recovery. The unexpected behaviour of the disentangled crystals is due to the “crystal melting from the sides” behavior followed by slow entanglement formation after complete melting.

In Figure 4.1, the heating rate dependence of the storage modulus during melting of nascent disentangled sample E (3.6×10^6 g/mol), at a constant strain of 0.5 % (inside the visco-elastic linear regime) and an angular frequency of 10 rad/s (inside the rubbery plateau frequency window) is followed.

From Figure 4.1 it is again evident that on melting of nascent disentangled UHMW-PE, the storage modulus decreases. The modulus of the melt measured at 142.5 °C, is lower than the equilibrium value of 1.92 MPa obtained for the fully entangled samples, as reported in the chapter 2, Figure 2.1. The low modulus is indicative for the presence of disentangled domains in the melt. The figure shows that on decreasing the heating rate, the onset of the decrease in the storage modulus occurs earlier. For example the onset of the modulus decrease occurs at 133 °C for 0.1 K/min and 1 K/min and at 135 °C for 5 K/min. Furthermore it is seen that with the decreasing heating rate, the modulus at 142.5 °C (i.e. after complete melting) increases. These observations can be explained with the melt mechanism proposed in chapter 3.

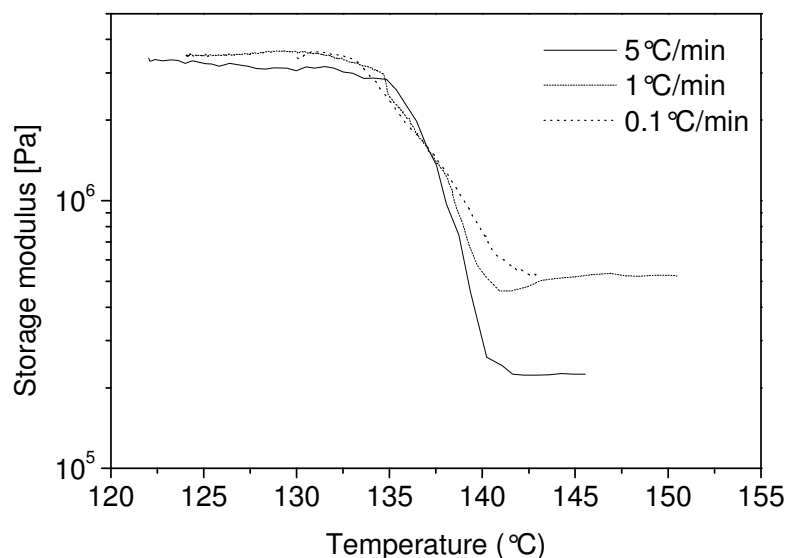


Figure 4.1: Storage modulus during melting of nascent disentangled UHMW-PE of molar mass 3.6×10^6 g/mol at different heating rates, a constant strain of 0.5 % and frequency of 10 rad/s.

As explained in chapter 3, melting at low temperatures occurs by the detachment of single chain stems from the side surface (AA' and BB' in Figure 4.2) rather than the complete randomization of the whole crystal. Therefore the storage modulus decreases already at 133 °C for 0.1 K/min. This temperature is 8 °C below the melting point of 141 °C observed when heating the same sample at 10 K/min. By decreasing the heating rate, the time given to the crystal to stay in the low temperature region is longer, thus the length of chain segments, AA' and BB', obtained by consecutive detachment of chain stems from the crystal surface and their diffusion in the melt increases. The detached chain stems are able to entangle with the surrounding chains and consequently the fraction of entangled amorphous phase increases. This increase in the entangled amorphous fraction is noticed in the NMR T_2 experiments, Figure 3.12. Due to the increase of the entangled fraction with the decreasing heating rate, the modulus at 142.5 °C (i.e. above the equilibrium melting temperature) increases. On the contrary, the initial modulus (0.6 MPa) at 142.5 °C of the disentangled sample heated above 10 K/min is higher than the corresponding modulus of the same sample heated at 5 K/min, 1 K/min and 0.1 K/min (see figure 4.1). This can be explained by the immediate gain in entropy on cluster melting ('chain explosion'), contrary to the consecutive detachment of chains from the crystal surface.

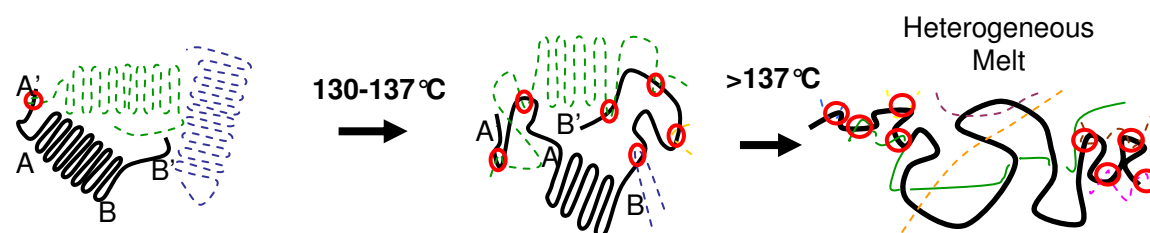


Figure 4.2: The melting process of disentangled nascent crystals during slow heating. On annealing below 137 °C, with the consecutive detachment of chain stems from the crystal substrate and their diffusion in the melt, normal entangled amorphous domains are formed. On heating above 137 °C, the center of the crystal melts, producing the mobile amorphous domains. The two amorphous phases, entangled and disentangled, do not mix even above the melting temperature. This leads to the origin of a melt having differences in the local mobility of the two amorphous components. Entanglements are circled.

We now follow the entanglement kinetics as a function of melting rate. To this end, we first melt the samples from 120 °C to 145 °C with the desired heating rate. Next, from 145 °C to 180 °C the samples are heated fast (~ 30 K/min) and the rubbery plateau G_N^0 is followed in time at 180 °C at constant strain (0.5 %) and angular frequency (10 rad/s).

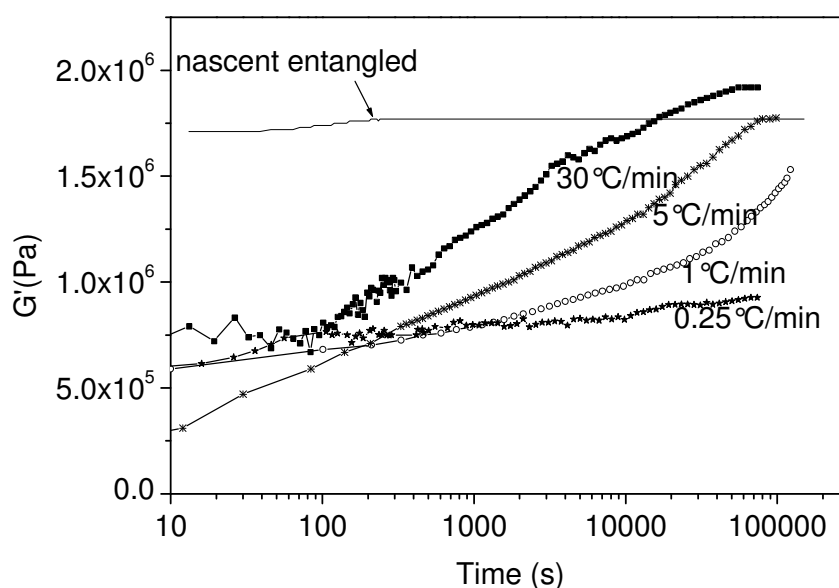


Figure 4.3: Plateau modulus as function time of the nascent disentangled and entangled samples melted at different heating rate (see text for details).

For the nascent entangled UHMW-PE grade, independent of the heating rate, the plateau modulus immediately reaches about 1.8 MPa. (Figure 4.3). This value is close to the anticipated plateau modulus of 1.9 MPa found for the mono-disperse polyethylenes (Figure 2.1).

The modulus of the nascent disentangled UHMW-PE sample gradually increases from 0.6 to 2.0 MPa and shows a strong dependence on the heating rate. The increase in modulus suggests a gradual tightening of the entanglement network (or equivalently decrease of M_e) due to diffusion/reptation. It is to be noted that in a thermodynamically non-equilibrium melt, containing disentangled and entangled domains, the existing rheological models are questionable, however we assume that $\langle M_e \rangle$ determined from equation (4.1) at least qualitatively holds in this situation.

In Chapter 2, when the nascent disentangled sample is heated fast (30 K/min), the time required for the buildup of modulus to reach the fully entangled state scales as the reptation process. On the contrary, for the same sample when the heating rate is decreased, the time required for the buildup of modulus to reach the fully entangled state strongly increases. When the nascent disentangled sample is heated *very slowly* (at 0.25 K/min) almost no buildup in modulus is observed, even when the sample is left for 30 hours at 180 °C. These results suggest that the kinetics of the entanglement process to reach the thermodynamic equilibrium state depends on the melting kinetics and mechanism. To understand the detailed mechanism of entanglements formation of the disentangled melt, we now turn to ^1H NMR measurements in the melt.

4.3.2 Influence of melting kinetics on the entanglements formation as probed by Solid state NMR

^1H NMR spectroscopy is a sensitive tool to probe the local polymer chain dynamics indicative of structural differences.⁸⁻²² This technique has proven to detect dynamic heterogeneities as well as chain order in polymer melts, even if the dynamics in different regions are very similar, that is, they have extremely low structural contrast.^{14,15} Since NMR is applied without isotope labeling and avoids the miscibility problems that exist between deuterated and protonated polyethylenes of highmolar mass ($>1 \times 10^6$ g/mol), advanced NMR is probably the most sensitive technique to detect heterogeneities in melts. In this section first the heterogeneous melt and the homogenous melt are compared using T_2 relaxation measurements. Thereafter the entanglements formation for different heating rates is measured.

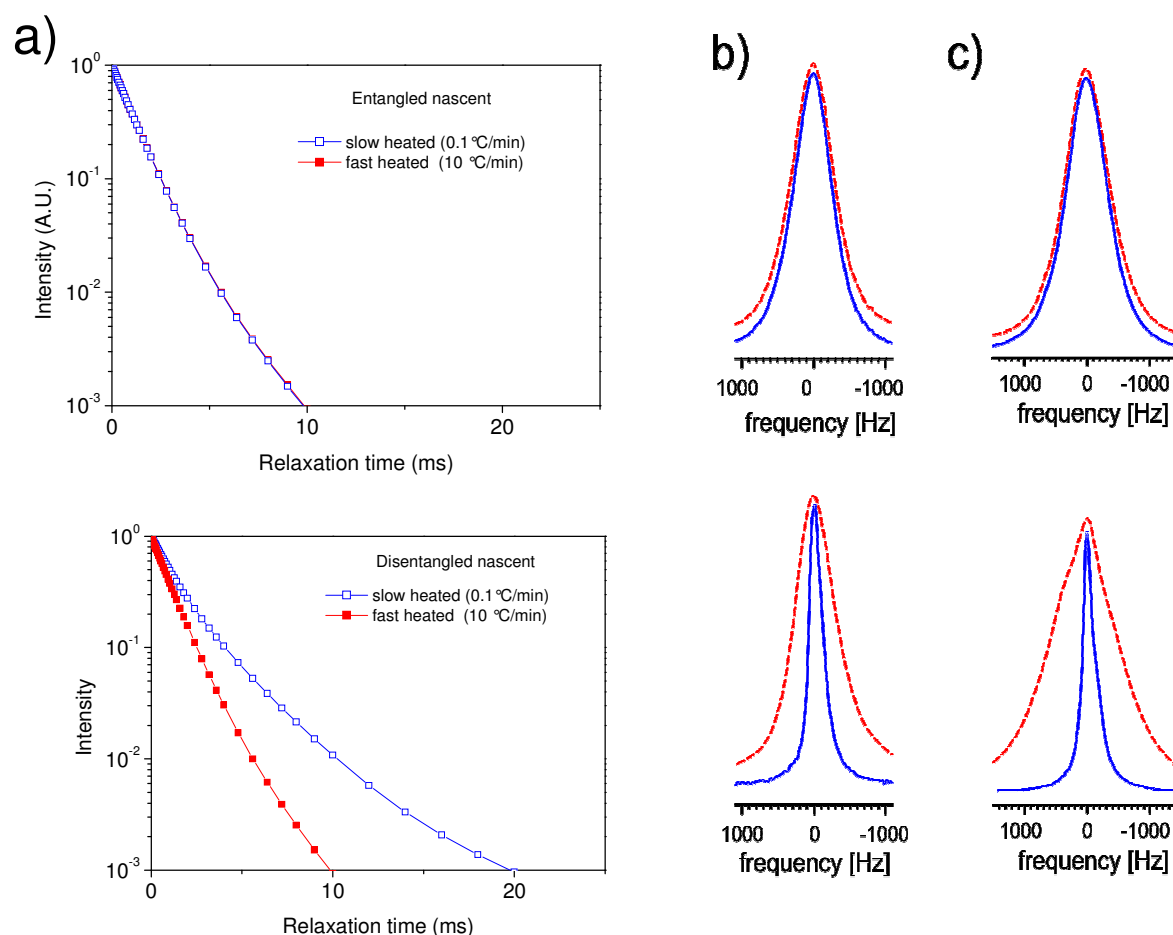


Figure 4.4: *NMR line shapes and transverse spin relaxation (T_2) curves of fast (10 K/min, filled red squares) and slow (0.1 K/min, unfilled blue squares) heated UHMW-PE melts of the initially entangled and disentangled nascent samples. Experiments are performed at 150 °C. The dynamic heterogeneity monitored by the variation of the line width in the T_2 -filtered spectra is shown in **b**) (10 ms T_2 relaxation filter time). **c**) Even more pronounced heating rate dependences in melts of the nascent disentangled samples are revealed applying double-quantum filtration (16 ms double-quantum excitation time).*

Standard spin-echo experiments probing kilohertz motions through spin–spin (T_2) relaxation of the protons¹⁶ already reveal pronounced differences between the heterogeneous and homogenous (entangled) melt. Figure 4.4a shows the transverse spin (T_2) relaxation curve for slow (0.2 K/min) and fast-heated melts (10 K/min) of the nascent entangled (top row) and nascent disentangled (bottom row) UHMW-PE. The melts are kept at 180 °C for 3 hrs before the experiments are performed at 150 °C.

In the nascent entangled sample the T_2 relaxation shown in the figure is independent of the heating rate. Hence, we designate such entangled melt as ‘homogeneous’, meaning that entanglements are homogeneously distributed.

In contrast, the nascent disentangled sample shows considerable differences in the relaxation behavior for different melting rates. The fast-heated sample relaxes faster than the slow-heated sample and the transverse spin relaxation curve can be described with a single relaxation time. It has to be noted that these experiments are performed after leaving the samples in the melt for 3 hrs, therefore, the disentangled domains are absent (Chapter 2).

Using the T_2 -relaxations as a filter, thereby suppressing the less-mobile fractions of the melt, significant differences in the peak width are observed in the NMR spectrum of the nascent disentangled melts, whereas the T_2 -filtered peak width of the nascent entangled sample is independent of the heating rate and similar to the peak width of the fast-heated nascent disentangled melt, Figure 4.4b. The narrower peak of the slow-heated melt indicates a higher local mobility in part of the sample. As the polyethylene chains are chemically uniform, the different local dynamics originate from a heterogeneous melt structure having disentangled and entangled domains. As is mentioned in chapter 3; quantitatively, the heterogeneous melt can be divided in an entangled amorphous fraction of 60 % and a disentangled amorphous fraction of 40 %. The entangled amorphous domains have a similar T_2 relaxation time of approximately 1 ms comparable to the normal entangled melt, and the disentangled amorphous have a higher local mobility with a T_2 relaxation time of approximately 2.5 ms. In fact, an increase in T_2 filter strength leads to suppression of larger less-mobile fractions of the sample and decreasing peak width in the slow-heated nascent disentangled melts, strengthening the idea of heterogeneity in the local mobility.

This conclusion is borne out by applying double-quantum NMR methods,¹⁵ which provide more detailed information on the local mobility of chain segments in polymer melt. The double-quantum filtered spectra displayed in Figure 4.4c, where the most mobile chains are selected, show an even higher contrast between the peak widths of the slow- and fast-heated nascent disentangled melts. Hence, we designate such melts as ‘heterogeneous’.

To investigate the influence of intermediate heating rates on the entanglements formation, ^1H NMR T_2 relaxation experiments are performed on a series of samples. As shown in chapter 2, the T_2 relaxation time of entangled polyethylene melts with a molar mass greater than 200.000 g/mol, is quantitatively related to the number of statistical segments between entanglements at temperatures about 100-150°C above T_g .^{9-11,22} (chapter 2).

The entanglement density can be determined from the plateau T_2 value (T_2^{pl}), since T_2^{pl} is related to the number of statistical segments between the entanglements.

$$T_2^{\text{pl}} = a T_2^{\text{rl}} N_u / n_{\text{ss}} \quad (4.2)$$

where a is molecular-structure specific constant ~ 6.2 for aliphatic polymers, and n_{ss} represents the number of elementary chain units per statistical segment in the Kuhn model, which for polyethylene is 9.25 CC bonds.²⁷ T_2^{rl} represents the decay time of the spin-spin relaxation in the rigid limit and is typically in the order of 13 μs . As described in chapter 2 the T_2^{pl} is not affected by constraints having lifetime greater than 1 millisecond. Such constraints do not necessarily contribute to the modulus. Similar to the rheology experiments presented in section 4.3.2, different samples of the same grade (grade E, 3.6×10^6 g/mol) are heated from 120 °C to 145 °C in the NMR spectrometer at different heating rates. Subsequently, from 145 °C to 160 °C, the samples are heated fast (10 K/min). Once the temperature is reached the experiment is started. To follow the entanglements formation a Hahn echo pulse sequence with 8 different echo times is applied. The Fourier Transform peak of the 8 echo times is integrated and the peak area is followed in time.

Figure 4.5 represents the integrated area of the Fourier transformed peaks of the NMR spectrum. The figure depicts the changes in the integral with different heating rates when a 4 ms T_2 relaxation filter is applied. Since in the normal entangled melt, the $T_{2,\text{entangled}}$ is approximately 1 ms, on the application of a 4 ms T_2 filter, the normal relaxation processes are mostly filtered. Thus hardly any intensity in the entangled melt is observed.

With decreasing the heating rates, a heterogeneous melt is formed. In this melt, disentangled domains exist having a higher T_2 relaxation time compared to the entangled domains. Thus the loss in the integral on the application of the 4 ms T_2 filter is associated with the decreasing fraction of the disentangled domains in time.

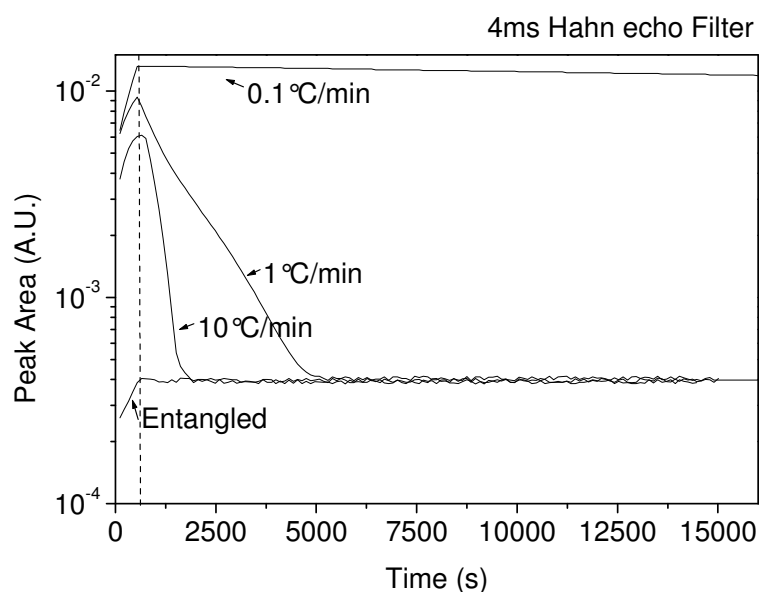


Figure 4.5: *The integral of the Fourier transformed peaks of the NMR spectrum using a 4 ms T_2 relaxation as a filter. The initially disentangled sample E (3.6×10^6 g/mol) is heated at different rates from 120 °C to 145 °C. Thereafter the samples are heated fast to 160 °C and the NMR spectrum was repeatedly measured in time.*

As for the fast heated samples discussed in section 2.3.4, the increase of in the integral during the first 700 s is related to the time required to reach the thermal equilibrium of the experiment. During this time the sample melts and the temperature increases to the set value of 160 °C. With increasing temperature the local mobility of the melt increases and hence the integral of the Fourier transformed peaks.

After 700 s, with time, clear differences are seen between the integrated peak areas of the samples heated at different rates. With time, the integrated peak area decreases faster with increasing heating rate. The decrease of the integrated peak area is indicative for a decrease of the mobile fraction (disentangled domains) in the heterogeneous melt due to entanglements formation, ultimately leading to the homogeneous distribution of entanglements in the initially heterogeneous melt.

For example, upon decreasing the heating rate from 10 K/min to 1 K/min resp. 0.1 K/min, the time required for the T_2 relaxation to reach the equilibrium homogenous state increases from 1750 s to 5000 s resp. more than a day, respectively. Qualitatively, these observations are in agreement with the rheological studies presented above. However for the same heating rate, the time needed for the T_2 relaxation to reach the equilibrium homogeneous melt state, is much shorter than the time needed for the modulus to build up. These findings suggest that the restriction in the local mobility (chain conformation) as probed by NMR between the

entanglements is realized much earlier than the entanglements probed by the stress relaxation (translational mobility) in the rheometry experiments.

Upon slow melting, 0.25 K/min, the transverse spin relaxation as well as the plateau modulus do not reach the equilibrium value. The long lived high local mobility of the chains in the disentangled domains suggests that the entangled chains do not come into contact with the disentangled chain segments present in the melt.

These observations can be explained by the proposed picture of the heterogeneous melt schematically shown in figure 4.6.



Figure 4.6: *Schematic picture of the heterogeneous melt. The melt consist of entangled (AA' and BB') and disentangled domains (AB). The de Gennes' virtual tube required for the cooperative reptation is absent in the disentangled domain since it is depleted with entanglements.*

In this picture, the entangled chains do not come into contact with the mobile part of the sample. Therefore the entangled chains do not provide a restriction in the chain conformation of the disentangled chain segments. Since restrictions in the chain conformations can not be achieved, the chains do not form the de Gennes' tube. Chain reptation requires entanglements to form a virtual tube, in which it can reptate. Since the tube is absent there is no preferred trajectory for the chain diffuse and consequently the normal chain reptation is slowed down considerably. Therefore the modulus does not buildup to the fully entangled state (Figure 4.3).

4.3.3 Additional experimental evidence for the existence of the heterogeneous melt

To further confirm the idea of a heterogeneous melt possessing disentangled and entangled domains, first the characteristics of a heterogeneous melt is discussed and thereafter the influence of molecular weight on the appearance of heterogeneity in the melt state and the mutual transformation from the heterogeneous to the homogeneous melt state is discussed. The rheological characteristics as they appear in a frequency sweep experiment are presented in figure 4.7.

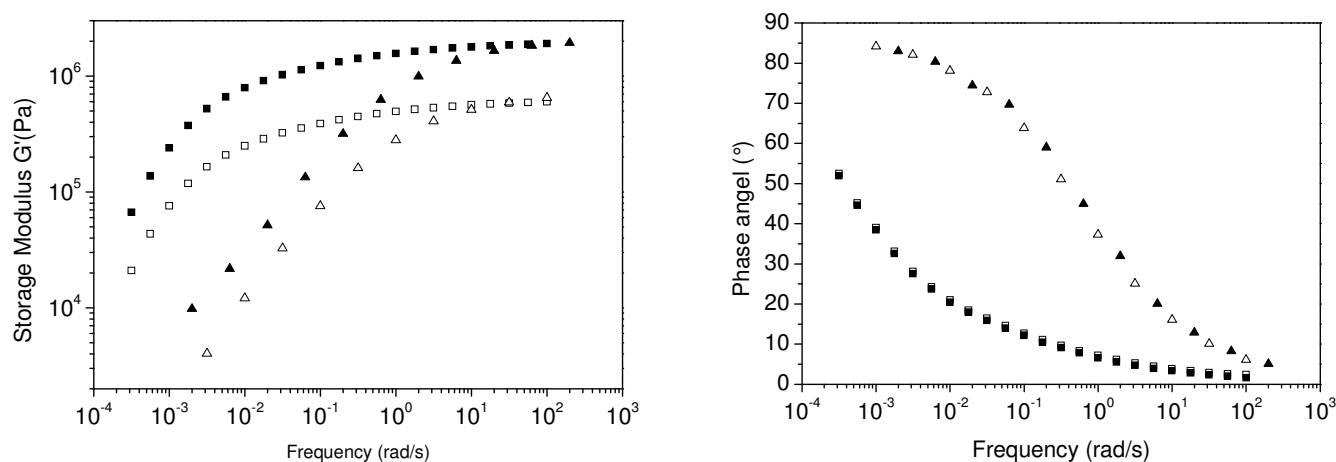


Figure 4.7: Linear viscoelastic response in oscillatory shear of the sample C (0.8×10^6 g/mol (\blacktriangle)) and sample E (3.6×10^6 g/mol (\blacksquare)) at the 180°C . The filled symbols represent the homogeneously entangled sample and the unfilled symbols represent the heterogeneous melt obtained after slow melting. (0.2 K/min) Prior to the experimentation the samples were left at 180°C for 4 hours.

In figure 4.7 the storage modulus vs. frequency of the entangled melts (possessing a homogeneous distribution of entanglements) of the sample C (0.8×10^6 g/mol) and sample E (3.6×10^6 g/mol), is compared with the corresponding heterogeneous melt. The heterogeneous melt is obtained on heating the samples slowly (0.2 K/min) from 120°C to 142°C followed by fast heating to 180°C . The figure shows a vertical shift along the modulus-axis in the entangled melt with respect to the melt having a heterogeneous distribution of entanglements. The phase angle in the two melt states is similar. This indicates that the stress relaxation time spectrum for the two melts are similar. Table 4.1 summarizes the time for complete stress relaxation and the time needed for full modulus to buildup.

Table 4.1 Characteristic terminal relaxation times of the nascent disentangled polymers studied at 180°C .

	Terminal stress relaxation time (s)	Time for modulus buildup (s)
Homogeneous melt (0.8×10^6 g/mol)	400	600
Heterogeneous melt (0.8×10^6 g/mol)	500	>experimental limit
Homogeneous melt (3.6×10^6 g/mol)	40000	54000
Heterogeneous melt (3.6×10^6 g/mol)	48000	>experimental limit

The characteristic experimentally determined stress relaxation time, (listed in Table 4.1) is estimated from the stress relaxation experiments. Here for the sake of comparison, the terminal stress relaxation time is defined as the time needed for the stress to decrease to: $G(t)/G_N = 0.02$. The modulus buildup time, that is, the entanglement formation process is obtained from the experimental data provided in Figure 4.3. The buildup time is defined as the time needed to buildup to $G(t)/G_N = 0.98$. It should be noted that for the fast-molten sample, independent of the molar mass, the time needed for full stress relaxation matches the time for the modulus to buildup as is shown in Chapter 2. However, for the slow-heated sample, apparently no correlation between the terminal stress relaxation time and the modulus build up time exists. These observations suggest that the heterogeneous melt consist of a composite of entangled and disentangled domains, where the disentangled domains have a very low modulus in the measured time scale. The disentangled domains do not contribute to the modulus, therefore only the stress relaxation of the entangled domains is measured. Consequently the phase angle of the homogenous and heterogeneous melt is invariant. However it is difficult to understand how stress relaxation is achieved, with almost unchanged terminal time, without complete reptation of chains beyond a tube length. The latter is required for the entanglement process. In section 4.4 a possible explanation for these observations, originating from T.C.B. McLeish is presented.¹⁸

4.3.4 Molecular weight dependence of the appearance of heterogeneity in the melt

The heterogeneity in the melt arises from melting of the disentangled mono-molecular crystals by consecutive detachment of chain stems. The fraction of the disentangled domain depends on the heating rate. To recall, on heating slowly, a melt state is created in which the entangled part $N_{\text{entangled}}$ (AA' and BB' in Figure 4.6) is large enough to inhibit the mixing of the two domains. In this case chain reptation required for the modulus buildup ceases. To confirm such a hypothesis the molecular weight desired for the appearance of the 'stable' heterogeneous melt is investigated.

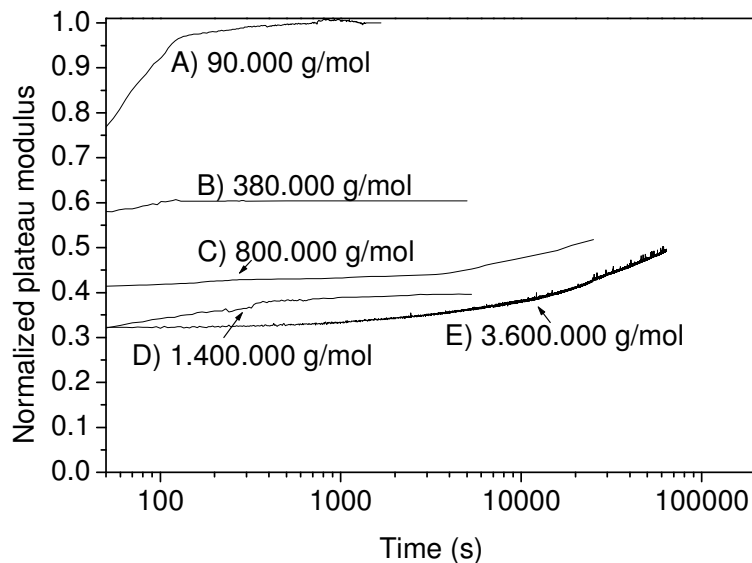


Figure 4.8: Normalized plateau modulus ($=G'(t)/G_N^0(100 \text{ rad/s})$) of the heterogeneous melt as a function of time for different molar masses. The heterogeneous melt is obtained on heating the nascent disentangled samples slowly, 0.1 K/min from 125-145 °C and 10 K/min from 145 °C to 180 °C. The experiments have been performed isothermally at 180 °C.

Figure 4.8 shows that the initial modulus at $t=50$ s increases with decreasing molar mass. The molar mass dependence of the initial modulus can be understood on considering that for the same annealing time (or heating rate), the entangled chain length ($N_{\text{entangled}}$) (i.e. AA' and BB' in Figure 4.2) for different molar masses having similar crystal thickness is a constant. Therefore the entangled volume fraction; $\phi_e = N_{\text{entangled}}/N$ increases when molar mass decreases. If we consider that the disentangled domains have “zero modulus” in the plateau modulus region, the resulting modulus of the composite melt will be:

$$G_{\text{heterogenous}} \approx \phi_e G_0 \quad (4.3)$$

In this simple equation the normalized plateau modulus presented in the figure 4.8 is equal to the volume fraction ϕ_e .

From the figure, it is evident that the heterogeneity of the samples B-E is stable in time. Whereas in the sample A (90.000 g/mol) the low modulus is lost in the order of the stress relaxation time. These results suggest that there is a critical molar mass, between 90.000 g/mol and 380.000 g/mol below which the sizes of the entangled and disentangled domains are too small to prevent the mutual diffusion by chain reptation.

4.3.5 From a Heterogeneous to a Homogeneous melt

To further strengthen our concept of the two different melt states, the mutual transformation from the heterogeneous to the homogeneous melt state is measured by means of rheometry. It is observed that this transformation can be enhanced considerably by successive crystallization/melting cycles. This causes a pronounced increase in modulus, indicating an increase in the entanglement density, until the value of the homogeneous entangled melt is reached (Figure 4.9). During crystallization of disentangled region AB, see Figure 4.2, parts BB' and AA' in the entangled domains are likely to be partially pulled towards the centre. On subsequent fast heating, due to entropic reasons, the domain sizes of the entangled regions AA' and BB' increase. The recovery of the homogeneous melt in Figure 4.9 precludes any chemical changes. Oxidation is also monitored by Fourier transform infrared spectroscopy and no chemical changes are found in the polymer left in the melt at 180 °C for a considerably long time.

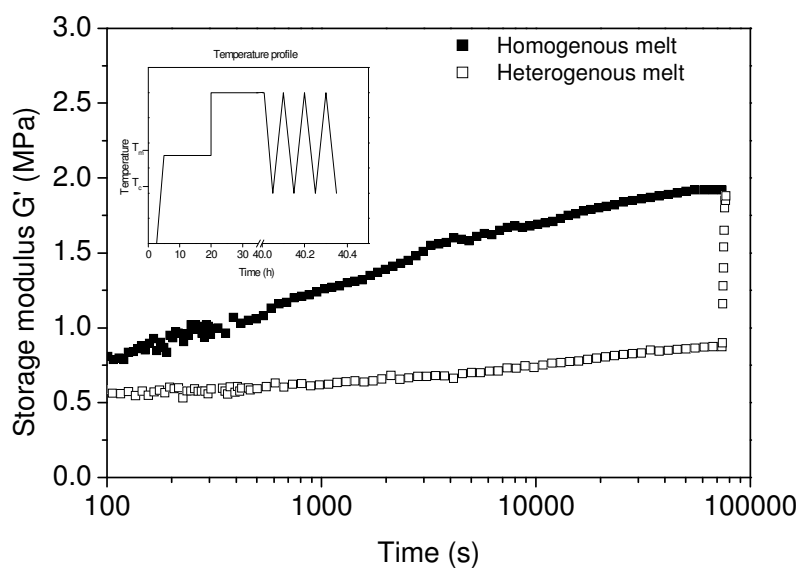


Figure 4.9: A possible route to transform the heterogeneous melt into a homogeneous melt. The sample studied is the grade E (3.6×10^6 g/mol). The figure shows a steep increase in the plateau modulus of the heterogeneous melt upon successive crystallization-melting cycles. After each cycle of crystallization and melting (as shown in the inlay), the modulus was measured at a fixed temperature of 180 °C and a frequency of 10 rad/s. The consecutive cycles (each data point during the steep build-up of modulus refers to a cycle) result in an increase in the plateau modulus, which ultimately reaches a constant value of approximately 2 MPa. This modulus value refers to the fully entangled state in the homogeneous melt.

4.3.6 Heterogeneity in polymer melts

The experimental observations presented above are now combined to develop a picture of the evolution of the homogeneous and the heterogeneous distributions of entanglements in the melt, after fast and slow heating. Initially, there are monomolecular, fully-disentangled crystals. On fast heating, the chain stems melt cooperatively, at temperatures higher than the true melting temperature. All parts of a chain start to move, after a short time the chains are mixed and the different chains entangle. Ultimately, the entanglements are homogeneously distributed along the chains, restricting the number of conformations that molecules can adopt at the local level, creating a tube and restricting the local mobility. In NMR this results in a broad peak (Figure. 4.4), whereas rheometry shows a build-up of the modulus (Figure. 4.3, 30 K/min). The time required for the entanglement process matches the time needed for complete stress relaxation.(Figure 2.7)

For slow melting, all data agree in accordance with the notion of a heterogeneous melt (Figure 4.2). When disentangled crystals are melted slowly, melting occurs by consecutive detachment of chain stems from the crystal surface that entangle with neighboring chain parts, forming tubes at both ends of the chain. Therefore the fraction of disentangled crystal (AB in figure 4.2) decreases. On further raising the temperature above 137 °C, part AB (see figure 4.2) also melts, but it retains its high mobility as demonstrated by NMR and corroborated by rheology. This means that it remains disentangled (it does not form a new tube as its ends are not free). The fraction of the disentangled domain (AB in figure 4.2) in the melt is dependent on the time the crystal is given to melt. This results in a higher initial modulus upon decreasing melting rate. (Figure 4.1). The resultant melt state is now heterogeneous in nature having entangled and disentangled domains. This causes the narrower peak and the slower T_2 relaxation in the NMR results (Figure. 4.4). By comparison with the fast heated samples the chain ends are now heterogeneously distributed, namely they only reside in the entangled domains, since the chain ends (A' and B' in Figure 4.2) melt first. The disentangled domains consists of high mobile chains segments, which are not effectively entangled in terms of modulus. As is clear from the T_2 relaxation experiments, the disentangled domains survive longer when the heating rate is decreased. This suggests that longer end-entangled fraction of the chains (AA' and BB' in figure 4.2) slow down the entanglement formation process of the remainder of the central parts. Upon melting slowly (below 0.25 K/min) the mixing of the two types of domains does not occur on an experimental time scale. Hence, although the central part of the chains are highly mobile locally, they seem "reluctant" to further penetrate by reptation in the already entangled sections. Therefore the formation of effective entanglements does not occur and the plateau modulus stays low. (Figure 4.3).

4.4 A theoretical Model

In the experiments presented above, compared to the fully entangled melt, in the heterogeneous melt a lower plateau modulus and viscosity is observed, whereas the terminal stress relaxation rates remain the same. Though thermodynamically unstable, the heterogeneous melt state is long-living, indicative for chain reptation beyond a tube length to be absent. Combining these findings, it is difficult to understand how stress relaxation is achieved without complete reptation of chains beyond a tube length, since all current theories of polymer melt dynamics, predict a correlation between stress relaxation and single-chain diffusion. These challenges in our understanding of the new melt have been addressed by T.C.B. McLeish in a recent paper. (Details of the model are presented in reference 18, below a short overview of the salient findings is presented)

4.4.1 Salient findings of the McLeish model on the heterogeneous melt¹

In the model, similar to the suggested hypothesis pictured in Figure 4.2, the heterogeneous melt is pictured as a melt having separated entangled regions and disentangled “cells”. In order to achieve a uniform entangled state the cells need to interpenetrate each other. In the model, chains leaving and entering the original “cells” must result in strong elastic deformations (F_{elast}) of the entangled material of the cell walls (eq 4.4).

$$\Delta F_{\text{elastic}} = \phi_e \left(\frac{N}{N_e} \right) k_B T \quad (4.4)$$

Where N is the degree of polymerization and N_e the average degree of polymerization between two entanglements. Therefore at a high degree of entanglement ($Z = N/N_e$) the penalty arising from the elastic distortions of the entangled network will be high. This will result in a free-energy barrier to chain motion. It is a property of this model that single-chain (non-cooperative) reptation may be strongly suppressed by elastic deformation of the entangled regions.

Although the model predicts that the diffusion of entire chains in the heterogeneous melt is strongly suppressed by the presence of the elastic entangled regions, partial reptation of chains is only strongly suppressed after an amount of chain (say n monomers) has left the entangled region, such that the resulting elastic penalty is of the order of the thermal energy. The model suggests that well entangled chains can be relaxed by partial reptation in the order

¹ The model presented originates from the work of T.C.B. McLeish in *Soft Matter* **2007**, DOI: 10.1039/b611620e. This model is presented for completeness of the work done on the heterogeneous melt.

of: $n = \sqrt{NN_e}$, and that the partial relaxation is in principle all what is required to relax stress completely.

From here it is estimated that in the heterogeneous melt a critical volume fraction, 0.1, of the entangled region exists for the melt state to stay long-living. It is stated further that a critical molecular weight arises from the competition of elastic distortion and the free-energy of confinement, in the order of 100.000 g/mol. From the estimations made at a single-chain level, and at a “one-loop” level of co-operative motion, McLeish concluded that; many-chain effects alter the physics quantitatively, but not qualitatively.

4.4.2 Comparison with experiments

From the McLeish model presented above, a few predictions/suggestion are being made:

- It is predicted that there should be correlations between annealing time, the modulus of the heterogeneous melt, and the subsequent rate of the modulus build-up. The longer the annealing time, the higher ϕ_e and therefore the larger the entangled fraction and initial modulus of the heterogeneous melt. At the same time, the elastic penalty for the whole chain reptation (and so chain diffusion) is also higher, so the rate of subsequent annealing will anti-correlate with the modulus. The predicted correlations of the annealing time and heterogeneous modulus are seen in Figure 4.1. It is observed that lower the heating rates (higher annealing time), induce higher heterogeneous modulus. The predicted anti-correlation of annealing time with the modulus the rate of build up is depicted in Figure 4.3.
- It is predicted that there is a molecular weight dependence for the time needed for the heterogeneous melt to reach the equilibrium entangled state. i.e. lower the molecular weight, the faster is the entanglement formation time. This effect can be seen in Figure 4.8, where lower molecular weight accelerates the rate of entanglements.
- The model predicts a critical molecular weight for a heterogeneous melt to stay long-lived. Experimentally it is found that; this critical molecular weight lies between a molar mass of 90.000 g/mol and 380.000 g/mol (Figure 4.8). This is in agreement with the predicted critical molar mass of 100.000 g/mol.

4.5 Conclusions

From the experimental evidences presented in this chapter, it is concluded that the resulting melt state upon melting of disentangled nascent crystals strongly depends on the time given to the crystals to melt.

On *slow* melting, melting occurs by consecutive detachment of chain stems from the crystal surface. Thus with time, the fraction of the disentangled crystal (AB in Figure 4.2) decreases. The detached chain stems form entanglements with neighboring chains (AA' and BB' in figure 4.2). With decreasing heating rate, the time provided for the melting process decreases, and the length of the entangled chain segments (AA' and BB') increases. Subsequently, when the remainder of the crystal is molten (AB in Figure 4.2) a heterogeneous melt state having entangled and disentangled domains is obtained. For the same molar mass the volume ratio of the entangled and the disentangled domains can be varied with the heating rate. With decreasing heating rate, the initial modulus of the heterogeneous melt increases because the volume of the entangled domains increases (Figure 4.1). When the same heating rate is applied to the nascent disentangled crystals having different molar masses, an increase in the initial modulus is observed with decreasing molar mass.

The NMR and rheology experiments show that with decreasing heating rate as the length of the of the entangled chain segments, AA' and BB' increases, the rate of the entanglements formation decreases (Figure 4.3). Ultimately it is possible to obtain a melt state where the partially disentangled (heterogeneous) melt state is retained.

With decreasing molar mass for the same heating rate, while the length of the entangled chain segments is similar, the remainder of the disentangled AB domain decreases. Ultimately, with decreasing the molar mass the disentangled domains become too small to retain the heterogeneous melt state.

The time required to reach the equilibrium entangled melt state on melting of the disentangled nascent crystals is probed by NMR and Rheology. While the NMR probes local restrictions in chain conformation, the rheological experiments probe the stress relaxation of the topological constraints(entanglements) To recall, in Chapter 2, it is shown that on fast heating the restriction in the local mobility (chain conformation) between the entanglements is realized much earlier than restriction of the segmental mobility arising from the entanglements formation. The restriction in the chain conformation provided due to the formation of entanglements, has been investigated with varying heating rates in this chapter. The observations are that with the decreasing heating rate the time required to restrict chain conformations at the local length scale increases. Ultimately it is feasible to melt the sample so slow that the restriction in the chain conformation can be inhibited, maintaining the high local mobility. Since in the disentangled domains restrictions in the chain conformations can

not be achieved, a tube is absent and consequently, since there is no preferred trajectory for the chain to diffuse, chain reptation is slowed down considerably.

Compared to the fully entangled melt in the heterogeneous melt a lower plateau modulus and viscosity is observed, whereas the stress relaxation rates remain the same. Though thermodynamically unstable, the heterogeneous melt state is long-living, indicative for chain reptation beyond a tube length to be absent. The observations are that stress relaxation is achieved without complete reptation of chains beyond a tube length. This is explained by the partial reptation of the chains since only a fraction of the whole chain is required for the stress relaxation.

4.6 References

- 1 De Gennes, P.G., *Scaling Concepts in Polymer Physics* **1979** (Cornell University Press, Ithaca, NY).
- 2 Doi, M.; Edwards, S.F., *The Theory of Polymer Dynamics* **1986** (Clarendon Press, Oxford).
- 3 Likhtman, A. E.; McLeish, T. C. B. *Macromolecules*, **2002**, *35*, 6332.
- 4 Graham, R. S.; Likhtman, A. E.; McLeish, T. C. B.; Milner, S. T. *J. Rheol.* **2003**, *47*, 1171.
- 5 McLeish, T. C. B. ;Milner, S. T. *Adv. Polym .Sci.* **1999**, *143*, 195.
- 6 Ferry, J. D. *Viscoelastic Properties of Polymers* 3rd edn **1980** (Wiley, NY).
- 7 Barham, P.; Sadler, D.M. *Polymer*, **1991**, *32*, 393
- 8 Cohen-Addad, J.P. *Prog. NMR Spectrosc*, **1993**, *25*, 1.
- 9 Fry C.G.; Lind A.C. *Macromolecules*, **1988**, *21*, 1292.
- 10 Gotlib, Y.Y.; Lifshits, M.I.; Shevelev, V.A.; Lishanskii, I.A.; Balanina ,I.V. *Poly Sci USSR*, **1976**, *18*, 2630.
- 11 Litvinov, V.M.; Barendswaard, W.; van Duin M. *Rubber Chemistry and Technology*, **1998**, *71*, 105.
- 12 Guillermo, A.; Cohen-Addad, J-P. ; Bytchenkoff, D. *J. Chem. Phys.* **2000**, *113*, 5098.
- 13 Brereton, M.G.; Ward, I.M.; Boden, N.; Wright, P. *Macromolecules*, **1991**, *24*, 2068.
- 14 Tracht,U.; Wilhelm M.; Heuer A.; Feng H.; Schmidt-Rohr K.; Spiess H.W. *Phys. Rev. Lett.*, **1998**, *81*, 2727.
- 15 Graf, R.;Heuer, A.; Spiess, H.W. *Phys. Rev. Lett.*, **1998**, *80*, 5738.
- 16 Schmidt-Rohr, K.; Spiess, H. W. **1994** *Multidimensional Solid-State NMR and Polymers* (Academic, New York).
- 17 Fetters, L.J.; Lohse D.J.; Greassley W.W. *J. Polym. Sci. Part B* **1999**, *37*, 1023.
- 18 McLeish T. C. B., *Soft Matter*, **2007**, DOI: 10.1039/b6111620e.

Chapter 5

Role of chain entanglements in crystallization; homogeneous vs. heterogeneous nucleation

In the previous chapters, it is shown that on the controlled melting of the single chains forming single crystals, it is feasible to obtain a heterogeneous melt state, having entangled and disentangled domains. The heterogeneous melt having local differences in the chain mobility, provides a unique opportunity to investigate the influence of entanglements on crystallization aspects. Using the differences in the transverse (T_2) relaxation times of the chains in the entangled and the disentangled domains, the initial stages of crystallization is followed on cooling the heterogeneous melt. The observations are that the disentangled chains segments crystallize faster than the entangled chains, which is indicative for the intramolecular homogeneous nucleation to occur faster than the heterogeneous nucleation. To follow the influence of the disentangled domains on the overall crystallization time, rheological studies are performed. With the increasing number of entanglements per unit chain, the time required for the onset of crystallization increases. In the sample from the same batch having lesser number of entanglements per unit chain, the crystallization time can be reduced by a decade.

5.1 Introduction

In previous chapters it is demonstrated that it is possible to obtain single chains forming single crystals, where chains are adjacently re-entrant. It is feasible to melt these crystals, either by simple consecutive detachment of chain stems from the crystalline substrate or by cluster melting, where several chain stems are involved (Chapter 3). The consecutive detachment of chain stems occurs at the melting temperature predicted from the Gibbs-Thomson equation, whereas the cluster melting occurs at much higher temperatures. Melting by consecutive detachment of chain stems from the crystal substrate and their diffusion in the melt, ultimately result into a new melt state having a heterogeneous distribution of physical entanglements (Chapter 4). With the combined DSC, rheology and solid state ^1H NMR studies it is shown that in the heterogeneous melt, the disentangled domains present within

Reproduced in part from:

Lippits, D.R.; Rastogi, S.; Höhne, G.W.M.; Mezari, B.; Magusin, P.C.M.M. *Macromolecules*, **2007**, in press.

the entangled matrix possess higher local mobility than the entangled domains, ultimately causing a lower elastic modulus. The fraction of the entangled and disentangled domains is maintained at higher temperatures leading to a thermodynamically non-equilibrium melt state. On the contrary, in the cluster melting where several chain stems (initially disentangled) can simultaneously adopt the random coil, entanglements that are formed get homogeneously distributed in the melt.

The heterogeneous melt having local differences in the chain mobility, which arises from the differences in the distribution of chain entanglements, provides a unique opportunity to investigate the influence of entanglements on the crystallization aspects.

Advanced NMR provides a distinction in the local mobility of the disentangled and the entangled domains. Crystallization, which is a nucleation and growth process, when probed by solid state NMR will give information on the differences in the crystallization kinetics of the disentangled and the entangled domains.

On cluster melting of the single chain forming single crystals, due to the entanglements formation, the elastic modulus probed by rheometry increases in time. During the modulus buildup this provides a range of samples (from the same synthesis batch) with varying number of entanglements. Making use of these series of samples the influence of entanglements on polymer crystallization is investigated by making use of advanced NMR and Rheometry.

5.2 Experimental section

5.2.1 Materials

To investigate the influence of entanglements on the crystallization behavior, the nascent disentangled UHMW-PE sample E of table 2.2 is used, possessing a molar weight of 3.6×10^6 g/mol. The homogenous melt is obtained by fast melting (10 K/min) the nascent disentangled UHMW-PE sample to the melt in the rheometer. Thereafter the entanglement density is controlled by leaving the sample for different times in the melt. The fully entangled melt state is obtained after leaving the initially disentangled samples for 3 hours in the melt at 180 °C to entangle. The heterogeneous melt state is obtained by leaving the nascent disentangled UHMW-PE sample to melt at 136 °C in the rheometer for 18 hours prior to fast heating to 180 °C. This sample is left at 180 °C for 15 minutes before being cooled to the crystallization temperature.

5.2.2 Experimental

Rheometry

The influence of the melt state on crystallization of UHMW-PE is investigated using oscillatory shear measurements in the linear viscoelastic region are performed using an Advanced Rheometrics Expansion System (ARES). Measurements are carried out using parallel plate geometry (8 mm diameter and thickness 1 mm) under a nitrogen atmosphere. The compressed samples are cooled from the different melt state with 1 K/min to 127 °C. Subsequently, at constant strain ($\gamma=0.1$ %) and frequency ($\omega=100$ rad/s) isothermal crystallization at 127 °C is followed by measuring the elastic modulus (G'). Khanna¹ and Boutahar² related the crystallinity of PE with the scaled modulus G' :

$$\frac{\varphi(t)}{\varphi(\infty)} = \frac{G'(t) - G'(0)}{G'(\infty) - G'(0)} \quad (5.1)$$

where $G'(0)$ is the initial modulus and $G'(\infty)$ is the plateau value reached at the end of crystallization. $\varphi(t)$ is the degree of crystallinity at time t and $\varphi(\infty)$ is the maximum degree of crystallinity of the samples.

Solid state ¹H NMR

NMR experiments are carried out without sample rotation on a Bruker DMX spectrometer operating at a ¹H NMR frequency of 500 MHz and equipped with a special (2-mm MAS) probe head that resists temperatures above 150 °C. The transverse relaxation time T_2 is measured using a two pulse sequence $90^\circ-\tau-180^\circ-\tau-aq$ with a variable τ time starting from $\tau=2$ μ s. The 90° pulse length is 5 μ s and the repetition time is 3 s, which proved long enough for quantitative measurements. The relaxation decay is characterized by 60 data points at properly selected echo times. This pulse sequence is chosen because it offers the possibility to both qualitatively as well as quantitatively analyse relaxation of the amorphous and crystalline components. Temperature calibration is carried out by monitoring the peak separation in the ¹H NMR spectrum of glycol and the melting-induced ¹H NMR line-narrowing of a series of compounds often used for DSC calibration.

The samples are cooled from the heterogeneous melt at 1 K/min to 128 °C inside the spectrometer. At the temperature of 128 °C, the samples are left isothermal. The real-time T_2 relaxation is monitored by repeatedly measuring 12 properly data points. In this way it is possible to follow the changes in the sample with 5 minutes intervals. ¹H NMR spin-spin relaxation decays are obtained from the total integral of the spectra after Fourier transformation, phase- and baseline correction. The relaxation decay is analyzed by a non-linear least-square fitting.

Solid state drawability

Samples crystallized from the heterogeneous melt are compression moulded at 50 °C. Standard tensile bars are cut having a length of 40 mm, width of 2 mm and thickness of 1 mm. The tensile tests are performed at 120 °C and at a drawing speed of 10- 20 mm/min using a Zwick Z100 tensile tester, equipped with a nitrogen oven. The draw ratio (DR) is determined from the separation of ink pre-printed on the surface of the samples. The obtained drawn samples are cooled to room temperature. The drawn samples are cut in 75 mm pieces. The thickness of the samples is determined by weighing the samples. Thereafter the samples are glued in a cart-board and a tensile test is performed at 100 mm/min. The tensile modulus is calculated from the 0.1 % to 0.2 % strain.

5.3 Results and discussion

5.3.1 Influence of a heterogenous distribution of entanglements in the polymer melt on crystallization

The heterogeneous melt state obtained on slow melting constitutes entangled and disentangled domains, provides an opportunity to investigate the influence of entanglements on polymer crystallization – especially the nucleation process, which has been a subject of dispute. It has been often debated that nucleation occurs via chain disentanglement from the entangled melt or via clustering of the disentangled domains pushing the entanglements within the amorphous phase.¹ As stated earlier in Chapter 3, advanced NMR is an experimental tool capable of making a distinction in the local mobilities of the disentangled and entangled domains in the melt. Differences in the local mobility in the melt are apparent from the two different relaxation times for the two amorphous domains as shown in Figure 3.12. The *normal* amorphous is related to the entangled domains and the *mobile* amorphous phase is related to the disentangled domains. Thus by following the crystallization aspects of the two domains at a fixed temperature it can be feasible to probe the nucleation process at the molecular length scale.

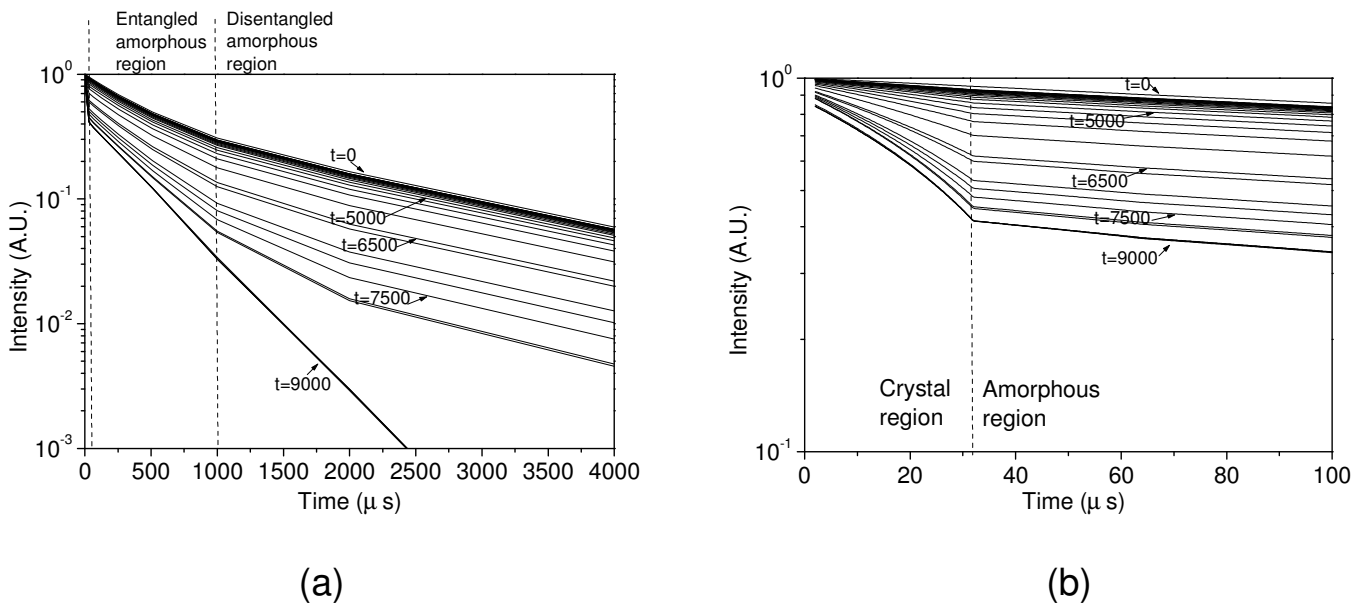


Figure 5.1: *Transverse spin relaxation curve (T_2) obtained using a Hahn-echo pulse program during iso-thermal crystallization at 127 °C. The sample is cooled from the heterogeneous melt state at 160 °C to 127 °C with 1 K/min. In the figure, two distinct slopes can be seen, a steep slope from 0-32 μs (Figure 5.1a), related to the crystalline phase, and 32-4000 μs related to the amorphous phases. A closer look of the T_2 – relaxation in the amorphous phase (Figure 5.1b) shows the presence of two slopes in the region $t=0$ to $t=6500$ s. The two slopes arise from the differences in the mobility of the disentangled and entangled amorphous phases.*

Figure 5.1 shows the transverse spin relaxation curves (T_2) of the heterogeneous melt during crystallization at 127 °C, recorded at an interval of five minutes. The heterogeneous melt is obtained by melting the nascent disentangled samples from 130 °C to 142 °C with a heating rate of 0.1 K/min followed by 10 K/min heating to 160 °C in the NMR spectrometer. The samples are left in the melt for 30 min at 160 °C, followed by 1 K/min cooling to 127 °C. Prior to the isothermal experiment the sample is left at 127 °C for 5 minutes to reach the thermal equilibrium.

In the experiment, the amorphous phases possess T_2 relaxation times in the order of 1 millisecond can be clearly distinguished from the crystalline phases possessing a T_2 relaxation time two decades faster, in the order of micro seconds. Consequence to the two very different relaxation times, the T_2 relaxation curve shows two distinct slopes as is evident from Figure 5.1a. The slope in the region of echo times of 0-32 μs is attributed to the crystal phase and the slope in the region greater than 32 μs to the two amorphous phases (entangled and disentangled domains). The large differences in the T_2 -relaxation times of the crystalline and

the amorphous phases facilitate the quantitative determination of the crystalline fraction by curve fitting the T_2 -relaxation data in the region of 0-100 μ s. From the Figure 5.1b, it is to be noted that the slope of the amorphous region, from $t=0$ s to $t=6500$ s does not change, while the crystalline component increases. Thus on curve fitting the amorphous fraction in the region of 32 μ s to 4 ms echo times, it is observed that the qualitatively determined T_2 relaxation times of the both amorphous phases remain nearly unchanged up to a crystallinity of approximately 45% (at $t=6500$ s). Since the T_2 -relaxation times of the two amorphous phases are almost constant, the relative fraction of the two amorphous phases can be determined by curve fitting of the T_2 -relaxation data in the region of 32 μ s to 4 ms echo times.

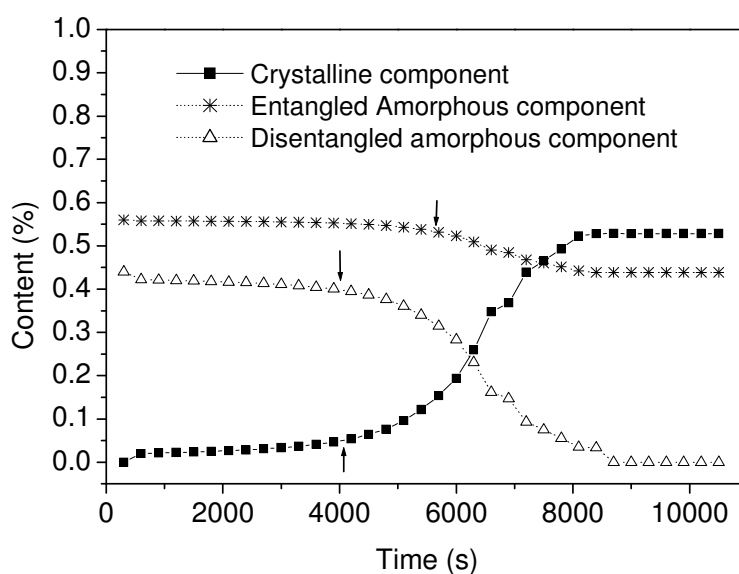


Figure 5.2: *Quantitative determination of the three components (crystalline, entangled and disentangled amorphous), during isothermal crystallization at 127 °C. The quantitative determination is obtained by curve fitting the T_2 -relaxation curve presented in Figure 5.1.*

Figure 5.2 shows the changes in the fraction of the crystalline and the amorphous (entangled and disentangled) components during isothermal crystallization at 127 °C. Arrows in Figure 5.1 correspond to the onset of the decrease in the fraction of the two amorphous phases and the increase in the crystalline fraction. It is to be noted that the decrease in the fraction of the mobile disentangled amorphous component occurs much earlier than the entangled amorphous component. With the decrease in the fraction of the disentangled amorphous component the simultaneous increase in the fraction of the crystalline component occurs. This is indicative for the earlier onset of the crystallization of the disentangled amorphous component compared to the entangled amorphous component. The role of entanglements in

the nucleation process becomes more evident by the rate at which the disentangled mobile fraction decreases relative to the entangled fraction – to quote for the given time while the entangled amorphous component decreases by approximately 10%, the disentangled fraction of approximately 40 % crystallizes completely. These studies clearly demonstrate the overriding influence of the homogeneous nucleation over the heterogeneous nucleation, provided that the chains are in the disentangled state. Homogeneous nucleation in the disentangled region followed by the crystal growth provides the possibility of crystalline disentangled domains in the solid state, likely to arise from intra-molecular crystallization.

Theoretical studies on intra-molecular nucleation have been performed by Hu et al.⁴ From their studies the authors concluded that the intra-molecular nucleation in a single homopolymer chain is independent of chain length and crystallization proceeds via homogeneous nucleation.

5.3.2 Influence of entanglements in the polymer melt on crystallization

To investigate the influence of entanglements on crystallization, the onset of crystallization with the increasing amount of entanglements is followed using rheometry. On fast melting of the nascent disentangled crystals, in Chapter 2, it is shown that the initially disentangled chains entangle with time in the order of the stress relaxation time. As the molar mass between the entanglements decreases, the elastic modulus increases. The inlay in the Figure 5.3 (from Figure 2.3) depicts the increase in the storage modulus for linear polyethylene having a molar mass of 3.6×10^6 g/mol with a polydispersity of 2.8 (sample E in table 2.2). The time required for the modulus to reach the entangled thermodynamically equilibrium state at 180 °C is approximately 10^4 seconds.

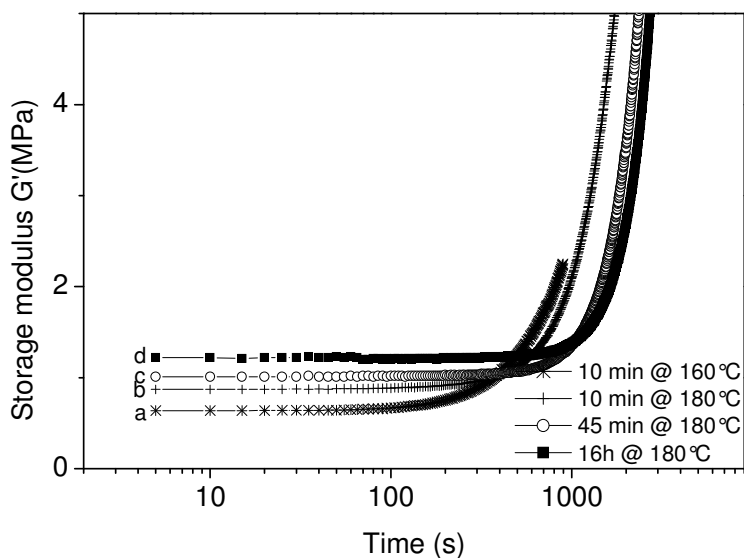


Figure 5.3: *The build up of elastic modulus with time during isothermal crystallization is recorded at 125 °C and 10 rad/s. Samples of the nascent disentangled UHMW-PE (sample E listed in table 2.2, 3.6×10^6 g/mol, are fast molten and left in the melt for; (a) 1 min, (b) 10 min, (c) 45 min, (d) 100 min. The onset in modulus refers to the onset in crystallization. The inlay shows the build up of plateau modulus of the fast molten sample at 180 °C with time. Points a, b, c and d in the inlay refer to different plateau modulus obtained on leaving the samples for different times.*

Experimentally, the onset of isothermal crystallization can be monitored by measuring the elastic modulus as a function of time at a constant strain and fixed frequency, where a strong increase in modulus indicates the onset of crystallization. Figure 5.3 shows that nascent disentangled crystals, heated fast to 180 °C and left in the melt for 1 minute before being cooled to an isothermal crystallization temperature of 125 °C (with 1 K/min), show an onset in the build up of modulus after approximately 250 seconds (curve *a* in Figure 5.3). When a sample of the same grade is heated to 180 °C and left in melt at 180 °C for 10 (curve *b*), 45 (curve *c*) and 100 (curve *d*) minutes, respectively, the onset of the modulus increase shifts to longer times. Differences in the onset of crystallization time can be as large as an order of magnitude. The shift in plateau modulus to higher values on going from curve *a* to *d* show an increase in the number of entanglements per chain with increasing residence time of the sample in the melt. From here it is concluded that with the increasing number of entanglements per chain the time required for the onset of crystallization increases.

On melting the disentangled nascent crystals slowly, a heterogeneous melt is evolved possessing disentangled and entangled domains. To recall NMR studies performed on the

heterogeneous melt show the crystallization of the disentangled domains much earlier than the entangled domains. To further investigate the influence of the disentangled regions on crystallization of the polymer, a rheological study on the heterogeneous melt is performed. Figure 5.4 shows the influence on crystallization of the heterogeneous and homogeneous entangled melt states with a different number of entanglements per unit chain.

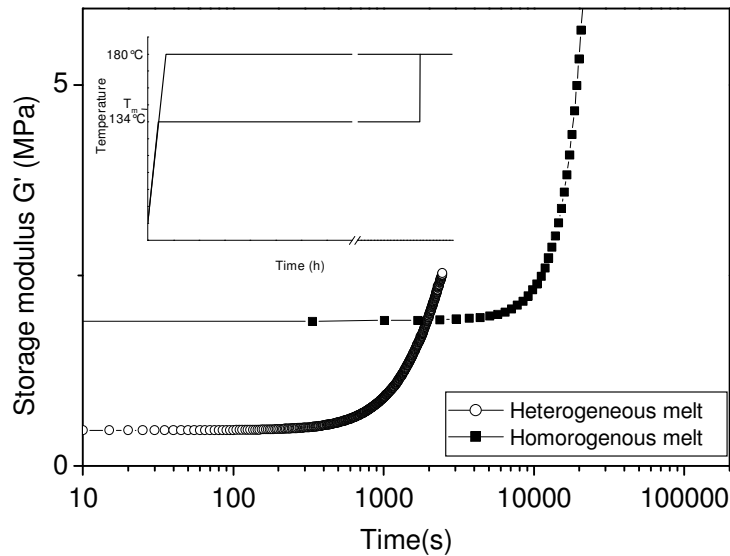


Figure 5.4: Isothermal crystallization behavior recorded by means of rheometry at 127 °C and 10 rad/s of the two different melt states, homogeneous and heterogeneous. The inlay shows the two different routes to obtain the two different melt states in the same polymer, nascent disentangled UHMW-PE.

To obtain the homogeneous entangled melt state, the disentangled nascent crystals are heated fast to 180 °C, left at 180 °C for 100 minutes and, subsequently, cooled to the isothermal crystallization temperature of (in this case) 127 °C. Whereas the sample possessing a heterogeneous distribution of entanglements is left at 136 °C for 18 hours prior to fast heating to 180 °C. This sample is left at 180 °C for 15 minutes before being cooled to 127 °C. In the heterogeneous sample, the onset of the storage modulus occurs a decade earlier than the homogeneously entangled melt. This shows a faster crystallization of the heterogeneous melt state, having on average a larger molar mass between entanglements, compared to the homogeneous entangled melt state.

Successive crystallization and melting of the heterogeneous melt state ultimately results into the homogeneous distribution of entanglements, as is shown in chapter 4. This process can be well understood by considering the rate of gain in entropy on melting.

5.3.3 Solid state drawing of disentangled melt-crystallized UHMW-PE

For polymers that show weak secondary bond interactions such as polyethylene, it is widely recognized that the solid-state (ultra) drawability is directly related to the entanglement density^{6,7} in the amorphous phase. Moreover, it is known, that the memory of a disentangled state is immediately lost upon (fast) melting, even of ultra-drawable, solution-crystallized, disentangled UHMPE samples.⁸ The experiments that supported this statement are repeated in a number of industrial laboratories, mainly because they presented an engineering and commercial disappointment, preventing the production of cheap - melt-processable disentangled, thus still ultra-drawable - polymers (that eventually possess excellent mechanical properties). The immediate loss in the modulus is explained as the entropy driven chain explosion process.^{9,10}

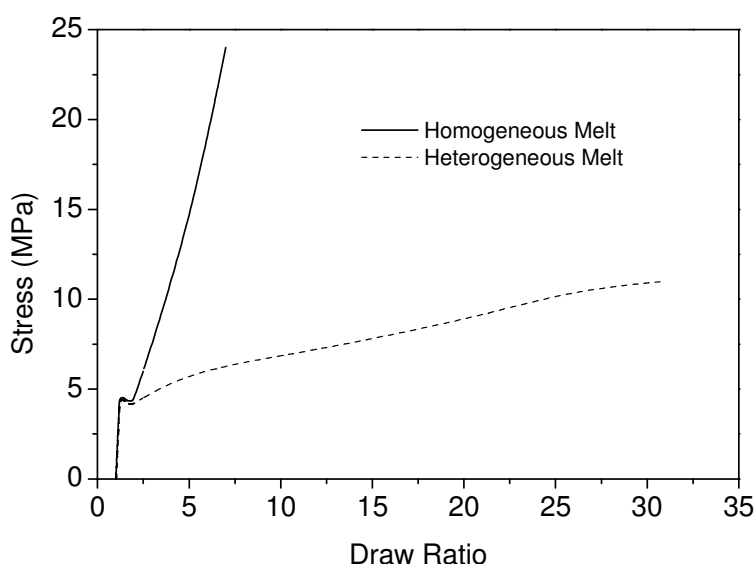


Figure 5.5: *The stress–strain curves of the polymer samples of the same grade crystallized from the heterogeneous and homogeneous melts. (Sample E, 3.6×10^6 g/mol) Experiments are performed in the solid state at 120 °C. The high draw ratio of crystals from the heterogeneous melt refers to the disentangled nature of the heterogeneous melt state. Crystals from the homogeneous melt show the usual strain hardening and limited draw-ratio.*

The easy deformation of the solution-crystallized and the nascent disentangled UHMPE samples is related to the disentangled domains in the amorphous phase of the semi-crystalline polymer.¹² In this chapter it is shown that in the heterogeneous melt, the disentangled domain crystallize faster/earlier than the entangled domains. Therefore it is anticipated that disentangled domains in the melt will form disentangled crystals. The presence of these

disentangled crystals is proved by the easy deformation of the semi-crystalline polymer in the solid state.

Solid-state drawability tests are performed on samples crystallized from the two different melt states, see Figure 5.5. From the results it is easily recognized that, compared to the samples crystallized from the homogeneous melt (obtained by fast melting nascent disentangled UHMW-PE), the samples crystallized from the heterogeneous melt (obtained by slow melting of the nascent disentangled UHMW-PE) sustain easy drawability. The easy drawability of the samples crystallized from the heterogeneous melt, is maintained even when the samples are left in the melt at 180 °C for several hours. These observations are in agreement with the retention of the disentangled domains in the heterogeneous melt obtained on slow melting of the disentangled nascent crystals (Chapter 4). Both rheology experiments depicted in Figure 4.3 and ^1H NMR experiments depicted in Figure 4.5 show, that the highly mobile disentangled domains (AB in figure 4.2) are maintained for several hours. These disentangled domains in the heterogeneous melt, when crystallized, form easily drawable crystals compared with the homogeneous samples. This drawability in the melt crystallized UHMW-PE is rather unique and unprecedented. The Young's modulus and tensile strength of the drawn tapes obtained from the heterogeneous melt are compared with the drawn tapes of the nascent disentangled UHMW-PE figure 5.6. For different draw ratios the tapes are obtained on solid state deformation of the semi-crystalline polymers at 120 °C. The thus obtained tapes are tested at 25 °C and at a test speed of 100 mm/min.

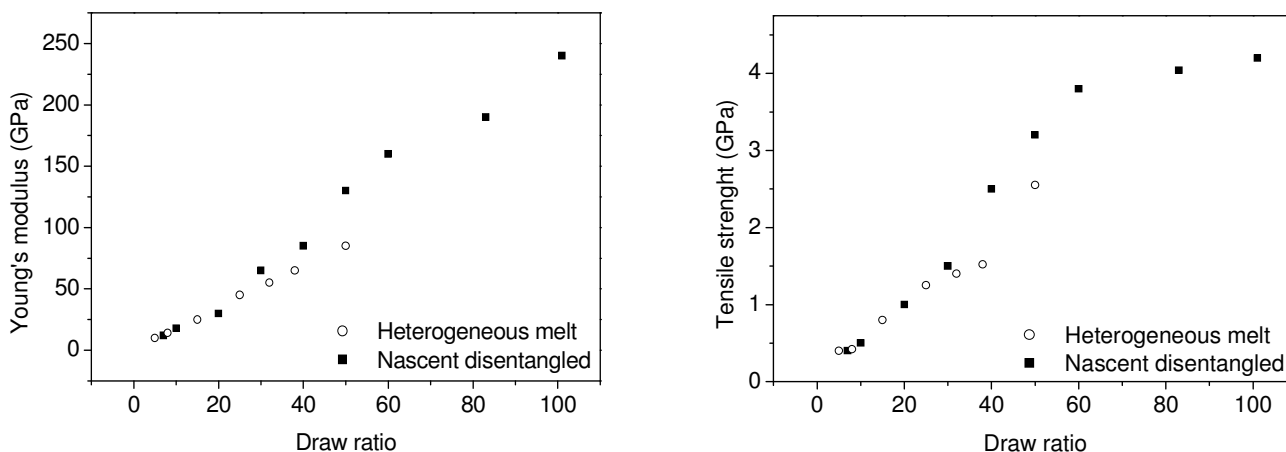


Figure 5.6: Young's modulus and tensile strength of the UHMW-PE samples crystallized from the heterogeneous melt and nascent disentangled UHMW-PE. Tensile test are performed at 25 °C and test speed of 100 mm/min. This figure serves the purpose of showing the difference between drawing UHMW-PE crystallized from a heterogeneous melt vs. sintered nascent disentangled UHMW-PE. The accuracy is limited in view of experimental inaccuracy in measuring the cross-sectional area of the tapes.

In accordance with the previous studies reported by Bastiaansen et al, both the Young's modulus and the tensile strength of the samples increases with the increasing draw ratio. The increase in the mechanical properties is explained by the increase in orientation.¹¹ The correlation of draw ratio with the mechanical properties of the nascent disentangled samples is similar to the findings reported by Bastiaansen et al.¹¹ The modulus and the tensile strength of the samples crystallized from the heterogeneous melt, show a slower increase with the draw ratio compared to the nascent samples. This difference can arise due to inhomogeneities in the distribution of entanglements present in the samples crystallized from the heterogeneous melt, where the disentangled crystals can be deformed easier than the entangled crystals. It is to be noted that the physical properties of the nascent disentangled samples are comparable with the commercially available UHMW-PE fibers, Dyneema[®],¹³ where the latter involves cumbersome solution processing.

5.4 Conclusion

On following the earlier stages of crystallization of the melt having disentangled and entangled domains, solid state ¹H NMR shows an earlier onset of crystallization of the chains residing in the disentangled domains compared to the entangled domains – indicative of the faster intra-molecular homogeneous nucleation compared to the normally anticipated heterogeneous nucleation. Rheological studies performed on the heterogeneous melt show a decade earlier onset of crystallization compared to the melt having the homogeneous distribution of entanglements. Nascent disentangled crystals provide an opportunity to follow the entanglement formation with the build up of the elastic modulus with time. Using a series of these samples, it is shown that with the increasing number of entanglements the onset of crystallization shifts to longer times for a fixed crystallization temperature.

When crystallized, the disentangled domains present in the heterogeneous melt form disentangled, easily drawable, crystals compared to the samples crystallized from the homogeneous melt. This easy deformation is indicative for the presence of (partial) disentangled crystalline domains in the solid state of sample crystallized from the heterogeneous melt. The easy deformation is maintained for even when the heterogeneously molten samples are left in the melt for several hours. These findings are in accordance with the earlier results (chapter 4), which showed a long living disentangled melt. The mechanical properties of the obtained fibers increase with the increasing orientation. This further supports the presence of disentangled crystalline domains in the samples crystallized from the heterogeneous melt.

5.5 References

1. Khanna, Y.P. *Macromolecules*, **1993**, 26, 3639.
2. Boutahar, K.; Carrot, C.; Guillet, J. *Macromolecules*, **1998**, 31, 1921.
3. Strobl, G. *Eur. Phys. J. E*, **2005**, 18, 295.
4. Hu, W.; Frenkel, D.; Mathot, V.B.F *Macromolecules*, **2003** 36, 8178.
5. Rastogi, S.; Lippits, D.R.; Peters, G.W.M.; Graf, R.; Yao, Y.; Spiess, H.W. *Nature Mat.*, **2005**, 4, 635.
6. Smith, P.; Lemstra, P.J. *Makrom. Chem.*, **1979**, 180, 2983.
7. Smith, P.; Lemstra, P.J. *J. Mater. Sci.*, **1980**, 15, 505.
8. Bastiaansen, C.W.M.; Meijer, H.E.H.; Lemstra, P.J. *Polymer*, **1990**, 31, 143
9. De Gennes, P. G. *C. R. Acad. Sci. Paris II*, **1995**, 321, 363.
10. Barham, P.; Sadler, D.M. *Polymer*, **1991**, 32, 393
11. Lemstra, P.J.; Bastiaansen, C.W.M; Rastogi, S.In: Salem DR (ed) *Structure formation in polymeric fibers*. Hanser, **2000**,185.
12. Bastiaansen, C.W.M. *Ph.D. thesis* **1991**
<http://alexandria.tue.nl/extra1/PRF7B/9104295.pdf>
13. Data reported here has been obtained on the commercially available DSM Dyneema[®] fiber.

Chapter 6

Implications of the melting kinetics on the melt state of the solution-crystallized UHMW-PE

From the series of experiments reported in previous chapters, it is evident that chain folding in the amorphous phase plays an important role on the melting behaviour of nascent polymers (Chapter 3). On melting of the nascent disentangled polyethylenes, fast or slow, different melt states having a homogeneous or a heterogeneous distribution of entanglements can be obtained. The different distributions of entanglements in the melt have a profound impact on the chain dynamics (Chapter 2, 4), and on the crystallization behaviour (Chapter 5). Another route to obtain the disentangled polymer is by dissolution of an entangled polymer in a good solvent. When crystallized from a semi-dilute solution, regularly stacked disentangled crystals are formed, having disentangled adjacently re-entrant folds in the amorphous region. In this chapter, the implications of the amorphous region on the melting behavior of the solution-crystallized polymers are discussed. The observations are that similar to the nascent disentangled crystals, it is feasible to melt these crystals by consecutive detachment of chain stems from the crystal substrate. Depending on the annealing temperature a clear distinction in the different melting processes is observed. A difference in the activation energies arises for the consecutive detachment of chain stems or melting of chain stems in clusters. The differences in the melting behavior, revealed during different heating rates, have consequences on the chain dynamics. Unlike the nascent disentangled sample where the modulus builds up with time, the immediate formation of entanglements occurs on fast heating of the solution-crystallized samples. In spite of the disentangled amorphous regions, in the nascent and solution-crystallized samples, the remarkable difference in the rate of entanglements formation is attributed to the differences in the stacking of crystals, prior to melt.

6.1 Introduction

In the previous chapters, the influence of the amorphous phase on the melting behaviour and its consequences on the chain dynamics in the melt state is discussed. Materials investigated are nascent disentangled polymers obtained by controlled synthesis. Another route to obtain disentangled polymers is by dissolution of entangled polymer in a good solvent. When crystallized from a semi-dilute solution, regularly stacked disentangled crystals are formed.

Reproduced in part from:

Rastogi, S.; Lippits, D.R. Terry A.E.; Lemstra P.J. In: Reiter G.; Strobl G.R. (ed) *Progress in understanding of polymer crystallization*. Lecture notes in physics, **2006**, 285.

Due to the removal of entanglements these so called solution-crystallized polymers can be drawn to high draw-ratios of over 100 times into fiber and tapes.^{1,2} The thus obtained fibers possess excellent modulus and tensile strength.

In the past, attempts were made to use disentangled solution-crystallized polymer for the melt-processing of the intractable UHMW-PE. The basic idea has been that the disentangled molecules will require considerably long time to (re)establish the equilibrium entanglement network. However, against the predictions, within the given experimental time, no memory effect of the disentangled state could be obtained. It was shown that after melting and crystallization of the solution-crystallized polymer the high drawability ($DR > 100$) in the solid state is lost, even when the polymer was left in the melt for a few seconds. The thus crystallized samples behave similar to the entangled melt crystallized samples.³⁻⁵ Rheological properties of the melt obtained from the initially disentangled crystals, such as G' , G'' and $\tan \delta$ are identical to the fully entangled melt state. In view of the long relaxation times for these high molar masses the absence of any memory effect was rather puzzling.

The immediate gain in modulus was addressed experimentally by Barham and Sadler⁶ and theoretically by de Gennes.⁷ Using neutron scattering techniques and deuterated polyethylene's, Barham and Sadler concluded that upon melting of the solution-crystallized polyethylene's, the radius of gyration, which is rather low for the folded-chain crystals, 'jumps' to its equilibrium value corresponding to a Gaussian chain (random coil). To explain the instantaneous increase in the radius of gyration, the authors introduced the term 'coil explosion', and suggested that the kinetics of this process is independent of the molecular weight, up to 400.000 g/mol. Considering a mono-molecular crystal, de Gennes pointed that, if a chain starts to melt, the free dangling end of the molten chain will create its own tube and will move much faster than anticipated from the reptation theory; independent of the molar mass provided that the other end of the chain is still attached to the crystal. Whatever is the cause for chain randomization upon melting, on crystallization from the melt, the favourable drawability in the solid state is lost.

In contradiction to the findings reported on the solution-crystallized UHMW-PE, in previous chapters, it is shown experimentally that it is possible to retain the disentangled melt state on slow melting of the nascent disentangled UHMW-PE crystals. To recall, in Chapter 5, it is shown that the on "slow melting" (~ 0.1 K/min), it is possible to obtain a heterogeneous melt state where the chain ends are distributed heterogeneously in the melt, which on crystallization retain some drawability. The heating rate dependence on the entanglements formation in the melt suggests that the gain in entropy or 'coil explosion' depends on the underlying mechanism of the melting process, which is dependent on the melting rate of the crystals.

In this chapter the influence of the amorphous interphase of the disentangled solution-crystallized UHMW-PE on the melting behaviour and its implications in the polymer melt is investigated. With similar approach of the studies performed on the disentangled nascent UHMW-PE presented in previous chapters, an attempt is made to explain the differences in the entanglements formation on melting of the disentangled solution-crystallized and nascent UHMW-PEs.

6.2 Experimental

6.2.1 Materials

Experiments are performed on the nascent disentangled UHMW-PE sample of molecular weight 3.6×10^6 g/mol and polydispersity of 2.8 (Sample E in Table 2.2). Solution-crystallized films are obtained on dissolving the degassed polymer powders at 135 °C in xylene⁹. 0.1 wt% anti-oxidant based on UHMW-PE is added to the solution. The hot solution is quickly transferred to an aluminum tray and left to cool slowly under quiescent conditions. Upon cooling, a gel is formed which is stapled onto a cardboard to prevent lateral shrinkage. The gel is left to dry for a week in a fumehood. The dry film is subjected to the experimental investigation. It has to be noted that all the experiments presented in this chapter have also been performed on the commercial available Montell 1900CM (M_w 4.2×10^6 g/mol, PDI 8). Since the results are similar only the work on the initially disentangled nascent Sample E is presented. The experiments on the polyethylene fiber are performed on the Dyneema[®] SK75, grade 538.

6.2.2 Experimental techniques

Differential scanning calorimetry (DSC)

DSC is performed using a standard Perkin-Elmer DSC-7. Samples of 0.7-2.0 mg mass is weighed with a precision balance and encapsulated in standard (crimped) aluminium pans of known mass. An identical empty pan is used as a reference. Nitrogen is purged at a rate of 25 ml/min. DSC is calibrated using indium and tin.

Rheometry

Oscillatory shear measurements in the linear viscoelastic regime are carried out on a Rheometrics ARES strain controlled spectrometer for a broad range of temperatures (140 °C-220 °C) angular frequencies ω (from 0.001 to 100 rad/s), and constant strain of 0.5 %. To follow the entanglements formation in the melt, the build-up of the plateau modulus with time is investigated. Prior to measurement, the disentangled nascent powders are first

compressed at 50 °C and 200 bars and the resulting disks of 8 mm diameter and 1 mm thickness are heated with in an ARES rheometer with the desired heating rate to 145 °C. Thereafter the samples are heated fast (~ 30 K/min) to 180 °C, and the modulus is followed in time at a constant strain of 0.5 % at a fixed frequency of 10 rad/sec or 100 rad/sec. The frequency is chosen to be in the plateau region of the fully entangled material. More detailed information of the experimental rheology of UHMW-PE can be found in the Appendix.

Solid state ¹H NMR.

NMR experiments are carried out without sample rotation on a Bruker DMX spectrometer operating at a ¹H NMR frequency of 500 MHz and equipped with a special (2-mm MAS) probe head that resists temperatures above 150 °C. The transverse spin-spin relaxation time T_2 is measured using a Hahn echo pulse sequence; 90° - τ - 180° - τ -acquisition, with a variable τ time starting from $\tau=2\ \mu\text{s}$. The repetition time is 3 s. ¹H NMR transverse relaxation functions are obtained from the total integral of the spectra after Fourier transformation, phase- and baseline correction.

To follow the formation of entanglements of the initially disentangled solution-crystallized melt, the samples are heated with 1 K/min inside the NMR spectrometer from 120 °C to 145 °C. Thereafter the samples are heated fast (10 K/min) to 160 °C and the experiment is started. A short Hahn echo experiment with 8 different echo times is used to follow the time dependence of the transverse spin-spin relaxation with 5 minutes interval.

6.3 Results and discussion

6.3.1 Crystal morphology of solution-crystallized UHMW-PE

To explain the differences in the entanglements formation on melting of the solution-crystallized and nascent UHMW-PE, it is essential to recall the morphological differences between the nascent disentangled UHMW-PE obtained in the powder-form on synthesis, and the solution-crystallized UHMW-PE films obtained on the slow evaporation of the solvent.

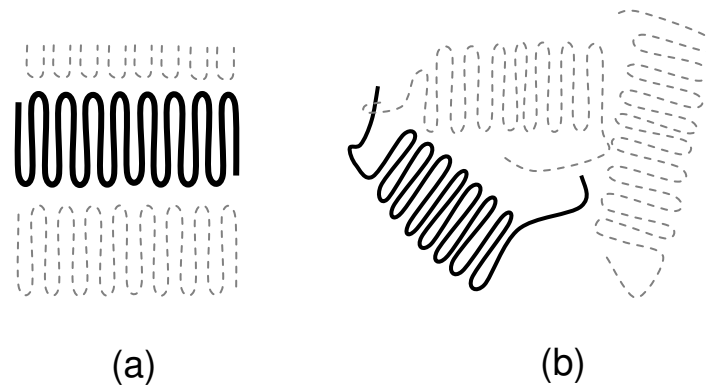


Figure 6.1: A simple 2D model envisaging the crystal stacking of (a) solution-crystallized disentangled polymer chains (after Rastogi et al.),¹⁰ and (b) nascent disentangled polymer chains. For the sake of simplicity the entanglements are not depicted as in figure 1.3.

Contrary to the solution-crystallized UHMW-PE, where crystals of equal thicknesses are regularly stacked (Figure 6.1a), in the nascent disentangled UHMW-PE, the as synthesised crystal flakes precipitate in the solvent, causing a non-regular stacking of the polymer crystals (Figure 6.1b). Consequence to the regularly stacked crystals, the solution-crystallized polymer thickens on annealing via lamellar doubling. Rastogi et al.¹⁰ observed by in-situ synchrotron measurements that upon heating the dry solution-crystallized films, above the alpha relaxation temperature, around 110 °C, the lamellar thickness doubles the initial value, from 12.5 nm to 25 nm. Some loss in the well-stacked lamellar arrangement after the doubling process (Figure 6.2) is observed. However, the drawability of the annealed solution-crystallized films is maintained even after the lamellar doubling. The retention of the drawability suggests the absence of entanglements formation.¹¹ These results suggest that regular stacking is a prerequisite for lamellar doubling, where the crystal thickens twice to its initial value even on fast heating (30 K/min).

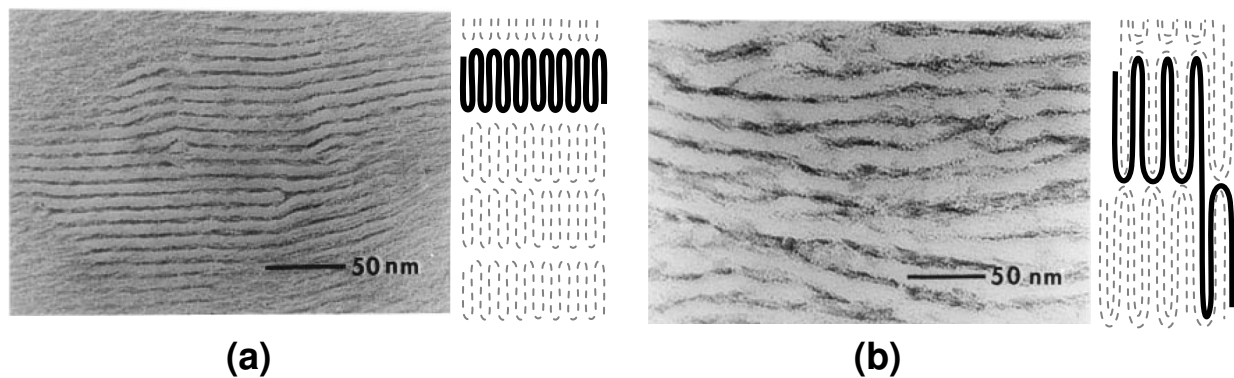


Figure 6.2: Electron micrograph (adapted from reference 10) and schematic representation for (a) the regular stacking of lamellar crystals of solution-crystallized UHMW-PE, below 110 °C and (b) after lamellar doubling above 120 °C.

Compared to the solution-crystallized samples the annealing behavior of the nascent disentangled UHMW-PE is very different. No lamellar doubling is observed but if the samples are left to anneal for long time (~ 20 hrs) at temperatures close to the melting point increase in the lamellar thickness up to 26 nm is observed.^{11,12} The differences in the chain mobility along the c-axis in the solid state of the two samples suggest remarkable morphological differences. Such morphological distinctions lead to differences in the melting behaviour of the solution-crystallised and the nascent polymer.

6.3.2 Melting behaviour of the solution-crystallized UHMW-PE

As is discussed in chapter 3, the amorphous interphase plays an important role in the melting behaviour of polymers. It is shown that nascent polymers having adjacent re-entrant folds in the amorphous, can “*feel*” its chain length. Therefore the observed melting temperature of nascent UHMW-PE of 141 °C for conventional heating rates, is 6 °C higher as anticipated from the Gibbs-Thomson equation for polyethylene⁷ [$T_m = 414.2 - 259.7/l$] for a lamellae thickness of 26 nm. On second melting the melt-crystallized having non-adjacent folds in the amorphous, melt at the temperature predicted by Gibbs-Thomson. Furthermore it is shown that the melting aspects involved in UHMW-PE can not be explained by existing thermodynamic concepts alone. Depending on the time the UHMW-PE samples are provided to melt, the melting mechanism/temperature can be different.

To recall, the lamella thickness of UHMW-PE crystallized from solution, double its initial value on annealing below the melting temperature to 25 nm. The melting temperature predicted from the Gibbs-Thomson equation for that lamellae thickness is 131 °C, 5°C lower than the experimentally observed melting point of 136°C. Furthermore, the high melting temperature of 136 °C, is lost on second heating where a melting temperature of 131 °C is measured¹⁶ The discrepancy of 5°C between the observed first melting point and that predicted by the Gibbs Thomson equation can not be explained by superheating effects alone, therefore it is indicative for the influence of kinetics in the melting processes similar to the nascent UHMW-PE.

To get insight in the melting mechanism, annealing experiments, below the melting point of 136 °C are performed on the solution-crystallized polymer similar to the experiments presented in chapter 3.5. In DSC, the sample is kept for a certain time at annealing temperatures ranging from 127 °C to 134 °C. Consequently, the sample is cooled to room temperature and reheated (at 10 K/min) to 150 °C. Two melting peaks are observed; at 131 °C and 136 °C, (Figure 6.3, inset).

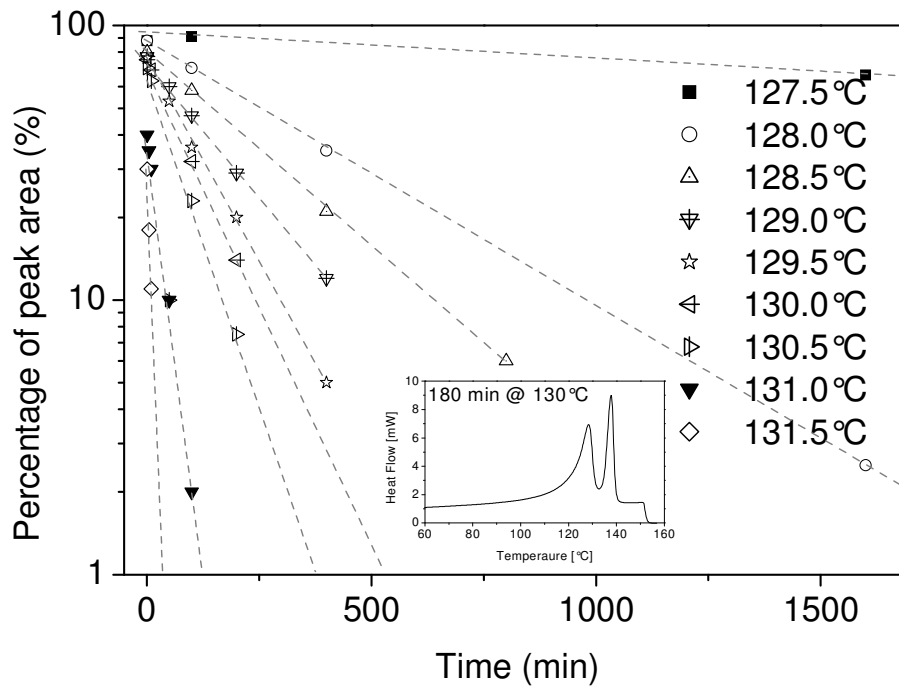


Figure 6.3: The relative decrease in the area of the 136 °C melting peak of the disentangled solution-crystallized UHMW-PE with annealing time at different temperatures. In the temperature region (127 °C – 132 °C) a first order behavior with only one time constant for each annealing temperature is observed. Inlay in the figure shows a DSC curve on heating a sample that is annealed for 180 min at 130 °C.

The peak at 131 °C is associated with the melting of material crystallized during cooling from the annealing temperature, and the peak at 136 °C to crystal domains in the initial state. The ratio between the areas of the two peaks changes with the annealing time at the given annealing temperature. Figure 6.3 shows an exponential decrease of the high temperature peak area with time having one characteristic time constant. Starting from a time law of Debye (Arrhenius) type for the fusion process the enthalpy change reads $H(T, t) = H_0(T)e^{-t/\tau(T)}$, and the time constant (τ) can be related to an activation energy by $\tau = \tau_0 e^{E_A / RT}$.

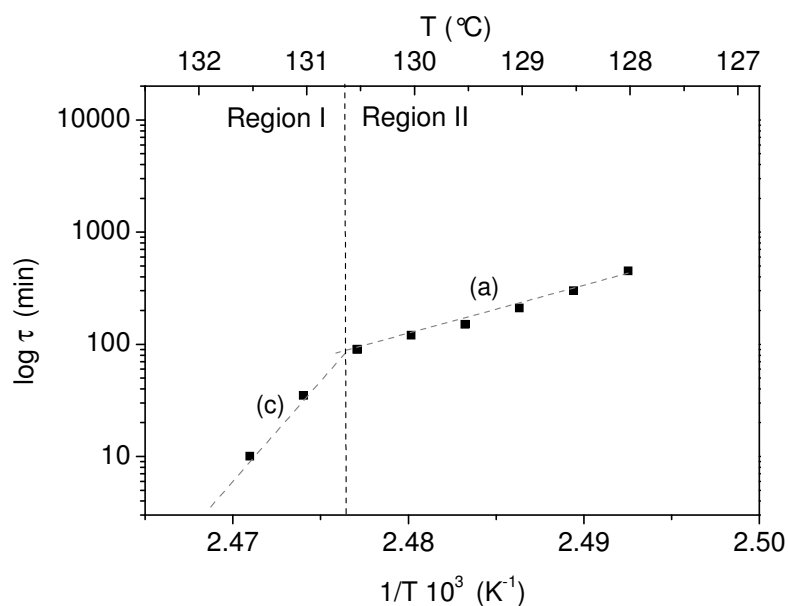


Figure 6.4: Arrhenius plot for solution-crystallized UHMW-PE. The different relaxation times at the given annealing temperatures (determined Figure 6.3) show two activated processes. The activation energy can be determined from the slope.

Figure 6.4 summarizes the relaxation times determined from Figure 6.3. In the explored temperature region, two different slopes (a) and (c) of the relaxation times are observed in the $\log \tau$ versus $1/T$ plot, indicating the involvement of two different activation energies at two different temperature regimes. Slope (c) for temperatures above 131 °C (region I) corresponds to activation energy of 4200 ± 1000 kJ/mol. Slope (a) for temperatures below 131 °C (region II) corresponds to activation energy of 700 ± 50 kJ/mol.

The presence of the two activation energies suggests the involvement of two different melting processes in the solution-crystallized polymer. The activation energy of (a) 700 ± 50 kJ/mol can be assigned to consecutive detachment of chain segments of $\sim 30 \pm 2$ nm (with enthalpy of fusion of a single CH_2 group 2.7 kJ/mol and C-C distance in the orthorhombic lattice along the c-axis 0.127 nm^{17}). This equals roughly one chain (stem) at the lateral surface of the lamellar crystal. These results suggest that, by providing the solution grown crystals enough time at 128 °C, the equilibrium melting point predicted by the Gibbs-Thomson equation of alkanes of 25 nm thickness; It is possible to isolate melting of the crystal fold planes, by removal of single chain stems from the crystal substrate. In this way the crystal lattice shrinks from the both sides. At temperatures above 131 °C, the activation energy of slope (c) corresponds to 4200 ± 1000 kJ/mol. This value is comparable to that of the nascent UHMW-PE samples presented in Figure 3.6, Table 3.2. This large activation energy is again associated to the breakdown of the crystal lattice by simultaneous randomization of at least 7-8 stems. This

result suggests that in the case of solution-crystallized UHMW-PE with an amorphous phase having adjacent or tight folds, the part of the chain that melts simultaneously corresponds to a length of 7-8 times the lateral thickness. If we assume the melting process to be caused by conformational dynamics a greater number of $-\text{CH}_2-$ groups are involved in the melting process of solution-crystallized UHMW-PE than in the melt crystallized sample with a random distribution of chains in the crystal and large loops in the amorphous phase. Since the number of $-\text{CH}_2-$ groups involved in the melting process is greater than the number of CH_2- groups present along the crystal thickness of the solution-crystallized UHMW-PE the chain “feels” its length. These results are further supported by solid state NMR studies by Yao et al¹⁸, which conclusively demonstrate that in the amorphous phase of the solution-crystallized sample CH_2- groups adopt restricted chain conformations compared to the melt crystallized samples. This is indicative for the presence of tight folds in the amorphous phase of the solution-crystallized samples.

If the number of $-\text{CH}_2-$ groups of the respective molecule, incorporated into the crystallite, is taken rather than its thickness, the Gibbs-Thomson equation is able to predict the high melting point of the solution-crystallized UHMW-PE.

When compared to the nascent disentangled UHMW-PE presented in Figure 3.6 the slopes (a) and (c) in Figure 6.4 are similar to the slopes (a) and (c) in Figure 3.6, whereas the slope (b), related to the melting of 3 chain stems of Figure 3.6 is absent. The absence of the slope (b) in Figure 3.6 suggests that within the temperature region of 128 °C to 130.5 °C the melting in the solution-crystallized samples mainly occurs by removal of single chain stems from the crystal substrate. Since slopes (a) and (c) in Figure 6.4 and Figure 3.6 are similar and the crystal thicknesses are comparable, this suggests that the activation energy required for the respective processes, namely, the removal of single chain stems from the surface followed by its diffusion in the melt (slope (a)) as well as the breakdown of larger parts of the crystal lattice (slope (c)), occurs independently of the morphological distinctions in the two samples.

However, the temperature regions where these melting processes occur in solution crystallized films are shifted parallel by nearly 5 K along the temperature axis, compared to the nascent material. To quote, a similar difference in the melting temperature of crystals of the same thickness is observed for alkanes and linear polyethylenes. For example, the melting temperature of alkanes of 25 nm thickness is 127 °C, whereas the melting temperature of linear polyethylene of similar thickness is 131 °C. This can be explained because of the differences in the topological constraints and the differences in the surface free energies. For example, in alkanes there are no entanglements, and the chains are always extended if the number of CH_2 units is less than 140.

Therefore, in the case of normal heating rates (10 K/min) the solution-crystallized UHMW-PE crystals melt at 136 °C and are consequently superheated by 8 °C. At 136 °C the crystal coil ‘explodes’. If melting occurs from the crystal sides by slow melting, this ‘coil explosion’ is circumvented. Melting in the different temperature regions (or with different heating rates) has implications on the chain dynamics and consequently the rate of entanglements formation from the disentangled to the entangled state.

6.3.3 Heating rate dependence on the chain dynamics –from the disentangled to the entangled melt.

To follow the entanglements formation in the melt, the build-up in the plateau modulus with time is investigated via oscillatory shear rheometry (in the linear visco-elastic regime). The average molecular weight between entanglements, $\langle M_e \rangle$, is inversely proportional to the entanglement density. This is related to the elastic modulus in the rubbery plateau region, G_N^0 by

$$G_N^0 = g_N \rho R T / \langle M_e \rangle, \quad (6.1)$$

where g_N is a numerical factor (1 or 4/5 depending upon convention), ρ is the density, R the gas constant and T the absolute temperature. As is shown above, the influence of the heating rate on the melting kinetics of the crystals is evident. In chapter 4, it is shown that in nascent disentangled polyethylene samples differences in the chain dynamics, arise due to different heating rates. Depending on the heating rate, differences appear in the rate of the formation of entanglements which is seen as a build up of plateau modulus.

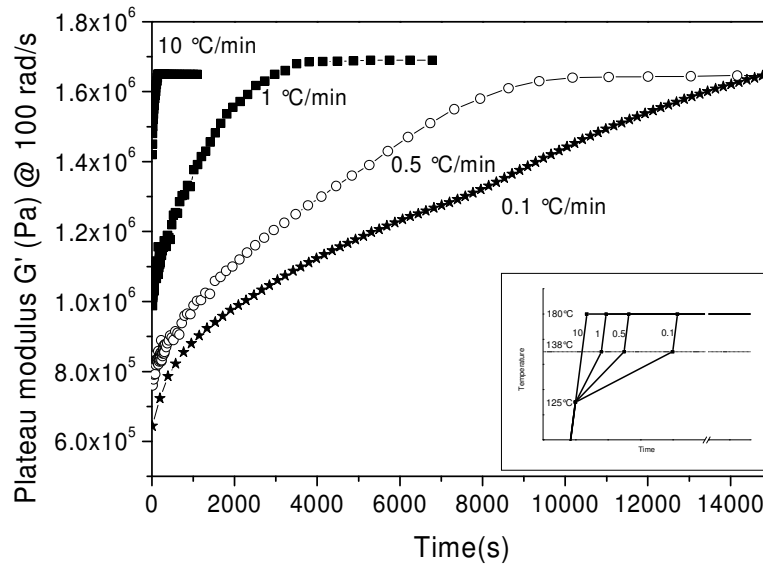


Figure 6.5: The build-up of plateau modulus in disentangled polymer melts obtained by melting solution-crystallized UHMW-PE, with time. Samples compressed at 50 °C, having diameter of 8 mm, thickness 1 mm, are heated with varying heating rate (10 K/min till 0.1 K/min) from 125 °C to 138 °C and then heated fast (30 K/min) to 180 °C in the rheometer (inlay). A constant strain of 0.5 % is applied at a fixed frequency of 100 rad/s. The frequency is chosen to be in the plateau region.

In Figure 6.5 the heating rate dependence of the formation of entanglements in solution crystallized samples is shown. The inlay in the figure describes the thermal history of the four different samples heated at a rate of 10 K/min, 1 K/min, 0.5 K/min, 0.1 K/min from 125 °C – 138 °C, respectively. The samples are heated from 138 °C – 180 °C at a heating rate of approximately 30 K/min. The heating profiles are performed in the ARES rheometer. Once the temperature of 180 °C is reached, the samples are subjected to a constant strain of 0.5 % at a fixed frequency of 100 rad/s. The frequency is chosen to be in the plateau modulus region of the fully entangled material. The change in modulus, corresponding to the entanglements formation, is followed as a function of time.

From the figure it is evident that with the increasing heating rate, the initial modulus increases. In the solution-crystallized samples, the rate of the entanglement formation is dependent on the initial state, i.e. lesser the number of entanglements at the initial state, larger is the time required for the build up of the modulus. The time required for the modulus build up to reach the fully entangled state, even for the material heated at a rate of 0.1 K/min is shorter than the reptation time required for a single chain of molar mass 4.2 million g/mol. These findings are in agreement with the proposed model of de Gennes,⁷ where he stated that the disentangled chains will reptate faster than the entangled chains.

Unlike in the solution-crystallized UHMW-PE, in the nascent disentangled UHMW-PE (even for the fast melted samples), the time required for the entanglements formation is similar to the experimentally observed stress relaxation time. These findings suggest that in the solution-crystallized samples the intermixing of the chains occurs faster than in the nascent disentangled samples. These differences are likely to arise due to the lamellar doubling in the solution-crystallized samples, which facilitates the intermixing of chains between the adjacent crystals. To investigate the melting of the solution-crystallized UHMW-PE on a molecular scale, ^1H NMR measurements are performed.

6.3.4 Melting mechanism of solution-crystallized UHMW-PE as probed by ^1H NMR

As shown in previous chapters, ^1H NMR spectroscopy is a sensitive tool to probe local mobility between the entanglements.²⁰⁻²² In the previous chapter 4, it is shown that the transverse spin (T_2) relaxation of the disentangled melt is faster than the entangled melt (Figure 4.4). Furthermore, the entanglement process causes an increase in the plateau modulus and a faster relaxation of the transverse magnetization (T_2). Both are related to an increase in entanglement density, see equations 6.1 and 4.2. The differences in the time required to reach the equilibrium state arise due to the different time-scale that the two techniques probe. To quote, the standard spin-echo experiments probe kilohertz motions through spin-spin (T_2) relaxation of the protons,²³ whereas rheology is sensitive for larger motions through chain stress relaxation. The latter requires a cooperative motion of the chain segments between the entanglements.

The time required in the spin-echo experiments to reach the equilibrium state is related to the intermixing of the chains, thereby restricting the chain conformations (i.e. local mobility between the entanglements) in the milli-second timescale. With decreasing heating-rate intermixing of the chains take longer time (Figure 4.5).

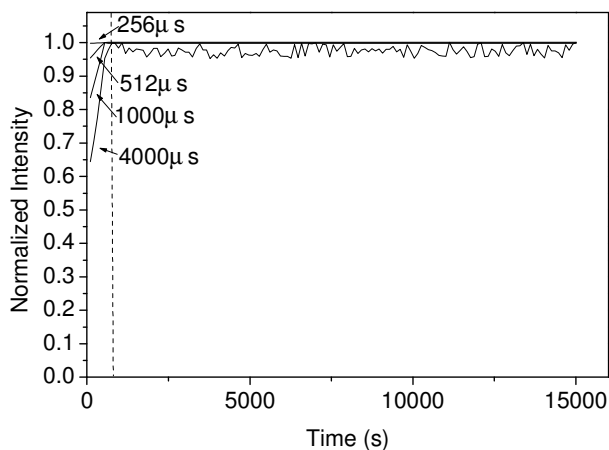


Figure 6.6

Figure 6.6: *The normalized area of the Fourier transformed peaks for different echo times at 160 °C as a function of time. The data is recorded on slow melting (heating rate of 0.1 K/min) of the solution-crystallized sample.*

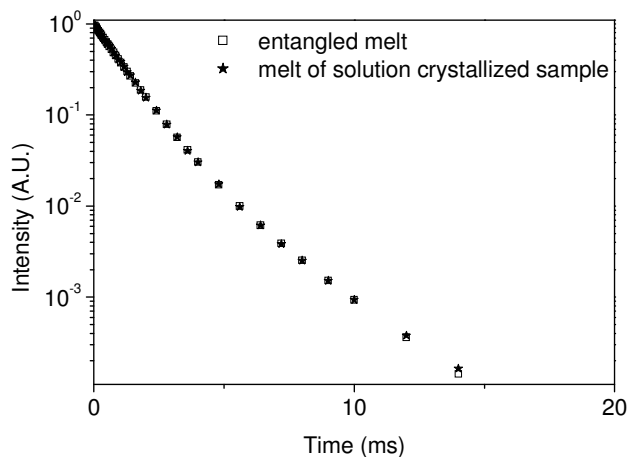


Figure 6.7

Figure 6.7: *T₂ relaxation curves of the entangled melt (unfilled squares) and the melt of the solution-crystallized sample of the same grade obtained on heating slowly (0.1 K/min) (stars). The data has been recorded at 160 °C.*

Figure 6.6 shows the time-dependence of the T₂ relaxation behavior of the melt obtained on melting of the disentangled solution-crystallized UHMW-PE samples at a heating rate of 0.1 K/min. The figure depicts the time dependence of the area of the Fourier transformed peaks at 4 different echo-times. From the data it is apparent that the T₂ relaxation behavior is constant in time. (Differences at the initial time are related to the time required for the sample to reach the thermal equilibrium). The T₂ relaxation curve of the thus obtained melt is compared with the fully entangled melt of a sample of the same grade. Figure 6.7 conclusively shows that the T₂ relaxation curves of both samples are the same. These observations are different from the disentangled nascent samples presented in the previous chapters, where the time required to reach the equilibrium T₂ relaxation time depends on the heating rate. While in the melt of the solution-crystallized samples the equilibrium T₂ relaxation time is reached immediately, in the nascent disentangled sample (even when the sample is heated fast) some time is required to reach the equilibrium state.

From here it is concluded that in the melt of the solution-crystallized samples, local chain restrictions, having a lifetime greater than a millisecond, are present. Therefore it is suggested that independent of the heating rate, in the melt the chains are intermixed. The presence of the intermixed chains in the melt arises due to the specific morphology of the solution-

crystallized samples. Independent of the heating rate, the morphology facilitates lamellar doubling prior to melt, thus providing the interdigitation of the chains in the solid state between the adjacent crystals. The interdigitation process in the solid state facilitates the intermixing of chains on melting, which invokes the immediate restriction in the chain conformations between the entanglements. This unique lamellar doubling is absent in the nascent powders, where no regularly stacking of the crystals exist. Therefore no interdigitation of the chains in the solid state occurs. Thus on melting some time is required for the intermixing of the chains, i.e. some time is needed to reach the equilibrium entangled state.

In the melt of the solution-crystallized samples, since the chains are already intermixed and restrictions in the chain conformations are present, the cooperative motion desired for the translational mobility is facilitated. Thus due to the feasible chain reptation (a) the appearance of a long lasting heterogeneous melt state is inhibited, and (b) the disentangled and the entangled domains as observed in the case of the nascent disentangled samples is absent.

These findings on the solution-crystallized samples strengthen the concepts laid in the previous chapters of this thesis.

6.3.5 Melt rheology of the disentangled UHMW-PE Fibers

Another example of disentangled polymers are the extended chain crystals, which can be obtained either via intervention of the hexagonal phase²⁴⁻²⁸ or via mechanical deformation of the disentangled crystals in the solid state.² To follow the entanglements formation in the extended chain crystals, rheological experiments are performed on the Dyneema[®] fibers. These fibers, made from UHMW-PE, exhibit high modulus and high strength due to the covalent bonding along the fiber direction. Since the modulus and the strength approaches the theoretical value for the polyethylene crystals, it is assumed that these fibers constitute extended chain crystals, making them an ideal material to follow the entanglements process.

It is to be noted that the melting process of the extended chain crystals would be remarkably different than the folded chain crystals. On melting, while the extended chain crystals will contract, the folded chain crystals will explode.

Samples for the rheological studies are prepared by bundling the fibers together. To avoid any air between the fibers, the fibers are compressed at 200 bars at 137 °C. Surface melting of the fibers at these temperatures facilitates a good coherence within the sample. Parallel plates of 12 mm diameter and 1 mm thickness are cut from the compressed samples. The samples are placed in the rheometer and are heated to 180 °C at a heating rate of 10 K/min.

At 180°C, the storage modulus at 100 rad/s is followed in time for a constant low strain of 1 %.

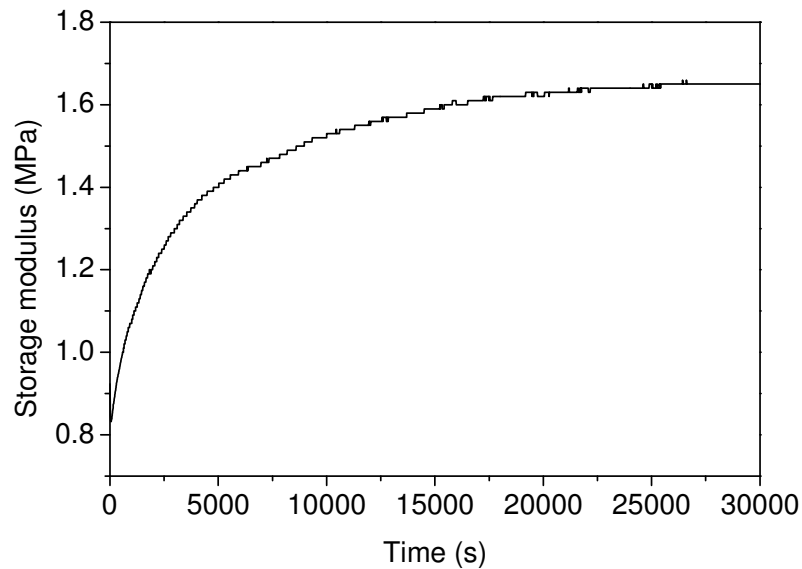


Figure 6.8: *The storage modulus in the compressed samples of the UHMW-PE fibers as a function of time at 180 °C. Measurements are performed at constant frequency of 100 rad/s and 1 % strain. The increase in the storage modulus is associated to the entanglements formation in the disentangled melt.*

The Figure 6.8 shows the entanglements formation in the initially disentangled melt obtained on melting of the extended chains in the fiber. The figure shows that the time required to reach the thermodynamically equilibrium entangled state is approximately 25000 s. This value is in agreement with the anticipated stress relaxation time for a molecular weight of $1-2 \cdot 10^6$ g/mol. These results suggest that in this case, the entanglements formation occurs by chain reptation. It has to be noted that the rheology experiments on these fibers are difficult, due to the considerable stress relaxation of melting, and the unavoidable air bubbles in the viscous polymer melt, thus no hard conclusion can be drawn. However the modulus buildup is in agreement with the entanglements formation process seen in the disentangled melt of the nascent and solution-crystallized UHMW-PE.

6.4 Conclusion

Similar to the disentangled nascent UHMW-PE in Chapter 3, the time dependence in the melting behavior of the solution-crystallized UHMW-PE samples cannot be explained by the thermodynamics alone. The implications of the melting kinetics on the resultant melt state are investigated. To summarize, when given enough time below the normally observed melting peak temperature of 136 °C (at a normal heating rate of 10 K/min), it is feasible to melt the solution-crystallized samples by simple consecutive detachment of chain stems from the crystal substrate. Depending on the annealing temperature a clear distinction in the different melting processes is observed. A difference in the activation energies arises for the consecutive detachment of chain stems or melting of chain stems in clusters.

The consecutive detachment of chain stems occurs at the melting point predicted from the Gibbs-Thomson equation, whereas higher temperature or time is required if the chain has to overcome the topological constraints. The differences in the melting behavior, revealed during different heating rates, have consequences on the chain dynamics.

Rheology experiments show that the modulus buildup depends on the heating rate, i.e. slower the heating rate, the slower is the buildup of modulus (or the entanglements formation). Unlike the nascent disentangled polymers, even on slow heating, no long living heterogeneous melt is observed.

The spin-echo NMR experiments performed on the melt show that the conformational mobility between the entanglements is restricted independent of the heating rate.

From these experiments it is concluded that in the melt of the solution-crystallized samples the chains are intermixed. The presence of the intermixed chains in the melt arises due to the specific morphology of the solution-crystallized samples. The unique morphology, lamellar stacking, facilitates lamellar doubling prior to melt. This provides the interdigitation of the chains in the solid state between the adjacent crystals. The interdigitation process in the solid state facilitates the intermixing of the chains on melting, which invokes the immediate restriction in the chain conformation between the entanglements. This unique lamellar doubling is absent in the nascent powders, where no regularly stacking of the crystals exist. In the melt of the solution-crystallized samples, since the chains are already intermixed and restrictions in the chain conformations are present, the cooperative motion desired for the translational mobility is facilitated. Thus due to the feasible chain reptation, the appearance of a long lasting heterogeneous melt state is inhibited, and the disentangled and the entangled domains as observed in the case of the nascent disentangled samples is absent.

6.5 References

1. Smith, P.; Lemstra, P.J.; Booij, H.C. *J. Polym. Sci. Part B: Polym. Phys.*, **1982**, *20*, 2229.
2. Lemstra, P.J.; Bastiaansen, C.W.M; Rastogi, S.In: Salem DR (ed) *Structure formation in polymeric fibers*. Hanser **2000**, 185.
3. Bastiaansen, C.W.M.; Meijer, H.E.H; Lemstra, P.J. *Polymer*, **1990**, *31*, 1435.
4. Lebars, P.J.R; Bastiaansen, C.W.M; *Macromolecules*, **1989**, 3312.
5. Bastiaansen, C.W.M. Ph.D. thesis , Eindhoven University of Technology, **1991**
<http://alexandria.tue.nl/extra1/PRF7B/9104295.pdf>
6. Barham, P; Sadler, D.M. *Polymer*, **1991**, *32*, 393.
7. ATHAS data bank (<http://web.utk.edu/~athas/databank/> Ed. M. Pyda)
8. De Gennes, P.G.C. *R. Acad. Sci. Paris series II*, **1995**, *321*, 363.
9. Smith, P.; Lemstra, P. *J. Mater. Sci.* **1980**, *15*, 505.
10. Rastogi, S.; Spoelstra, A.B.; Goossens, J.G.P.; Lemstra, P.J. *Macromolecules* **1997**, *30*, 7880.
11. Rastogi, S.; Lippits, D.R.; Terry, A.E.; Lemstra, P.J. In: Reiter G.; Strobl G.R.(ed) *Progress in understanding of polymer crystallization*. Lecture Notes in Physics, Springer **2006**, 285-328.
12. Rastogi, S.; Kurelec, L.; Lippits, D.R.; Cuijpers, J.; Wimmer, M.; Lemstra, P.J; *Biomacromolecules*, **2005**, *6*, 942.
13. Corbeij-Kurelec, L. Ph.D. thesis, Eindhoven University of Technology, Chain mobility in polymer systems **2001** Chapter 3 ISBN 90-386-3032-8
<http://alexandria.tue.nl/extra2/200113706.pdf>
14. Wunderlich, B.; Czornyj, G, *Macromolecules* **1977**, *10*, 906.
15. Depending on the experimental methods used, different numerical Gibbs-Thomson equations exist, see Cho, T.Y.; Heck, B.; Strobl, G.; *Colloid Polym Sci.* **2004**, *282*, 825. A difference arises because of different surface free energy values resulting in a somewhat different melting temperature of 136°C for a crystal thickness of 25nm. But such discrepancies in the calculated melting temperatures have no implications on our experimental findings.
16. Tervoort-Engelen, Y.M.T., Lemstra, P.J, *Polym. Comm*, **1991**, *32*, 345.
17. Considering 1/3rd lesser neighbor interactions on the surface than in bulk, the detachment energy and its diffusion into the melt is likely to be 2.7kJ/mol since the melting enthalpy of the bulk is 4.11kJ/molCH₂ a value obtained from the ATHAS data bank (<http://web.utk.edu/~athas/databank/welcome-db.html>).
18. Yao, Y; Graf, R; Rastogi, S.; Lippits D.R.; Spiess, H.W, **2007** , manuscript in preparation.
19. Cohen-Addad, J.P. *Prog. NMR Spectrosc*, **1993**, *25*, 1.
20. Fry, C.G.; Lind, A.C. *Macromolecules*, **1988**, *21*, 1292.
21. Gotlib, Y.Y.; Lifshits, M.I.; Shevelev, V.A.; Lishanskii, I.A.; Balanina, I.V. *Poly Sci USSR*, **1976**, *18*, 2630.
22. Brereton, M.G.; Ward, I.M.; Boden, N.; Wright, P. *Macromolecules*, **1991**, *24*, 2068.
23. Schmidt-Rohr, K.; Spiess, H. W. **1994** *Multidimensional Solid-State NMR and Polymers* (Academic, New York).
24. Bassett, D.C. *Polymer*, **1976**, *17*, 460.
25. Wunderlich, B.; Grebowicz, *J. Adv Polym Sci*, **1984** , *60/61*, 1.
26. Rastogi, S.; Hikosaka, M.; Kawabata, H.; Keller, A. *Macromolecules*, **1991**, *24*, 6384.
27. Maxwell, A.S.; Unwin, A.P.; Ward, I.M. *Polymer*, **1996**, *37*, 3293.
28. Kowalewski, T.; Galeski, A. *J. Appl. Polym. Sci.* **2003**, *44*, 95.

Chapter 7

Influence of the addition of single walled carbon nanotubes on the melt rheology of UHMW-PE

In the previous chapters an in-depth research is presented on the rheological aspects of the disentangled polyethylenes obtained by controlled synthesis. It is shown that the entanglements formation (and thereby viscosity) can be tailored by varying the melting process of the disentangled nascent crystals. The rheological properties of the UHMW-PE melt can be also influenced by the addition of the nano-particles. In this chapter the influence of single-walled carbon nanotubes (SWNTs) on the melt rheology of UHMW-PE is presented. To homogeneously disperse the single-walled carbon nanotubes in the intractable UHMW-PE matrix, the exfoliated tubes in water and a surfactant are sprayed on the fine powder of the nascent UHMW-PE. The SWNTs are adsorbed on the surface of the polymer powder. A composite film is prepared from the solution of the polymer powder dissolved in xylene. The high viscosity of UHMWPE in solution prevents coagulation of the adsorbed SWNTs. Scanning electron microscopy (SEM) of the films reveals that SWNT bundles are randomly dispersed in the UHMWPE matrix. The observed "shish-kebab" morphology in the SEM pictures of the film shows that the polymer chains tend to crystallize from solution as chain-folded crystals (kebab). The nanotube surface can act as a nucleating site (shish). The orientation of the dispersed SWNTs in UHMWPE matrix is achieved on solid-state drawing the solution-crystallized films. Crystallization of the UHMWPE melt followed by rheometry shows that the presence of SWNTs enhances the overall crystallization rate. The observed rheological behavior of the UHMWPE/SWNT nanocomposites is rather unusual. Varying the content of SWNTs, the dynamic viscosity/storage modulus shows a minimum. The decrease in viscosity is attributed to the selective adsorption of the high molar mass fraction onto the nanotubes surface. The increase in viscosity upon further increasing the nanotube content is attributed to the formation of an elastic nanotube-polymer network. The formed nanotube-polymer network is conductive at percolation threshold of 0.6 wt % SWNTs.

7.1 Introduction

The discovery of carbon nanotubes (CNTs) possessing unique electronic, thermal, optical and mechanical properties and their potential use in the next generation of composite materials has lead to considerable attention in academia and industry. CNTs have the ability to affect the material properties at low loading due to their extremely high aspect ratio (length to diameter ratio) of up to 1000.²⁻⁷ This offers CNTs an important advantage over conventional

Reproduced in part from:

Lippits, D.R.; et al. *Macromolecules* **2006**, *39*, 658.

Zhang, Q.; Rastogi, S.; Chen, D.; Lippits, D.R.; Lemstra, P.J. *Carbon* **2006**, *44*, 778.

fillers. However, for intractable polymers this potential has not been realized, mainly because of the difficulties in the solubility. In solution, strong interactions between the CNTs result in their agglomeration. Different approaches are reported to improve the dispersion of CNTs in solvents or polymers. One of the approaches is the chemical modification of the CNT surface, i.e., functionalization at defect sites. In this method, active sites are introduced onto the surface of CNT by chemical oxidation, for instance, via adding concentrated H_2SO_4 and/or HNO_3 .⁸ When required these nanotubes can be functionalized⁹⁻¹⁴. Single-walled carbon nanotubes (SWNTs) and multi-walled carbon nanotubes (MWNTs) functionalized with poly(vinyl alcohol) (PVA) in esterification reactions can be dissolved in highly polar solvents such as DMSO and water.¹⁵ Polystyrene nanocomposites with functionalized SWNTs demonstrated a percolated SWNT network structure with 1.5 wt% of SWNTs, whereas the threshold for a percolated network is 3 wt% for unfunctionalized SWNTs¹⁶. Even though chemical functionalization of CNTs improve the solubility, the method is relatively complex, especially the procedures of the separation and the collection of functionalized CNTs from by-products such as amorphous carbon and catalysts.

The dispersion of CNTs in solvents or polymers in presence of surfactants is another important method that does not require chemical reactions. A single-step solubilization scheme has been developed in which nanotubes are mixed with surfactants in low-power, high-frequency sonicators. This process enhances the exfoliation of CNT bundles without much breakage of the tubes. CNTs suspended in aqueous media as individuals or bundles surrounded by surfactants^{17,18} such as, sodium octylbenzene sulfonate, sodium dodecylbenzenesulfate (SDS), or copolymers¹⁹ (or oligomers) such as poly(m-phenylenevinylene) (PmPV), poly(aryleneethynylene)s (PEEs), poly(vinyl pyrrolidone) (PVP), Gum Arabic (a highly branched arabinogalactan polysaccharide, etc.²⁰⁻²²

CNTs in solutions can be dispersed by dissolving a polymer into the suspended solution. Zhang et al. reported that both the tensile yield strength and the tensile modulus of PVA/PVP/SDS/SWNT are approximately doubled compared to PVA.²³ Regev et al.²⁴ prepared SWNT/SDS/PS composites using latex technology, which exhibit excellent conductive properties with a percolation threshold of 0.28 wt% of SWNTs. Brittain et al. adopted a similar approach for dispersion of silicate in PMMA via in-situ suspension and emulsion polymerisation.²⁵ So far the preparation of CNT-polymer composites using the surfactant dispersion method is limited to water-soluble polymers or polymers in a latex form. The third method is direct mixing of CNT into the polymer with a twin screw melt mixer.²⁶ However, this method is limited to low viscous polymer materials.

In this chapter a spraying method similar to that is used for surface coatings in industrial applications is reported to disperse SWNTs in the intractable UHMW-PE. The rheological aspects of the thus obtained nano-composites are investigated.

7.2 Experimental

7.2.1 Materials

Experiments are carried out on purified HiPco (>95% pure) SWNTs. Two different grades of UHMW-PE are used in this study. A commercially available UHMW-PE (Montell 1900 LCM) (Grade A) with an average molecular weight of $M_w \sim 4.2 \times 10^6$ g/mol and $M_w/M_n \sim 8$ and a self synthesized UHMW-PE (Grade B) with $M_w \sim 3.6 \times 10^6$ g/mol and $M_w/M_n \sim 2.8$. Sodium dodecylbenzenesulfate (SDS) is used as a surfactant, and xylene as a solvent. Both were purchased from Aldrich. It has to be noted that contrary to the samples used in the previous chapters, these samples are both entangled.

7.2.2 Experimental techniques

Environmental Scanning Electron Microscopy (ESEM)

ESEM is used to observe the resultant morphologies of the nanocomposites. A voltage of 1 KV is used to observe the surface of polymer. Relatively good conducting SWNTs cannot be distinguished in the poor conducting polymer matrix. To enhance the contrast the samples are gold sputtered.

Rheometry

Oscillatory shear measurements in the linear viscoelastic region are performed using an Advanced Rheometrics Expansion System (ARES). Measurements are carried out using parallel plate geometry (8 mm diameter) at 160 °C in nitrogen atmosphere. Frequency sweeps with an angular velocity between 0.001 and 100 rad/s are performed in the linear viscoelastic regime at low strain of 1 %. Samples are left to equilibrate for 15 minutes prior to measurement. The obtained values are corrected for the true dimensions between the plates.

Electrical conductivity

Electrical conductivity of the nanocomposites is measured at room temperature with a two-probe method.

7.3 Results and discussion

7.3.1 Dispersion of SWNTs in UHMW-PE

To disperse SWNTs in UHMW-PE, an aqueous solution of SWNTs is prepared using SDS as surfactant, according to a reported method.²⁴ A 20 ml solution containing 0.044 g SWNTs and 1 wt% SDS based on H₂O is ultra sonicated for 15 min and then centrifuged at 3000 rpm for 20 minutes. After sonification, about 90 % of SWNTs are suspended in the aqueous solution, whereas the remainder is deposited. The morphology of the suspension of SWNTs is shown in Figure 7.1. From the figure it may be stated that the SWNTs are dispersed in the form of fine bundles with an average diameter of ~10 nm. These bundles are rather flexible to coil back, forming loops.

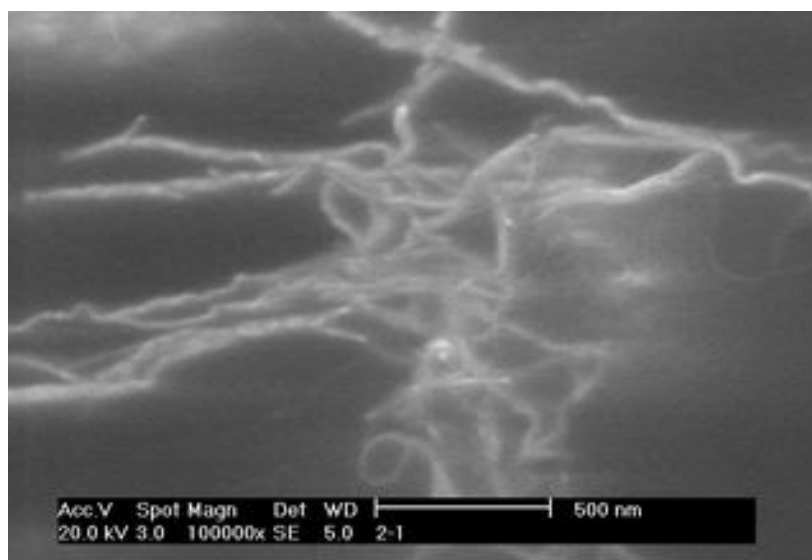
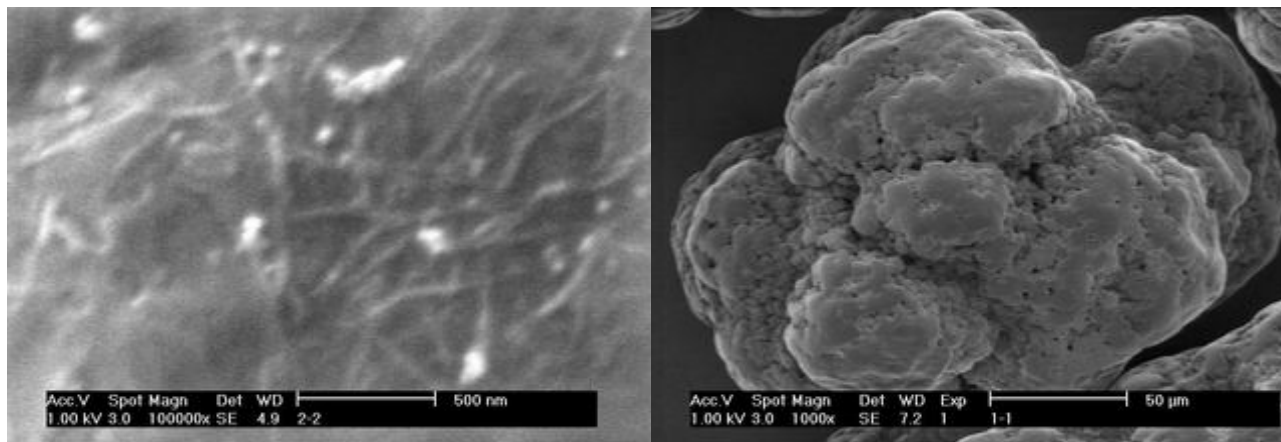


Figure 7.1: SEM image of SWNT dispersed in water, SDS is used as a surfactant for the dispersion.

The surface morphology of the nascent (i.e. directly from the reactor) UHMW-PE (Grade A) used in this work is shown in Figure 7.2a. Many micro-concaves are present on the uneven surface of the polymer powder. This morphology results in enhancement of high surface area, which facilitates the adsorption of micro-objects for example air. Therefore, in the process of casting films, to avoid air bubbles, the adopted first step is to degas air on the surface of the polymer powder by keeping the nascent powder in a vacuum container for an hour.

The aqueous solution containing 0.2 wt% of SWNTs is uniformly sprayed on the surface of UHMW-PE. On drying, SWNT coated polymer powders are obtained. Figure 7.2b shows that the SWNTs are adsorbed on the surface of the powder. The individual SWNT bundles can be distinguished. The interaction between SWNT and UHMW-PE is strong to an extent that

when the dried SWNT-UHMW-PE powders are immersed into water again, on sedimentation of the powder the water retains its transparency.



(a)

(b)

Figure 7.2: SEM images of (a) the surface morphology of nascent UHMW-PE (Grade A) powder, (b) SWNTs absorbed on the surface of UHMW-PE. The adsorption is achieved after spraying an aqueous solution of SWNTs on the UHMW-PE surface (0.6 wt% SWNTs)

Figure 7.3 depicts an image of UHMW-PE powders and their blends with different content of SWNTs. Compared to UHMW-PE, the coated powders are relatively dark because of the adsorption of the nanotubes on the surface of the polymer powder. The powders become gray when 0.1 wt% of SWNTs is adsorbed and black on the adsorption of 0.6 wt% of SWNTs.

Solution-crystallized films are obtained on dissolving the degassed coated polymer powders at 135 °C in xylene.²⁸ 0.1 wt% anti-oxidant based on UHMW-PE is added to the solution. The high viscosity of the polymer solution (1 wt% of UHMW-PE in xylene) prevents aggregation of the tubes in xylene. The hot solution is quickly transferred to an aluminum tray and left to cool slowly under quiescent conditions. Upon cooling, a gel is formed which is stapled onto a cardboard to prevent lateral shrinkage. The gel is left to dry for a week in a fumehood. The dry film is subjected to the experimental investigation. Obviously, the UHMW-PE film without SWNT is transparent, while the film with 0.1 wt% SWNTs shows translucency and the other with 0.6 wt% content is relatively opaque.



Figure 7.3: *UHMW-PE powders and SWNT-UHMW-PE powders with a weight percentage of 0.1 % and 0.6 % SWNTs, prepared by the spraying technique.*

7.3.2 Solution-crystallized films of SWNT/UHMW-PE nanocomposites

SEM images of the solution crystallized films having SWNT often reveal a ‘Shish-Kebab’ structure, Figure 7.4. Shish-Kebabs are normally observed in extensional flow field where the high molar mass fraction of UHMW-PE is extended and crystallizes into a fibrous structure (‘shish’). The remaining part that stays in solution as random coil nucleates onto the fibrous structures,²⁹ forming chain-folded crystals. In SWNT/UHMW-PE composites the nanotubes can also form fibrous like ‘shish’ structure. The folded chain crystals can directly nucleate onto the nanotube surface. From the SEM pictures alone, Figure 7.4, it is impossible to make a distinction between the different mechanisms involved in the resultant shish-kebab like structures.

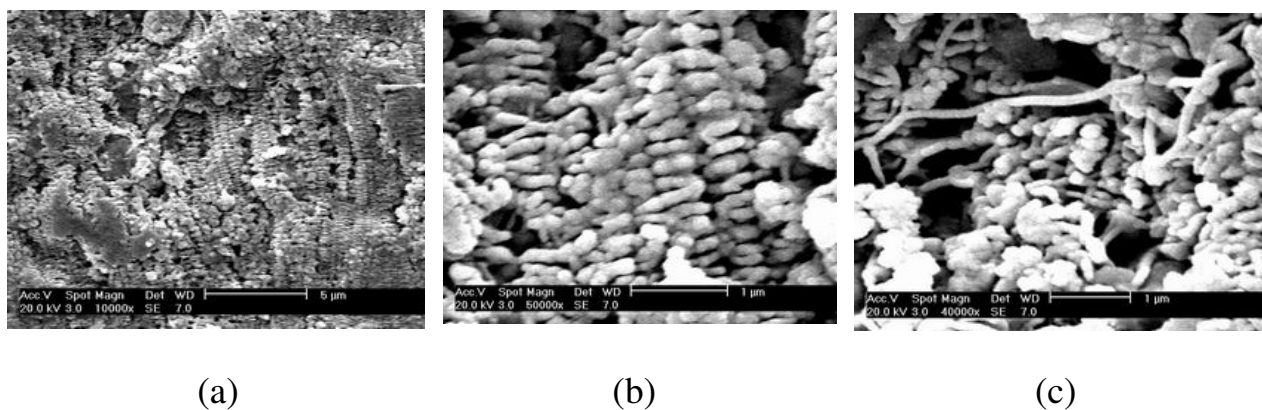


Figure 7.4: SEM images of crystallized 0.6 wt% SWNT/UHMW-PE nanocomposites. (a) Shish-Kebab like morphology in solution-crystallized films of the nanocomposite. (b) and (c) are the magnified regions of (a).

SEM images of the cross-section of the solution-crystallized UHMW-PE films with 0.6 wt% of SWNTs are shown in Figure 7.5. The undrawn films exhibit an interesting micro-structure. As shown in the Figures 7.5a and 7.5b, SWNT bundles are embedded in the UHMW-PE matrix. The bundles seemingly have a large diameter of several tens of nanometers. The sample is gold-sputtered because the polymer cannot endure a high voltage and the applied low voltage of 1 KV results into lower resolution. Therefore, considering the gold layer of about 10 nm, the SWNT bundles are likely to be about 10 nm of the diameter, comparable to the SWNT bundles in aqueous solution shown in Figure 7.1. Thus it can be stated that on dissolution of SWNT coated UHMW-PE coagulation of the SWNTs does not occur. The anticipated coagulation process of SWNTs is prevented because of the high viscosity of the UHMW-PE solution.

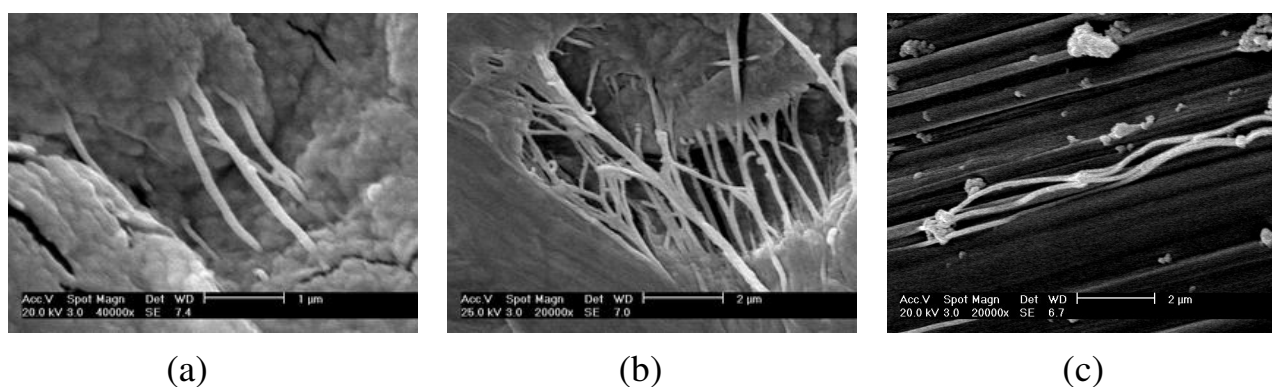


Figure 7.5: SEM images of the solution crystallized SWNT-UHMW-PE nanocomposite films with 0.6 wt% SWNTs. The image (a) is from the film that is not drawn, and (b) is from the end part of the film drawn at 120 °C. (c) is an image from a spun nanocomposites fiber

As expected, the SWNTs orient or align upon drawing the composite film. Similar to the UHMW-PE without nanotubes, the SWNT/UHMW-PE composites can be spun from solution. (Figure 7.5c) Despite the good drawability and orientation of the SWNTs, the SWNTs/UHMW-PE spun fibers do not show any enhancement in mechanical properties.

7.3.3 Crystallization of UHMW-PE in the presence of SWNTs

The influence of SWNTs during crystallization of UHMW-PE is investigated using dynamic rheometry. Compression molded samples are left inside the rheometer to relax at 180 °C for an hour. Subsequently, the samples are cooled from 140 °C to 128 °C at 1 K/min. At constant strain ($\gamma=0.1$ %) and frequency ($\omega=100$ rad/s) isothermal crystallization at 128°C is followed by measuring the elastic modulus (G'). Khanna³⁰ and Boutahar³¹ related the crystallinity of PE with the scaled modulus G' :

$$\frac{\varphi(t)}{\varphi(\infty)} = \frac{G'(t) - G'(0)}{G'(\infty) - G'(0)} \quad (7.1)$$

where $G'(0)$ is the initial modulus and $G'(\infty)$ is the plateau value reached at the end of crystallization. $\varphi(t)$ is the degree of crystallinity at time t and $\varphi(\infty)$ is the maximum degree of crystallinity of the samples.

The Figure 7.6 shows that upon increasing the SWNT content in the composite, the onset of crystallization occurs earlier. Also the speed of crystallization is faster with increasing amount of the SWNTs. The Table 7.1 shows that the onset of crystallization is 5 times earlier and 3 times faster when 0.1 wt% of SWNTs is added to UHMW-PE. Considering the applied low strain (0.1 %) the enhancement of nucleation / crystallization on addition of SWNTs suggest that the 'shish-kebab' structure, shown in Figure 7.4, is not due to the orientation of the high molar mass fraction, but is likely a result of the crystallization of the polymer chains onto the nanotube surface, where the SWNT surface acts as a nucleation site for PE chains to crystallize.

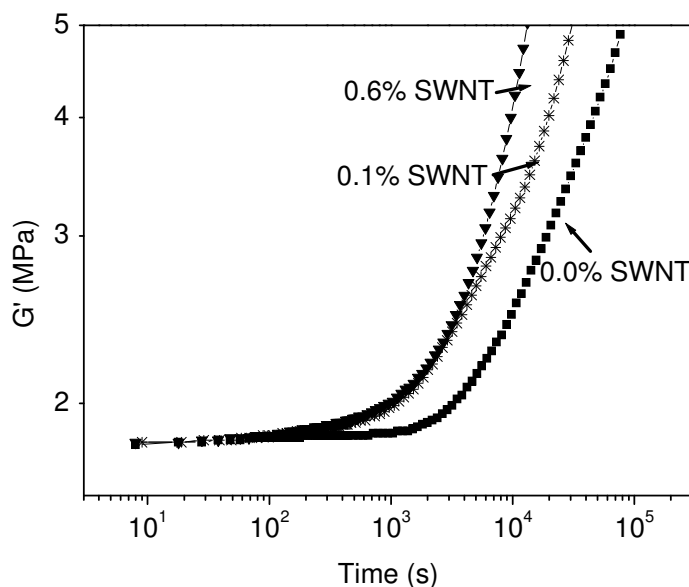


Figure 7.6: Isothermal crystallization at 128 °C of SWNTs/UHMW-PE composites at constant strain and frequency.

Table 1. Represents the onset, and crystallization speed of polyethylene in SWNT/UHMW-PE composite. The quantitative data is obtained from the Figure 7.6.

Content of SWNTs (wt%)	Onset of crystallization (s) ^a	Crystallization speed (%/s) ^b
0.0	1000	5.45×10^{-3}
0.1	210	17.4×10^{-3}
0.6	140	53.7×10^{-3}

^aDetermined at 1% of the total crystallinity within the given time of the experiment

^bDetermined at 50% of the total crystallinity within the given time of the experiment

7.3.4 Rheology of SWNT/UHMW-PE nanocomposites

Oscillatory shear measurements are performed on samples in the viscoelastic region at low strain ($\gamma=1\%$) at different frequencies ($\omega=10^{-3}$ - 10^2 rad/s) and temperatures ranging between 160°C-220°C. The master curves are obtained by using the time-temperature superposition principle. Since the SDS concentration in the nanocomposites is similar to the tube concentration, first experiments are performed to study the influence of SDS on UHMW-PE. From Figure 7.7, it is evident that there is no measurable influence of SDS on the rheological behavior of UHMW-PE on SDS loadings ranging from 0.1 to 1 wt%. In the 5 wt% SDS sample a decrease in storage modulus is observed (7 %), were the phase angle remains unchanged.

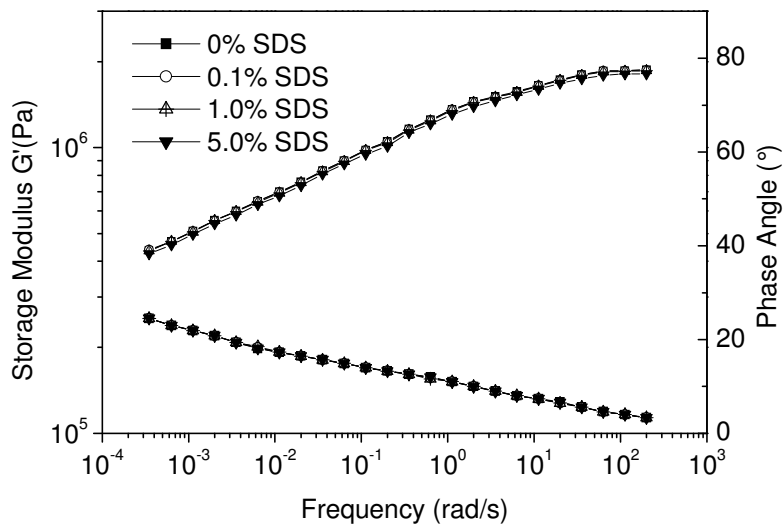


Figure 7.7: Storage modulus G' of UHMW-PE with varying concentration of SDS surfactant.

On dispersing SWNTs with SDS in UHMW-PE a complicated rheological situation arises that may be attributed to interactions between polymer and nanotubes. Such interactions are described in ref 32 and reproduced here in Figure 7.8.

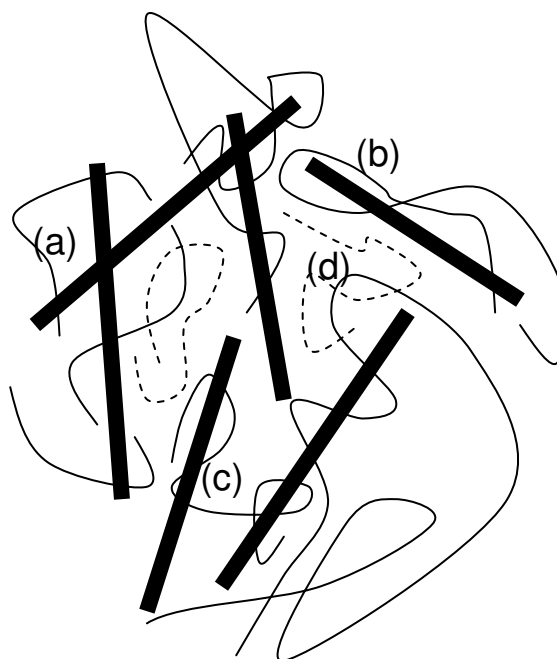


Figure 7.8: Illustration of nanotube–polymer interactions. This composite contains different network types. Nanotube–nanotube network formation (a), Nanotube–polymer interaction (adsorption) (b). Nanotube–polymer–nanotube bridging (c), Polymer–polymer network (d) (from reference 32)

The Figure 7.8 (a) depicts a SWNT-SWNT network due to overlap of two nanotubes; (b) depicts a PE-SWNT network where the polymer may be entangled or adsorbed on the nanotube; (c) depicts SWNT bridging by polymer; (d) refers to polymer network formation through temporary entanglements.

Figure 7.9a shows the master curves for the storage modulus at 160 °C varying from 0 to 0.2 wt% of SWNT/UHMW-PE composite. The figure is divided into two regions, Region I and Region II. In the Region I, considering the high molecular weight ($\sim 4 \times 10^6$ g/mol) of the polymer, the probing time in the experiment is too short for chains to relax. Therefore UHMW-PE behaves rubber-like and G' is nearly independent of frequency. The resulting plateau modulus originates from a combination of the elastic polymer network and the elastic nanotube network.

In the Region II that lies at low frequencies, a striking observation is that at these low frequencies, the storage modulus decreases considerably with an addition of low amount of SWNT in UHMW-PE ranging from 0.05 to 0.2 wt %. Whereas at high frequencies (100 rad/s) in the Region I, the storage modulus decreases to a much lesser extent.

The phase angle, δ , for the different compositions of SWNTs are depicted in Figure 7.9b. In the figure, it is seen that upon increasing the amount of SWNTs from 0 wt% to 0.1 wt% the phase angle increases in the Region II, indicating that the composite behaves less elastic than the pure polymer.

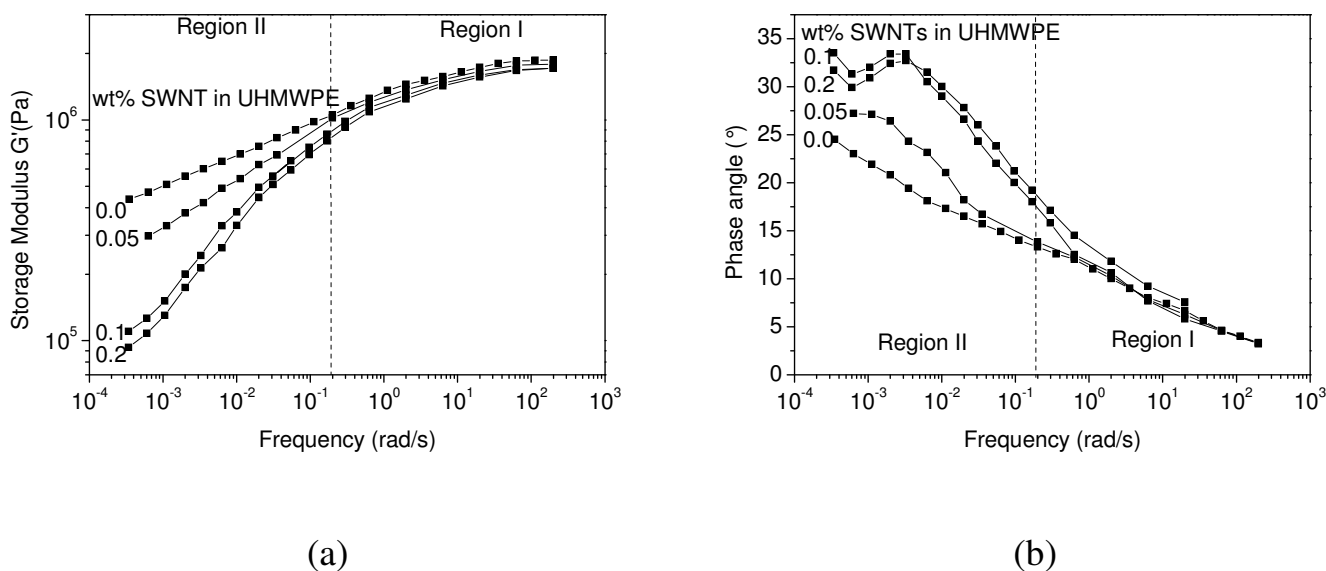


Figure 7.9: **a)** Storage modulus G' of UHMW-PE with varying SWNT content of 0-0.2 wt% at 160 °C. **b)** Phase angle of UHMW-PE with varying SWNT content of 0-0.2 wt% at 160 °C.

To my knowledge there are no studies that report the observed decrease in storage modulus for such a low loadings of nanotubes. But similar effects are reported in some recent studies where nanofillers (0.5-3 nm) are blended with linear polymers.^{1,33,34}

On increasing the SWNT content beyond 0.2 wt%, the storage modulus at low frequencies is independent of frequency, showing a second plateau in the Region II, see Figure 7.10a. It is known from literature, that interconnected structures of anisometric fillers result in an apparent yield stress which is visible in the dynamic measurements by a second plateau, as seen in the region II.³⁵ The interconnected structure (nanotube network) is described in Figure 7.8(a) In the Figure 7.10a, the second plateau is observed at low loading of 0.6 wt% of SWNTs. With increasing amount of SWNTs in the polymer matrix the second plateau modulus increases. This increase is attributed to more pronounced connectivity of the nanotubes.

The phase angle depicted in the Figure 7.10b shows a subsequent decrease with the increasing amount of SWNTs in the Region II. The phase angle goes through a maximum. The frequency at which the phase angle shows a maximum increases with increasing amount of SWNTs in the polymer matrix. The shift of the maximum to higher frequencies indicates a more dominant nanotube network with increasing SWNTs concentration. Presence of a maximum also suggests a change in the viscoelastic response with frequency -i.e. from viscous to elastic like response on going from Region I to II.

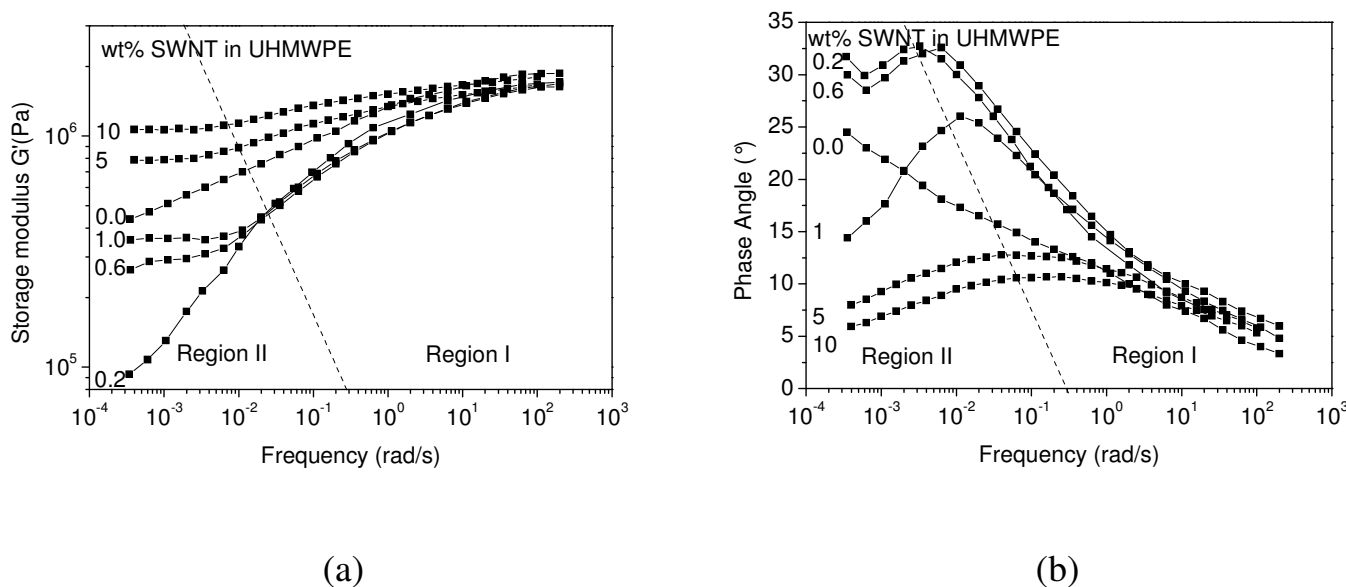


Figure 7.10: Storage modulus G' and phase angle of UHMW-PE filled with different concentrations of SWNTs, at 160 °C. (a) The storage modulus varies with the amount of nanotubes. Distinct variations at low and high frequencies are observed. (region II and I) The corresponding changes in the phase angle are depicted in (b).

These observations are similar to liquid-to-solid or liquid-to-gel transitions observed by Winter et al³⁶ in their gel studies. Similar effects have been reported for melt mixed polypropylene/MWNT³⁷ composites, polycarbonate/MWNT composites³⁸ and Polyamide 6/MWNT composites³⁹.

The distinct minimum in dynamic viscosity with the varying amount of SWNTs becomes more evident in Figure 7.11a where the dynamic viscosity at low frequency (3.5×10^{-4} rad/s) is shown as a function of SWNTs content. The figure depicts a minimum in the dynamic viscosity at 0.1-0.2 wt% of SWNTs. The variation in the storage or plateau modulus as a function of SWNTs content, at high frequency (100 rad/s) is given in Figure 7.11b. The plateau modulus decreases up to approximately 1 wt% after which the modulus increases.

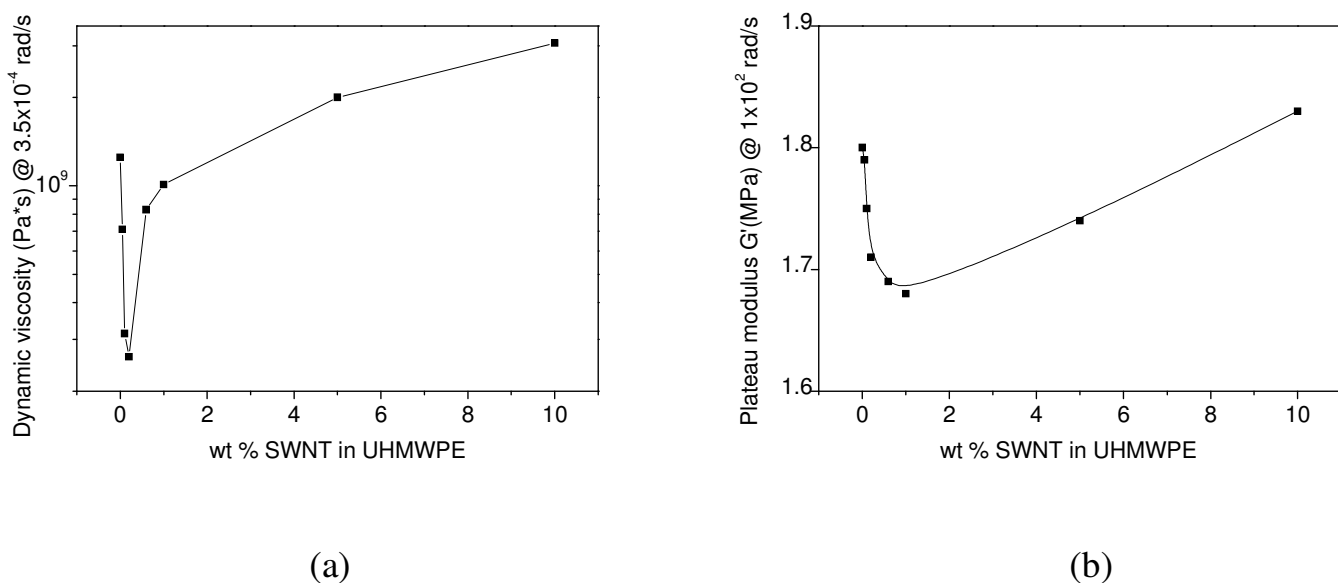


Figure 7.11: The figure depicts changes in dynamic viscosity and plateau modulus with the varying concentration of nanotubes. (a) Dynamic viscosity in region II at 0.00035 rad/s of the SWNT/UHMW-PE (Grade A) nanocomposites shows a significant drop with the addition of 0.1-0.2 wt% of SWNTs. (b) Plateau modulus in region I at 100 rad/s of the SWNT/UHMW-PE nanocomposites also registers a minimum in the modulus with increasing concentration of SWNTs.

The minimum in storage modulus (or dynamic viscosity) with increasing amount of SWNTs, at both high and low frequencies, requires an explanation. What follows is a possible explanation for the drop in the viscosity at relatively low content of nanotubes.

First, we recall that UHMW-PE used for the present studies has a broad molar mass distribution. Due to the van der Waals interaction PE chains tend to be adsorbed on the nanotubes. (also suggested by the crystallization studies, Figure 7.6) The probability of the

high molar mass to remain adsorbed on the nanotubes will be higher than the low molar mass chains. The adsorbed polymer, especially of high molar mass, can be considered as an immobilized part of the nanotube. Thus the polymer forming the remaining matrix will effectively have a lower average molecular weight than the pure polymer (dashed chains in the illustration of Figure 7.8). This would cause faster relaxation of chains thus a decrease in the storage modulus (or viscosity) and subsequently a higher phase angle, as depicted in the Figure 7.9. The observed drop in viscosity at such a low concentration of filler is in agreement with recent findings reported elsewhere. To quote, Mackey et al⁴⁰ reported decrease in viscosity in polystyrene filled with cross-linked polystyrenes, whereas Jain et al¹ observed a similar drop in viscosity using silica nanoparticles as filler. In nanocomposites filled with silica, an explanation provided for the viscosity drop was the selective physico-adsorption of polymer chains onto nano-particles surfaces. Independently, preferential adsorption of high molar mass component in polydisperse UHMW-PE on silica particles was observed by Maurer et al.⁴¹

When the nanotube content is increased beyond 0.2 wt % the nanotube network is formed. The formation of this network gets evident from the appearance of the plateau region at lower frequencies. The elastic strength of this network increases with increasing amount of the nanotubes.

To strengthen the concepts on selective adsorption of high molecular weight fraction, experiments are performed on a grade (Grade B) having molecular weight similar to the Grade A but a lower polydispersity, i.e. 2.8 instead of ~10. Figure 7.12 shows that similar to the Grade A (Figure 7.10) the storage modulus in the region II of the Grade B becomes independent of frequency at a SWNTs concentration of 0.6 wt%. This implies the formation of a mechanical nanotube network. However, unlike the Grade A, the Grade B does not show a minimum in the storage modulus in the Region II. This can be explained by the difference in polydispersity; since in the Grade B all polymer chains are relatively long ($M_n \sim 1.3 \times 10^6$ g/mol) and are of similar length, no clear distinction in the molecular weight between the polymer matrix before and after the adsorption of chains to nanotubes exist. Therefore increasing the nanotube content simply results into a stronger nanotube network.

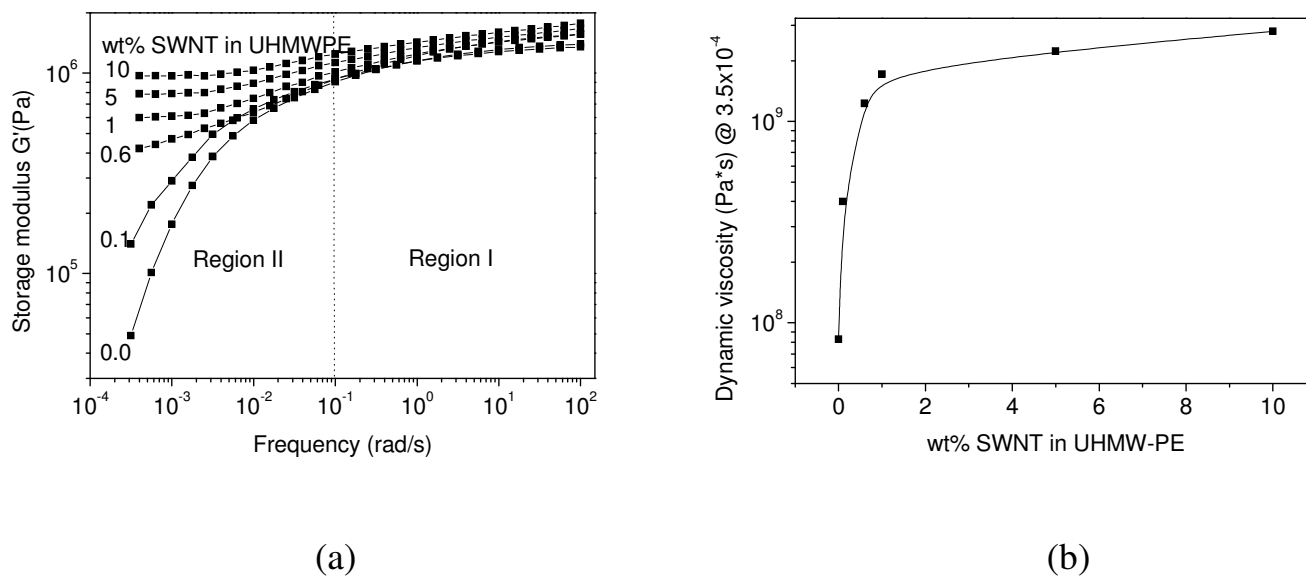


Figure 7.12: Storage modulus G' of SWNTs/UHMW-PE (Grade B) at 160 °C. (a) The modulus as function of frequency and wt % of SWNTs (b) Storage modulus at 0.00035 rad/s (region II) with different wt % of SWNTs.

In addition to it, many reported studies in literature also do not observe the drop in dynamic viscosity.^{32,37-40,42} Since in literature, composites with lower molecular weight are investigated (less than 400.000 g/mol), it seems plausible that a critical molecular weight of the polymer exists for the preferred adsorption mechanism. For example, in low molecular weight polymer the polymer/nanotube interaction (for the given experimental time) will be sufficiently small, which favors easier desorption of polymer from the nanotube surface. Results in Figure 7.13 describe our observations on a commercial HDPE grade, having a molecular weight of 100.000 g/mol and a polydispersity of 4. Similar to the results reported in literature no decrease in viscosity is observed. When compared to the UHMW-PE studies, these results strengthen the hypothesis that preferred adsorption only occurs when a chain is sufficiently long to remain adsorbed on the nanotubes.

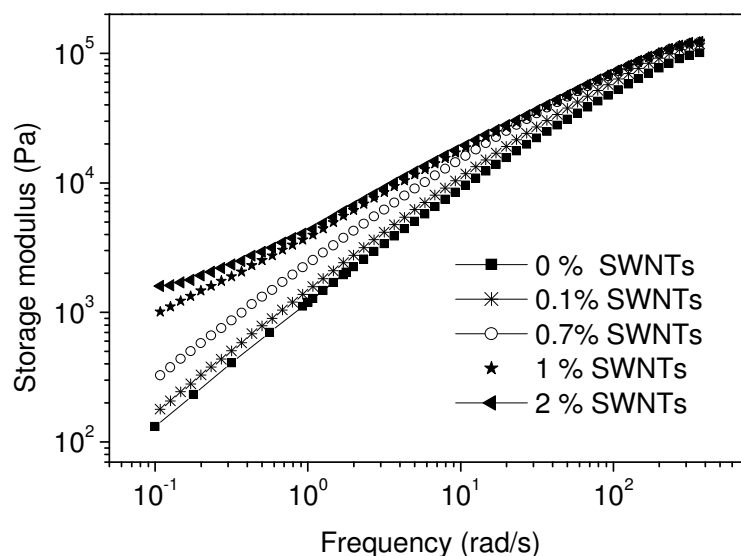


Figure 7.13: Storage modulus G' of SWNTs/HDPE at 160 °C as a function of frequency and wt % of SWNTs.

In the Figures 7.10 and 7.12, the second plateau modulus in the Region II at low frequencies of the SWNTs/UHMW-PE polymer network ranges between 4 to 6 x 10⁵ Pa for 0.6 to 1.0 wt% of SWNTs. This network modulus is higher than that reported in literature for similar CNT loadings in a relatively low molar mass polymer. Pötschke P. et al³² associated the origin of the modulus to the network formation between the carbon nanotubes linked by the polymer chains. (polymer nanotube bridging (c) in Figure 7.8). In the case of SWNTs/UHMW-PE nanocomposites the origin of the high modulus can be explained by the stronger polymer-nanotube interaction compared to the low molar mass nanotube composites. Since the diameter of a random coil of UHMW-PE is estimated over 120 nm, whereas the diameter of SWNTs ranges between 6-10 nm. Considering the large radius of gyration of UHMW-PE compared to the diameter of SWNTs, the polymer chains are likely to entangle with the nanotubes. Thus the nanotubes that are in proximity can be easily connected by the long polymer chains. This is likely to result in a decrease in chain mobility and an enforcement of the nanotube network by the polymer chain. Since the molecular weight of the polymers (4.000.000 g/mol) used in our studies is considerably higher compared to that reported for low molar mass (50.000-150.000 g/mol), bridging of the nanotubes with the polymer is more likely to happen at lower nanotube concentration. In addition to it the polymer interaction for the long chains with the nanotubes will be stronger for the same loading of nanotubes in the polymer.

Experiments reported above clearly demonstrate that the viscoelastic response of polymer/CNT composites is strongly influenced by the polydispersity. The simple spraying technique used to obtain the UHMW-PE nanocomposites opens an opportunity to overcome the intractable problem of UHMW-PE.

7.3.5 Electrical conductivity of SWNTs/UHMW-PE nanocomposites

Figure 7.14 shows that the SWNT/UHMW-PE nanocomposites are conductive at a SWNT loading of 0.6 wt%. It is generally accepted that when the nanotube loading reaches the conductivity threshold, a conductive network exists in which the nanotubes form a conductive path. For or a conductive network to be formed, nanotubes do not require real overlap of the nanotubes, since a conductive network can be formed through hopping and tunneling processes. However further increase in SWNT content to 1 wt% or higher does not show a pronounced increase in conductivity, there it is assumed that the network is formed by geometrical overlapped nanotubes at 0.6 wt% SWNTs. The threshold for the mechanical network formation probed with rheology, where geometrical overlap is required is in agreement with the sudden increase in electrical conductivity. The low threshold for rheological changes and electrical properties are comparable to that reported for other nanotube composites. This indicates that the simple spraying technique is adequate to generate a well dispersed SWNTs/UHMW-PE composite. The threshold value for percolation can be further lowered with improved dispersion of SWNTs in a solvent.

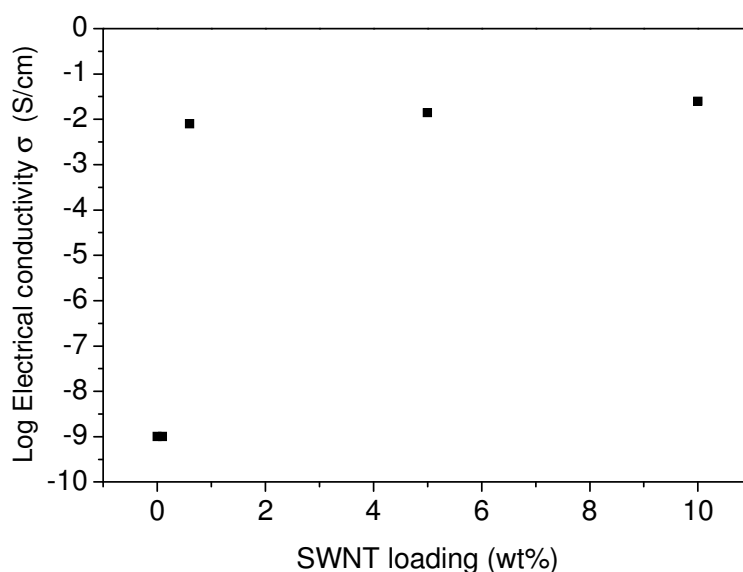


Figure 7.14: Electrical conductivity of SWNTs/UHMW-PE nanocomposites (Grade B).

7.4 Conclusion

A new simple method of spraying SWNTs on the surface of UHMW-PE particles is used to prepare SWNTs/UHMW-PE nanocomposites. Considering the simplicity of the technique, this method can be applied in general. The UHMW-PE coated with the nanotubes is dissolved in xylene. It is shown that in solution due to the high viscosity of the UHMW-PE the SWNTs do not coagulate. SEM images reveal a good distribution of the SWNTs in the polymer matrix after crystallization from the solution. The ‘Shish-Kebab’ type of morphology observed in these films suggests that the nanotubes act as a nucleating agent for the polymer chains. This is further strengthened by following crystallization behavior from the melt, using oscillatory rheometry as a tool. The observations are that the onset of crystallization and the crystal growth rate enhances considerably with increasing concentration of nanotubes in the polymer matrix. For an example, isothermal crystallization probed by rheometry shows enhancement in crystallization by a factor of three at low loadings of 0.1 wt% of SWNTs. Solution casted films having a concentration of SWNTs, less than 3 %, are drawable. However, the drawability decreases with increasing concentration of SWNTs.

Conductivity and linear viscoelastic measurements reveal that a threshold of 0.6 % of SWNTs is required to form a nanotube network within the polymer matrix. This threshold value is comparable to other SWNTs polymer-composites reported in literature.^{32,37-40,42} This proves that the adopted spraying technique in the intractable UHMW-PE is effective. The resulting network increases electrical conductivity by nine orders of magnitude.

The network formation that occurs in the melt from and above 0.6 wt % of SWNTs dispersed in polymer is observed as a plateau modulus at low frequency in the oscillatory shear measurements. The strength of the network increases with increasing concentration of the nanotubes.

A comparison with the reported data on the SWNTs/polymer network modulus for the same concentration of SWNTs shows that the strength of the network formed in UHMW-PE is higher than that for the low molecular weight polymers. A plausible explanation of the higher network modulus is that the high molecular weight polymers will have higher probability to entangle with the dispersed nanotubes. This result into a stronger network formation at low loadings of SWNTs compared to other polymer/CNT composites.

The polydispersity of UHMW-PE in nanocomposites has a distinct impact on the viscoelastic behavior of the nanocomposites. The observations are that in a polydisperse UHMW-PE sample with increasing concentration of SWNTs a clear minimum exists in dynamic viscosity (modulus). However, such a minimum is not realized in a sample having a relatively sharp molar mass distribution. Selective adsorption of the high molar mass fraction on the

dispersed SWNTs seems to be a possible explanation for the observed minimum. Due to the selective adsorption of the high molar mass the apparent molar mass of the polymer matrix decreases, consequence to it phase angle shows a more viscous like response as anticipated for the lower molar mass.

7.5 References

1. Jain S.H. Ph.D thesis, Eindhoven University of Technology, *Nano-scale events with macroscopic effects in PP/silica nanocomposites* **2005** ISBN 90-386-3046-8
<http://alexandria.tue.nl/extra2/200511823.pdf>
2. Ijima, S. *Nature* (London) **1991**, 354, 603.
3. Bethune, D.S.; Kiang, C. H.; De Vries, M. S.; Gorman, G.; Savoy, R.; Vazque Z.; Beyers, R. *Nature* (London) **1993**, 363, 605.
4. Yakobson, B. I.; Smalley, R. E. *Science* (New York) **1997**, 85, 324.
5. Kong, J.; Franklin, N.; Zhou, C.; Chapline, M.A.; Peng, S.; Cho, K.; Dai, H. *Science* (New York) **2000**, 287, 622.
6. Walters, D. A.; Ericson, L. M.; Casavant, M. J.; Liu, J.; Colbert, D. T.; Smith, K. A.; Smalley, R. E. *Appl. Phys. Lett* **1999**, 74, 3803.
7. Baughman, R. H.; Zakhidov, A. A.; de Heer W. A. *Science* (New York) **2002**, 297, 787.
8. Shaffer, M.S.P; Fan, X.F.; Windle, A.H; *Carbon* **1998**, 36, 1603.
9. Eitan, A.; Jiang, K.; Dukes, D.; Andrews, R.; Schadler, L. S. *Chem. Mater.* **2003**, 15, 3198.
10. Rinzler A.G.; Lui, J.; Dai, H.; Lui, H.; Nikolaev, P.; Huffman, F.J. ;Rodriguez-Macias, F.J.; Boul, P.J.; Lu, A.H.; Heymann D.; Colbert, D.T.;Lee, R.S.;Fischer, J.E.; Rao, A.M.; Eklund, P.C.; Smalley , R.E. *Appl Phys* **1998**, 67, 29.
11. Chen, J.; Hamon, M. A.; Hu, H.; Chen, Y.; Rao, A. M.; Eklund, P. C.; Haddon, R. C. *Science* (New York) **1998**, 282, 95.
12. Viswanathan, G.; Chakrapani, N.; Yang, H.; Wei, B.; Chung, H.; Cho, K.; Ryu, C. Y.; Ajayan, P. M. *J. Am. Chem. Soc.* **2003**, 125, 9258.
13. Hill, D. E.; Lin, Y.; Rao, A. M.; Allard, L. F.; Sun, Y.-P. *Macromolecules*, **2002**, 35, 9466.
14. Lin, Y.; Zhou, B.; Fernando, K. A. S.; Liu, P.; Allard, L. F., Sun Y.-P. *Macromolecules* **2003**, 36, 7199.
15. Shaffer, M. S. P.; Windle, A. H. *Adv. Mater.* **1999**, 11, 93
16. Mitchell, C. A.; Bahr, J. L.; Arepalli, S.; Tour, J. M.; Krishnamoorti, R. *Macromolecules* **2002**, 35, 8825.
17. Islam, M. F.; Eojas, E.; Bergey, D. M.; Johnson, A. T.; Yodh, A. G. *Nano Lett.* **2003**, 3, 269.
18. Moore, V. C.; Strano, M. S.; Haroz, E. H.; Hauge, R. H.; Smalley, R. E. *Nano Lett.* **2003**, 3, 1379.
19. Levi, N.; Czerw, R.; Xing, S.; Iyer, P.; Carroll, D. L. *Nano Lett.* **2004**, 4, 1267.
20. Bandyopadhyaya, R.; Nativ-Roth, E.; Regev, O.; Yerushalmi-Rozen, R. *Nano Lett.* **2002**, 2, 25.
21. Chen, J.; Liu, H.; Weimer, W. A.; Halls, M. D.; Waldeck, D. H.; Walker, G. C. *J. Am. Chem. Soc.* **2002**, 124, 9034.
22. Ausman, K. D.; Piner, R.; Lourie, O.; Ruoff, R. S.; Korobov, Mikhail. *J. Phys. Chem.* **2000**, 104, 8911.

23. Zhang, X.; Liu, T.; Sreekumar, T. V.; Kumar, S.; Moore, V. C.; Hauge, R. H.; Smalley, R. E. *Nano Lett.* **2003**, *3*, 1285.
24. Regev, O.; Elkati P. N. B.; Loos, J; Koning C. E. *Adv. Mater.* **2004**, *16*, 248
25. Huang X.; Brittain W.J. *Macromolecules* **2001**, *34*, 3255.
26. Bhattacharyya, A. R.; Potschke, P.; Abdel-Goad, M.; Fischer, D.; *Chem. Phys. Lett.* **2004**, *392*, 28.
27. Sharma-Garkail K Ph.D. thesis, Eindhoven University of Technology *Easily processable ultra high molecular weight polyethylene with narrow molecular weight distribution* **2005** ISBN 90-386-2836-6 <http://alexandria.tue.nl/extra2/200510552.pdf>,
28. Smith, P.; Lemstra, P. J. *J. Mater. Sci.* **1980**, *15*, 505.
29. Pennings, A.; Kiel, A.M. *Kolloid Z.Z Polymere* **1965**, *205* 160.
30. Khanna, Y.P. *Macromolecules*, **1993**, *26*, 3639.
31. Boutahar, K.; Carrot, C.; Guillet, J. *Macromolecules*, **1998**, *31*, 1921.
32. Pötschke P.; Abdel-Goad M.; Alig I.; Dudkin S.; Lellinger D.; *Polymer*, **2004**, *45*, 8863.
33. Mackay, M.E.; Dao, T.T.; Tuteja, A.; Ho, D.L.; Brooke van, H.; Kim, H.C.; Hawker, C.J.; *NatureMaterials* **2003**, *2*, 762.
34. Roberts,C.; Cosgrove, T.; Schimidt, R.G.; Gordon, G. V. *Macromolecules* **2001**, *34*, 538.
35. Shenoy AV. Rheology of filled polymer systems. Dordrecht:Kluwer Academic Publishers, **1999**.
36. Winter H.H.; Mours M. *Adv. Polym. Sci.* **1997**, *134*, 165.
37. Kharchenko S.B.; Douglas J.F., Obrzut J., Grulke E.A., Migler K., *Nature materials*, **2004**, *3*, 564.
38. Pötschke P., Fornes T.D., Paul D.R., *Polymer*, **2002**, *43*, 3247.
39. Meincke O.; Kaempfer D.; Weickmann H.; Friedrich C.; Vathauer M.; Wart H.; *Polymer* **2004**, *45*, 739.
40. Mackay, M.E.; Dao, T.T.; Tuteja, A.; Ho, D.L.; Brooke van, H.; Kim, H.C.; Hawker, C.J.; *NatureMaterials* **2003**, *2*, 762.
41. Maurer, F.H.J.; Schoffeleers, H.M.; Kosfeld, R., Uhlenbroich, T.H.; *Progress in Science and Engineering of Composites*, Tokyo **1992**, 803.
42. Du F.; Scogna R.C.;Zhou W.; Brand S.; Fischer J.E.; Winey K.I.; *Macromolecules* **2004** *3*.

Appendix

Experimental rheology of UHMW-PE

The material investigated in this thesis is linear Polyethylene possessing a molar mass ranging from 10^5 to 5×10^6 g/mol. The nascent disentangled grade of 3.6×10^6 g/mol and polydispersity of 2.8 (Sample E in table 2.2) is used to prove the concept of entanglements formation upon melting disentangled polymer crystals. The disentangled melt state is probed by Rheometry and advanced NMR (Chapter 2 and 4) and the influence of the disentangled state is seen in the crystallization studies (Chapter 5).

Given the high sample stiffness of the UHMW-PE samples, the measurements are not straight forward. In this appendix the precautions that were taken to correctly measure the UHMW-PE samples using rheology are described.

Compression temperature

First the nascent powders are compressed in a hot press at 50°C (i.e. below the α -relaxation temperature) and 200 bars in a mould of 30×50 mm. Using this procedure for the nascent disentangled grades, coherent films are obtained. For the entangled nascent UHMW-PE, (i.e. the commercially available Montell grade of molar mass 4.2×10^6 g/mol and polydispersity 8) coherent samples are only obtained by compression moulding above 120°C . By varying the compression temperature from 50°C to 130°C , no influence is seen on the rheological measurements in the melt.

Sample geometry

The torsion compliance of the rheometer force transducer used is equal to 1.3×10^{-6} NM/rad. If the sample stiffness approaches the spring constant of the instrument ($1/\text{compliance}$), the transducer becomes instable therefore considering the high stiffness of the UHMW-PE samples, samples having 8 mm diameter and 1 mm thickness are cut out of the 30×50 mm plate instead of the more frequently used 25 mm diameter plates. For these samples modulus values up to 10^7 Pa can be measured without transducer instabilities. To correctly measure the rheological behavior, it is required a good contact between the sample surface and the parallel plates. Given the high melt-viscosity of the UHMW-PE it is crucial that the thickness

variation in the solid state of the measured sampled is very low. Therefore only samples with a thickness variation in the solid state below 0.05 mm are selected for measurements. Figure A.1 illustrates the difficulties of a stiff sample between two parallel plates.

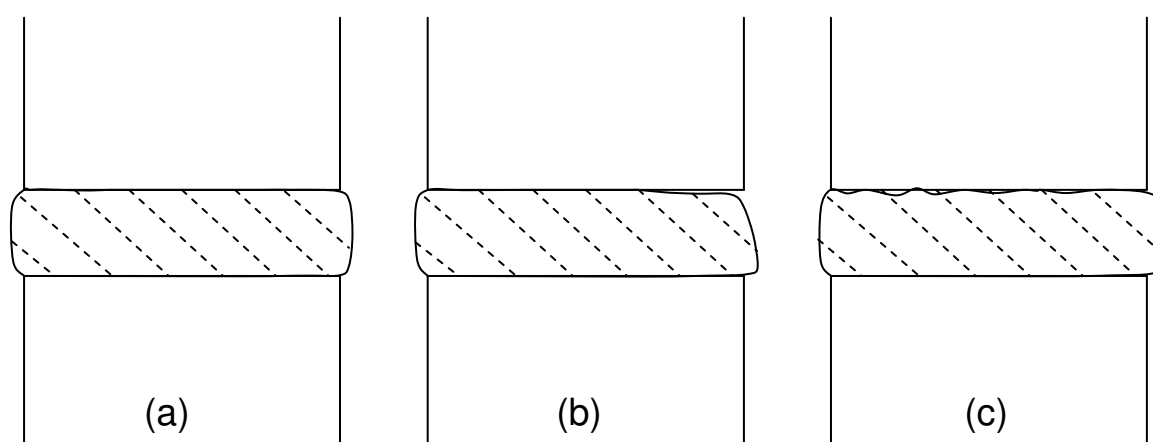


Figure A.1: Sketch of a stiff sample between the parallel plates. (a) depicts a correct measurement. (b) depicts a measurement of sample with a too large thickness variation. Therefore the sample does not touch the parallel plates completely. (c) depicts a sample with a rough surface. This rough surface smoothens after application of a normal force in the rheometer.

Rheological measurement

To make sure the sample touches completely the two parallel plates, a normal force of 500 g is applied. By varying the normal force from 0 to 2000 g, it is observed that, if the sample is touching the plates completely, the normal force has no influence on the performed rheological experiments. After the experiment, the roughness of the sample is evaluated by the eye to make sure that the sample completely touched the two plates during the experiment.

To monitor any possible slippage between sample and plates, all measurements are monitored by an oscilloscope which is connected to the rheometer. It is observed in a strain-sweep experiment (i.e. dynamic modulus as a function of applied strain at a constant frequency and temperature), that the applied strain (and the measured torque) is a perfect sine function from a strain of 0.1 % to 1.5 %, whereas at a strain greater than 2 % some noise on the applied strain signal is observed. Therefore the applied strain in all measurements is kept low at 0.5 %. It has to be noted that although some noise is observed, the measured modulus is not affected up to an applied strain of 8 %.

To prevent any chemical modification of the sample all measurements are performed in nitrogen atmosphere and the 1 wt% of Irganox anti-oxidant is used.

After the measurement.

After the measurements the sample diameter is measured. Generally, it is observed that the diameter shrinks on average about 5% in the case of the disentangled UHMW-PE and up to 20% in the entangled (commercial) UHMW-PE. This difference can be understood by considering the different stress needed to compress the samples in the solid state. The change in the diameter of the sample is only observed directly on melting. Therefore it is assumed that the diameter is constant during the measurement. If a diameter change of the sample of more than 5% is observed, the measurement is discarded.

To check for any oxidation/degradation of the samples, infrared spectroscopy is used. Furthermore size exclusion chromatography is performed to check the molecular weight of the samples before and after the measurement. To check if any cross linking during the measurements has occurred, 1 wt % of the measured sample is crystallized from decalin solution. After evaporation of the solvent the solution-crystallized film is drawn at 125 °C. It is observed that the drawability and the resultant properties of the measured sample are in line with the experiments performed on solution-crystallized nascent powders.

From these experiments it is concluded that the samples are chemically stable.

Concluding remarks

By following the above mentioned procedure all measurements shown in this thesis could be reproduced several times in different laboratories, by different people. It has to be noted that although the rheology experiments of the UHMW-PE sample are important to prove the concept of entanglements formation in a disentangled polymer melt, similar findings are observed with nascent disentangled samples possessing lower molecular weights (3.8×10^5 g/mol) and by different techniques i.e. advanced NMR, crystallization studies, drawability.

Samenvatting

Polymeren zijn van groot belang, zowel in de natuur als in de moderne maatschappij. In tegenstelling tot de polymeren in de natuur, de zogenaamde bio-polymeren, zijn de door de mens gemaakte polymeren thermisch stabiel en worden ze voor het overgrote deel verwerkt via de gesmolten toestand (plastics). In het geval van thermoplastische polymeren (>70% van alle synthetische polymeren) legt de sterke toename van de viscositeit van de smelt met toenemend moleculair gewicht een limiet op aan de verwerkbaarheid.

Experimenteel is aangetoond dat de (nul-)viscositeit van de polymere smelt, η_0 , schaalt met het gewichtsgemiddelde moleculair gewicht volgens $M_w^{3.4}$. Dit impliceert dat de smeltviscositeit bij een verdubbeling van het moleculair gewicht met meer dan een factor 10 toeneemt! Aangezien eigenschappen van polymeren in de vaste fase, zoals sterkte en taaierheid, toenemen met toenemend moleculair gewicht, is het verwerken van thermoplastische polymeren (bijv. spuitgieten, extrusie, vezelspinnen) vaak een compromis tussen het gemak van het verwerken via de smelt, d.w.z. voorkeur voor laag molgewicht (makkelijke vloeï), en eigenschappen met een voorkeur voor hoog/hoger molgewicht.

De huidige kennis van de polymeren in gesmolten toestand is al ver ontwikkeld en gebaseerd op een simpel maar elegant model van P.G. de Gennes (Nobel prijs voor de Natuurkunde), het zogenaamde reptatie model. In dit model wordt verondersteld dat de polymeerketen in de gesmolten toestand verstrengeld is met zijn naburige ketens. Deze andere ketens zorgen voor het ontstaan van een virtuele 'buis' dat het pad van de keten dusdanig vernauwt dat de keten zijn eigen contour lengte moet volgen (Brownse beweging). De beperkte ketenbewegelijkheid leidt tot een karakteristieke tijd voor een keten om over zijn eigen lengte te diffunderen, en daarmee ook de viscositeit, met M^3 . Het verschil met de experimenteel gevonden relatie van $\eta_0 \sim M_w^{3.4}$ kan worden verklaard door "contour lengte fluctuaties", d.w.z. fluctuatie gedreven rekking en contracties van een keten langs de 'tube'. In **Hoofdstuk 2**, wordt aangetoond dat zorgvuldig gesynthetiseerde hoog moleculair gewicht polyethyleen (PE) monsters met een smalle molgewichtverdeling de voorspellingen van het reptatie model inderdaad volgen, d.w.z. η_0 schaalt met M^3 . Het voordeel van hoog molgewicht polyethyleen is dat de keten uiteinden geen rol van betekenis spelen en daarom genegeerd kunnen worden. **Als gevolg van deze resultaten is (ultra) hoog molgewicht polyethyleen (UHMW-PE) gebruikt als model materiaal in dit proefschrift.**

In de vaste fase kunnen verstrengelingen (warpunten, in het Engels: "entanglements") eenvoudig verwijderd worden door het polymeer op te lossen. In verdunde oplossing, beneden de zogenaamde overlap concentratie ϕ^* , kunnen verstrengelingen helemaal verwijderd worden. In het geval van kristalliseerbare polymeren zoals PE, kan het gereduceerde aantal verstrengelingen permanent gemaakt worden doordat de lange molecuul

ketens gevouwen keten kristallen vormen: een goed bestudeerd fenomeen in de polymeer fysica.

Een meer elegantere en ook een technologisch meer geavanceerde manier om PE kristallen te produceren die helemaal ontstrengeld zijn, is via directe polymerisatie in de reactor. Bij lage polymerisatie temperaturen en lage katalysator activiteit zullen individueel groeiende ketens aparte gevouwen keten kristallen vormen. In het uiterste geval zijn de groeiende ketens ver genoeg uit elkaar om kristallen te vormen bestaande uit een enkel molecuul, de zogenaamde mono-moleculaire kristallen.

Als een compleet ontstrengelde PE structuur verkregen is door kristallisatie, vanuit oplossing en/of via directe polymerisatie, is de intrigerende vraag of deze ontstrengelde toestand behouden kan blijven na het opsmelten en wat de tijd schaal is om een volledig verstrengelde evenwicht polymeren smelt te vormen? **Deze vraag is het hoofd onderwerp van dit proefschrift: uitgaande van een niet-evenwichts ontstrengelde toestand zal het gedrag tijdens het smelten en de keten dynamica in gesmolten toestand gevolgd worden tot in het evenwicht, dus de volledig verstrengelde toestand.**

In **Hoofdstuk 2** wordt aangetoond dat uitgaande van de ontstrengelde toestand - in dit geval nieuw gevormde (nascent) UHMW-PE poeder verkregen door polymerisatie in oplossing via metallocene katalyse- het tijd kost om de plateau modulus, indicatief voor het vormen van verstrengelingen in de smelt, 'op te bouwen'. De vorming van verstrengelingen schaalt als het reptatie proces (M_w^3). Naast de rheologisch metingen is vaste stof NMR gebruikt om de verandering in keten mobiliteit te volgen. De zeer verschillende tijdschaal van de ontstrengelde smelt naar de evenwicht smelt, zoals gemeten met NMR en via Rheologie experimenten, suggereert dat de restricties in de lokale keten mobiliteit, zoals die in de NMR experimenten gevolgd wordt, eerder gevormd worden, in vergelijking met de restricties in de mobiliteit van keten segmenten zoals die gemeten worden in de rheologie experimenten.

Een eigenaardig fenomeen van nascent reactor poeders is het hoge smeltpunt dat dicht tegen het zogenaamde evenwichtssmeltpunt van PE aan ligt. Dit fenomeen heeft onderzoekers gedurende vele jaren voor vraagtekens gesteld. Verschillende verklaringen zijn gegeven, zoals de groei van gestrekte keten kristallen in plaats van gevouwen keten kristallen, of uitgebreide reorganisatie tijdens het smelt proces. Al deze verklaringen werden nooit onderbouwd door experimentele data. De observaties laten namelijk zien dat nascent kristallen "normale" gevouwen keten kristallen zijn zonder reorganisatie tijdens het smelten.

In **Hoofdstuk 3** wordt aangetoond dat het ongebruikelijke hoge smeltpunt van nascent UHMW-PE gerelateerd is aan de strak gevouwen (naar de aanliggende) ketens in het kristal. Tijdens het smelten "voelt de keten zijn eigen lengte" in tegenstelling tot bijvoorbeeld uit de smelt gekristalliseerde samples, waar een keten in meerdere gevouwen kristallen is ingebouwd, waardoor de keten in contact staat met meerdere ketens. Het smelt mechanisme zoals is besproken in hoofdstuk 3 kan worden gebruikt bij het gecontroleerd smelten van nascent UHMW-PE. Door het verlagen van de opwarm snelheid, zal het smelt proces starten

met het loslaten van enkelvoudige segmenten van het (laterale) oppervlak van het kristal. In dit proces zijn de keten uiteinde gesmolten en in staat om met andere keten uiteinden van partieel gesmolten kristallen te verstrengelen. De kern van het molecuul is echter nog steeds in het kristal, d.w.z. in de strak gevouwen keten conformatie. Na volledig smelten ontstaat er een heterogene smelt, omdat het centrale deel van de ketens niet in staat is om te verstrengelen met andere ketens tijdens het smelt proces. Deze heterogene smelt wordt besproken in **Hoofdstuk 4**. Vaste stof NMR experimenten tonen aan dat de tijd die nodig is om de keten conformatie op lokale schaal in te perken toeneemt met afnemende opwarm snelheid. Met de toenemende tijd die nodig is om de keten conformaties lokaal in te perken, zal de tijd toenemen voor de modulus om toe te nemen naar de evenwichtstoestand. Uiteindelijk is het mogelijk om het monster zo langzaam op te warmen dat de restrictie in keten conformaties in een deel van het sample kan worden voorkomen, waardoor de gedeeltelijke hoge lokale mobiliteit gehandhaafd blijft. Omdat de restrictie in de keten conformatie niet bereikt kan worden zal de coöperatieve beweging, nodig voor de translatiemobiliteit, afwezig zijn. Hierdoor zal de keten reptatie afgeremd worden en zal een, langdurig bestaande, gedeeltelijke onverstrengelde smelt ontstaan. Deze nieuwe gesmolten toestand heeft een verlaagde plateau modulus en verlaagde viscositeit; daarentegen is de stress relaxatie snelheid onveranderd. De stress relaxatie, zonder diffusie van keten voorbij een “tube” lengte, wordt verklaard door de partiële reptatie van ketens, waarbij beweging van slechts een gedeelte van de keten genoeg is voor stress relaxatie.

De consequenties van de heterogene smelt toestand wordt besproken in **Hoofdstuk 5**. In dit hoofdstuk wordt aangetoond dat ontstrengelde ketensegmenten sneller kristalliseren dan verstrengelde ketensegmenten. Deze observaties suggereren dat intra-moleculaire homogene kernvorming sneller verloopt dan heterogene kernvorming. Daarnaast is na kristallisatie van de heterogene smelt de verstreikbaarheid opmerkelijk hoog, wat indicatief is voor een ontstrengelde toestand in een deel van het kristal (verstreikbaarheid is gerelateerd aan de ingevangen verstrengelingen zoals hierboven besproken is)

Het smeltgedrag van uit oplossing gekristalliseerde UHMW-PE is als referentie besproken in **hoofdstuk 6**. Op dezelfde wijze als bij de nascent ontstrengelde kristallen, is het mogelijk om deze gevouwen kristallen te smelten door het opeenvolgend loslaten van ketensegmenten van de kristalsubstraat. Het verschil in smelt gedrag, als gevolg van de verschillende opwarm snelheden, heeft consequenties voor de ketendynamica in de smelt. In tegenstelling tot de nascent onverstrengelde samples, waar de modulus in de tijd toeneemt, vormen de verstrengelingen in de vanuit oplossing gekristalliseerde samples zich meteen na het (snel) smelten. Het opmerkelijke verschil in de snelheid van het vormen van verstrengelingen kan toe geschreven worden aan het verschil in opstapeling van de kristallen voordat de kristallen gesmolten worden.

De vanuit oplossing gekristalliseerde kristallen verdubbelen hun kristalgrootte, waarbij de ketensegmenten in de regelmatig opgestapelde kristallen met elkaar vermengen. Dit versnelt

het vormen van verstrengelingen na het smelten. Daarentegen is in de nascent ontstregelde monsters geen regelmatige opstapeling geobserveerd.

Een alternatieve route om de smelt viscositeit te verlagen door het mengen van enkelwandige koolstof nanovezels (SWNTs) is verkend in **Hoofdstuk 7**. Door de hoeveelheid van SWNTs te variëren is er een minimum in de dynamische viscositeit/opslag modulus geobserveerd. De verlaagde viscositeit wordt toegewezen aan de selectieve adsorptie van de hoog moleculaire fractie op het nano-vezel oppervlak. De verhoging van de viscositeit na het verder verhogen van de concentratie nan-vezels wordt toegewezen aan het ontstaan van een elastisch nanovezel-polymeer netwerk.

De concepten gepresenteerd in dit proefschrift, gebaseerd op experimentele bewijsvoering, kunnen een belangrijk effect hebben op nieuwe verwerkingstechnieken voor UHMW-PE, zoals het sinteren van UHMW-PE voor veeleisende toepassingen (zoals kunstmatige knie en heup prothesen) als kunstmatige knie- en heupprothese en het oplossingsvrij verwerken van UHMW-PE tot vezels en tapes.

Acknowledgment

At the initial stage of the research project presented in this thesis, it was challenging to convince others of the concept of a disentangled polymer melt. The experiments performed at that stage showed that we were dealing with an interesting polymer melt, although a clear hypothesis to explain the findings, as we have now, was lacking. I would like to thank Sanjay especially for this period. It was a period of strong discussions, but also a period where I needed Sanjay the most, since at that stage we were the only “believers” of our findings. Although honestly, it took me also some time to believe our experiments. A simple time-sweep experiment to follow the entanglements formation of the molten nascent disentangled melt was repeated over 20 times.

For this period I would also like to thank Prof. Piet Lemstra for the critical comments. Probably you were not convinced initially, I would like to thank you the opportunity of performing this research and for the support you gave at the writing stage.

Furthermore I would like to thank;

- DSM (especially Paul Hamm, Robert Kirschbaum, Rein Borggreve, Harm van der Werff, Médard Schoenmakers) for their input and for the opportunity to combine this research project with my sporting career.
- Prof. Christian Bailly for your contribution to the discussions and going to the thesis critically during the writing phase.
- Gerrit Peters and Prof. H.E.H. Meijer for the discussions we had and for the opportunity to use the Rheometers in your lab.
- Prof. H.W. Spiess, for the inspiring discussions and for the opportunity for us to use the Solid State NMR equipment in your laboratory in Mainz.
- Prof. T.C.M. McLeish for the model you wrote on the heterogeneous melt and for experimental suggestions.
- Prof. G.W.H. Höhne for the time you took for discussing about the melting behaviour of polyethylene. Although you are retired, it was nice to see the flame in you when discussing.
- Bing Wang for synthesizing the nascent disentangled PE materials in the DSM laboratories.
- Yefeng Yao and Robert Graf, for helping me with the solid state NMR experiments and for the collaboration we had in our projects.

I would like to thank;

- Pieter Magusin and Brahim Mezari for the possibility to perform solid state NMR experiments in Eindhoven and for the valuable time you took to discuss.
- Saied Talebi, Kirti Garkhail and Rob Duchateau for providing the synthesized materials which further strengthened our hypothesis.
- Lada Kurelec, Bob van de Gender for their contribution during the initial stages of this research.
- Juul Cuijpers for performing the TM-DSC experiments.

In short I would like to thank Joost Valeton and Wouter Gerritsen for their help with DSC. Peter Koets for helping with the drawing experiments, Sachin Jain and Han Goossens for the discussion on the nano-additives. Cees Bastiaansen for discussing on the rheology of solution crystallized UHMW-PE. Victor Litvinov for discussing the NMR results.

Next I would like to thank Prof. R. Larson, Prof. G. Strobl, Prof. M.A. Michels, Prof. D. Frenkel, Prof. M. Laun, for their time and for their input in the work.

I would like to thank the people of Sanjay's group in Eindhoven i.e. Nilish, Sai, Esther, Juul, Ann and especially Luigi for discussion. I would like to thank the rest of the SKT group for the inspiring atmosphere that I have been working.

Voor de ondersteuning tijdens mijn promotie in combinatie met mijn roeicarrière zou ik graag mijn moeder, Helen, Meindert, Rutger, Willemijn en mijn roeicoaches Jan, Ad, Lucas, Rick willen bedanken. Voor de discussies tijdens de koffie over de belangrijke zaken in het leven wil ik graag Dirk-Jan, Maartje, Worst, Het Tachoshuis, de bootslieden Jo en Frans en de leden van roeivereniging ESR Thêta bedanken.

Curriculum Vitae

The author of this thesis was born in Geldrop (Noord-Brabant), The Netherlands on May 3rd, 1977. After finishing secondary school (VWO, Augustinianum SG, Eindhoven) in 1995, he studied Chemical Engineering at the Eindhoven University of Technology. At the end of 2002, he completed his Masters thesis entitled 'Kinetics of melting in polymers; different states of melt and its influence on physical properties' under supervision of Prof. dr. S. Rastogi and Prof. dr. P.J. Lemstra.

At the beginning of 2003 he joined DSM Venturing and Business development and later DSM Performance Materials. The Ph.D. study described in the thesis is performed in the Faculty of Chemistry & Chemical Engineering, group Polymer Technology (SKT) (Chair: Prof. dr. P.J. Lemstra) in the research group of Prof. dr. S. Rastogi. During his Ph.D.-study, the author completed the four modules of the course 'Register Polymeerkundige (RPK)' organized by the 'National Dutch Graduate School of Polymer Science and Technology' (PTN, Polymeer Technologie Nederland).

From 1995 till 2007 the author was active in the sport of rowing on international level. During his Master and Ph.D. study he competed at the Olympic Games of Sydney, 2000 where he won a silver medal, and at the Olympic Games of Athens. For his achievement in sport and study the author received the Honorary Medal of the Eindhoven University of Technology.